Novel EGFR family member binding antibodies as cancer therapeutics

Von der Fakultät Energie-, Verfahrens- und Biotechnik der Universität Stuttgart zur Erlangung der Würde eines Doktors der Naturwissenschaften (Dr. rer. nat.) genehmigte Abhandlung

Vorgelegt von

Lisa Schmitt

aus Karlsruhe

Hauptberichter:	**Prof. Dr. Roland Kontermann**
Mitberichter:	**Prof. Dr. Tilman Brummer**

Tag der mündlichen Prüfung: **12. Dezember 2017**

Institut für Zellbiologie und Immunologie

der Universität Stuttgart

2018

Table of Contents

Abbreviations

2xTY	rich bacterial medium
3D	three dimensional
3M6	αHER3 antibody – Seribantumab variable domain with C89S mutation
4D5	αHER2 antibody – Trastuzumab variable domain/precursor
A	alanine
a	adenine
aa	amino acid
ADCC	antibody-dependent cellular cytotoxicity
Akt	protein kinase B
ALT	alanine aminotransferase
Amp	ampicillin
APS	ammonium persulfate
AUC	area under the curve
BAD	Bcl2-associated death promoter
BiTE	Bispecific T-cell engager
c	cytosine
C / Cys	cysteine
CDC	complement-dependent cytotoxicity
CDR	Complementarity determining region
C_H	constant region of the heavy chain
C_L	constant region of the light chain
CR	cysteine rich
CTX	cholera toxin
D	aspartic acid
Da / kDa	(kilo) Dalton ((10^3) g/mol)
DAPI	4',6-Diamidin-2-phenylindol
ddH_2O	double distilled water
DI	extracellular domain I
DII	extracellular domain II
DIII	extracellular domain III
DIV	extracellular domain IV
DMEM	Dulbecco's Modified Eagle Medium
DMSO	Dimethyl sulfoxide
DNA	deoxyribonucleic acid
dNTP	deoxynucleotide triphosphate
dox	doxycycline
DTT	dithiotreitol
E	glutamic acid
E.coli	*Escherichia coli*
e.g.	exempli gratia / for example
EC_{50}	half maximal effective concentration

ECD	extracellular domain
ECL	enhanced chemiluminescence
EGF	epidermal growth factor
EGFR	epidermal growth factor receptor
ELISA	enzyme-linked immunosorbent assay
ErbB	erythroblastic leukemia viral oncogene homolog
Erk	extracellular signal-regulated kinase
EtOH	ethanol
F	phenylalanine
$F(ab)_2$	antigen binding fragment dimerized via hinge region
Fab	Fragment antigen binding
FACS	Fluorescence activated cell sorting
Fc	Fragment crystallizable
FCS	fetal calf serum
FDA	(U.S.) Food and Drug Administration
FITC	fluorescein isothiocyanate
g	guanine
G / Gly	glycine
G418	aminoglycoside antibiotic
Gal12	Galectin 12 (beta-galactoside-binding)
GDP	guanosine diphosphat
GEF	Guanosine exchange factor
GFP	green fluorescent protein
glc	glucose
Grb2	Growth factor receptor-bound protein 2
GTP	guanosine triphosphat
h	hour
HB-EGF	heparin-binding EGF-like growth factor
HCl	hydrochloric acid
HEK	Human embryonic kidney
HEPES	4-(2-hydroxyethyl)-1-piperazineethanesulfonic acid
HER	human epidermal receptor
His	histidine
His_6	hexahistidine
HPLC	high performance liquid chromatography
HRG	heregulin
HRP	horseradish peroxidase
hu	human
I	isoleucine
i.e.	id est / that is
i.p.	intraperitoneal
i.v.	intravenous
IC_{50}	half maximal inhibitory concentration
IgG	immunoglobulin G

IMAC	immobilized metal ion affinity chromatography
IPTG	isopropyl-β-D-thiogalactopyranoside
k	kilo (10^3)
K	lysine
kb	kilo base pairs
kb	kilo base pairs
kcps	Kilo counts per second
L	leucine
L1	leucine-rich/ligand binding domain 1
L2	leucine-rich/ligand binding domain 2
LB	lysogeny broth
m	milli (10^{-3})
M	molar
M	methionine (in amino acid sequences)
mAb	monoclonal antibody
MAPK	mitogen-activated protein kinase
MEK	MAPK/Erk kinase
MFI	mean fluorescence intensity
MHC	Major histocompatibility complex
mo	mouse
MPBS	PBS containing milk powder
mTOR	mammalian target of rapamycin
mTORC1	mammalian target of rapamycin complex 1
mTORC1	mTOR complex 1
mTORC2	mammalian target of rapamycin complex 2
MW	molecular weight
n	nano (10^{-9})
N	asparagine
n.d.	not determined
n/a	not applicable
NaCl	sodium chloride
NaOH	sodium hydroxide
NFκB	nuclear transcription factor kappa B
NGF	Nerve growth factor
nm	nanometer (10^{-9}m)
NR	not reported
NTA	nitrilotriacetic acid
o/n	over night
OD	optical density
p	phospho- (-OPO_3^{2-})
P	proline
P/S	penicillin/streptomycin
PAA	Polyacrylamide
PAGE	polyacrylamide gel electrophoresis

PBA	PBS containing sodium azide
PBS	phosphate buffered saline
PBST	PBS with TWEEN 20
PCR	polymerase chain reaction
PDGF	platelet derived growth factor
PE	phycoerythrin
PEI	polyetylenimine
PFA	Paraformaldehyde
PH	pleckstrin homology
pH	negative decadic logarithm of the H_3O^+ concentration
PI	propidium iodide
PI3K	phosphatidylinositol 3-kinase
PIP_2	phosphatidylinositol 4,5-bisphosphate
PIP_3	phosphatidylinositol 3,4,5-trisphosphate
PKD1	Phosphoinositide-dependent protein kinase 1
PLC	phospholipase C
pM	pico molar (10^{-12} M)
PPB	periplasmic preparation buffer
PTEN	Phosphatase and Tensin homolog
puro	puromycin
PVDF	polyvinylidene difluoride
Q	glutamine
QCM	quarz crystal microbalance
R	arginine
Raf	rapidly accelerated fibrosarcoma
Ras	rat sarcoma
Rb	retinoblastoma
RIPA	radio immune precipitation buffer
RNA	ribonucleic acid
rpm	rotations per minute
RPMI	Roswell Park Memorial Institute
RSK	ribosomal-S6 kinase
RT	room temperature
RTK	receptor tyrosine kinase
S / Ser	serine
sc	single-chain
scDb	single-chain diabody
scFv	single-chain fragment variable
scTRAIL	single-chain TRAIL
SD	standard deviation
SDS	sodium dodecyl sulfate
Sec	size exclusion chromatography
SH2	Sarc homology 2
SH3	Sarc homology 3

Shc	SH2 containing transforming protein C
SOS	son of sevenless
Src	sarcoma
t	thymine
T / Thr	threonine
$t_{1/2}\alpha$	initial half-life
$t_{1/2}\beta$	terminal half-life
TAA	tumor-associated antigen
TAE	tris-acetate-EDTA
TCEP	tris(2-carboxyethyl)phosphine
TE	Tris-EDTA
TEMED	Tetramethylethylenediamine
Tet	tetracycline-inducible
TGF-α	transforming growth factor alpha
TKI	tyrosine kinase inhibitor
TMB	3,3',5,5'-Tetramethylbenzidine
TN1	trypton N1
TRAIL	TNF-related apoptosis-inducing ligand
Tris	tris(hydroxylmethyl)-aminomethane
UV	ultraviolet
V	valine
v/v	volume by volume
VEGF	vascular epithelial growth factor
V_H	variable domain of the heavy chain
V_L	variable domain of the light chain
W	tryptophane
w/o	without
w/v	weight per volume
WB	western blot
Y / Tyr	tyrosine
α	anti-
µ	micro (10^{-6})

Abstract

As conventional anticancer therapeutics often lack specificity and thus lead to toxicities to healthy tissues, monoclonal antibodies implicating specific targeting and low toxicity profiles have become attractive therapeutic drug candidates. ErbB receptors are valuable targets for antibody-mediated tumor therapy. The receptor tyrosine kinase (RTK) HER2 is a well-established tumor antigen whose overexpression is associated with adverse prognosis in breast cancer. The kinase impaired RTK HER3 has only recently emerged as target for antibody-mediated tumor therapy. In this study, a panel of scFv selected by phage display from the naïve human antibody gene libraries HAL7 and HAL8 were characterized. Two novel human monoclonal antibodies, IgG 2-35 and IgG 3-43, were developed from the candidates revealing highest affinity to cell surface expressed HER2 and HER3, respectively. IgG 2-35 bound to HER2 expressing cancer cells with EC_{50} values between 200 and 330 pM. Furthermore, IgG 2-35 was able to reduce EGF mediated proliferation of two HER2 overexpressing cancer cell lines. IgG 3-43 bound to an epitope conserved between human and mouse HER3. The bivalent IgG bound recombinant bivalent HER3 with subnanomolar affinity (K_D = 220 pM) and HER3-expressing tumor cells with EC_{50} values in the low picomolar range (3 - 30 pM). The antibody competed with heregulin for binding to HER3-expressing cells, efficiently inhibited both, heregulin induced and basal phosphorylation of HER3 as well as downstream signaling, and induced receptor internalization and degradation. Furthermore, IgG 3-43 inhibited heregulin-dependent proliferation of several HER3-positive cancer cell lines. Inhibition of tumor growth and prolonged survival was demonstrated in a FaDu xenograft tumor model in SCID mice. The findings demonstrate that IgG 3-43 efficiently blocks activation of HER3, thereby inhibiting tumor cell growth both *in vitro* and *in vivo*.

Zusammenfassung

Herkömmliche Krebsmedikamente sind oft unspezifisch und greifen daher auch gesundes Gewebe an. Monoklonale Antikörper versprechen spezifisches Targeting von Tumorzellen und geringe Toxizität, was sie zu attraktiven Kandidaten für Tumortherapeutika macht. Rezeptoren der EGFR-Familie sind wertvolle Zielstrukturen für die Antikörpervermittelte Tumortherapie. Die Rezeptortyrosinkinase HER2 ist ein etabliertes Tumorantigen, dessen Überexpression mit einer schlechten Prognose in Brustkrebs assoziiert ist. Die Rezeptortyrosinkinase HER3 wurde hingegen, unter anderem aufgrund ihrer eingeschränkten Kinaseaktivität, erst in jüngerer Zeit als strategisch wichtiges Tumorantigen bekannt. In der vorliegenden Arbeit wurde ein Set an variablen Antikörperdomänen, die zuvor mittels Phage-display aus einer Antikörpergenbibliothek isoliert wurden, als einzelkettiges variables Fragment (scFv) exprimiert und gescreent. Aus den Kandidaten mit den besten Bindungseigenschaften zu ihren zellulären Antigenen wurden zwei neuartige humane monoklonale Antikörper, IgG 2-35 und IgG 3-43, entwickelt. Die Antikörper wiesen hohe Affinität zu HER2 beziehungsweise HER3 auf. IgG 2-35 band HER2-exprimierende Krebszelllinien mit EC_{50}-Werten zwischen 200 und 330 pM. Zudem konnte IgG 2-35 die EGF vermittelte Proliferation in zwei HER2 überexprimierenden Krebszelllinien reduzieren. IgG 3-43 erkannte ein Epitop, das bei humanem und murinem HER3 konserviert ist. Die Affinität zwischen dem bivalenten Antikörper und rekombinantem bivalentem HER3 wurde mittels Quarzkristallmikrowaage-Technik gemessen und lag mit einer Dissoziationskonstante von 220 pM im subnanomolaren Bereich. HER3 exprimierende Krebszelllinien band IgG 3-43 mit EC_{50}-Werten im niederen pikomolaren Bereich (3-30 pM). Der Antikörper konkurrierte mit Heregulin um die Bindung von HER3 exprimierenden Zellen, inhibierte die Phosphorylierung von HER3 sowie von nachgeschalteten Signalmolekülen, und induzierte die Internalisierung und Degradierung des Rezeptors. Zudem inhibierte IgG 3-43 die Heregulin-abhängige Proliferation mehrerer HER3-positiven Krebszelllinien. Die Inhibierung von Tumorwachstum und ein verlängertes Überleben wurde in einem FaDu Xenograft-Modell in SCID-Mäusen nachgewiesen. Die erzielten Ergebnisse bestätigen, dass IgG 3-43 in effizienter Weise die Aktivierung von HER3 blockiert und dadurch das Wachstum von Tumorzellen sowohl *in vitro* als auch *in vivo* inhibiert.

1 Introduction

1.1 The EGFR family of receptor tyrosine kinases

Multicellular organisms depend on growth factors for their development, growth and homeostasis. They are required for cell-cell communications underlying embryonic tissue induction, fate determination, cell survival, apoptosis, tissue specialization and cell migration[1]. For the transduction of extracellular signals, growth factor receptors are needed. For its role in development, physiology, and human cancer, the epidermal growth factor (EGF) family of RTKs, also called ErbB or HER receptors, is one of the most extensively studied family amongst the receptor tyrosine kinases (RTKs)[1].

The majority of growth factor receptors are composed of extracellular, transmembrane, and cytoplasmic tyrosine kinase domains[2]. The ErbB family belongs to the type I receptor tyrosine kinases and has four members: EGF receptor, also termed ErbB1 or HER1, ErbB2/Neu/HER2, ErbB3/HER3 and ErbB4/HER4[3]. All family members share a certain general structure: they comprise a glycosylated extracellular (ligand-binding) domain, a single membrane-spanning region and a cytoplasmic domain consisting of a juxtamembrane domain, a typical protein tyrosine kinase segment, and a tyrosine-rich carboxyterminal tail[4,5]. Additional regulatory sequences in this cytoplasmic domain are subjected to autophosphorylation and phosphorylation by heterologous protein kinases[6]. The extracellular N-terminal domain contains four subdomains. The leucine-rich subdomains I (L1) and III (L2) directly interact with the ligand. The cysteine-rich subdomain II (CR1) contains the dimerization loop responsible for receptor-receptor interaction (reviewed by Wieduwilt & Moasser, 2009). Although the four glycoproteins are closely related, some important differences exist. The most intriguing one is that ErbB3 has an impaired tyrosine kinase activity[7]. Nonetheless it is noteworthy that, upon trans-phosphorylation by another ErbB family member, it leads to very potent activation of downstream signaling[8]. EGFR and ErbB4 display fully functional receptors with both, the ability to bind ligands and a functional intracellular tyrosine kinase domain[1]. ErbB2 in turn is unique in that it has no known ligand but is the preferred dimerization partner for other ErbB receptors[1,9,10]. The existing differences implicate, that each ErbB receptor has a distinct physiological role. Moreover, the physiological

characteristics of the four receptors are strongly interdependent, because their signaling can be modified by ligand-induced formation of ErbB receptor heterodimers or heterooligomers that are capable of generating unique signaling responses[11,12]. ErbB receptors are expressed in epithelial, mesenchymal, and in neuronal cells and their progenitors[5]. Although ErbB receptors are membranous proteins connecting the cells to their surroundings, nuclear localization of ErbB receptors has also been described[13].

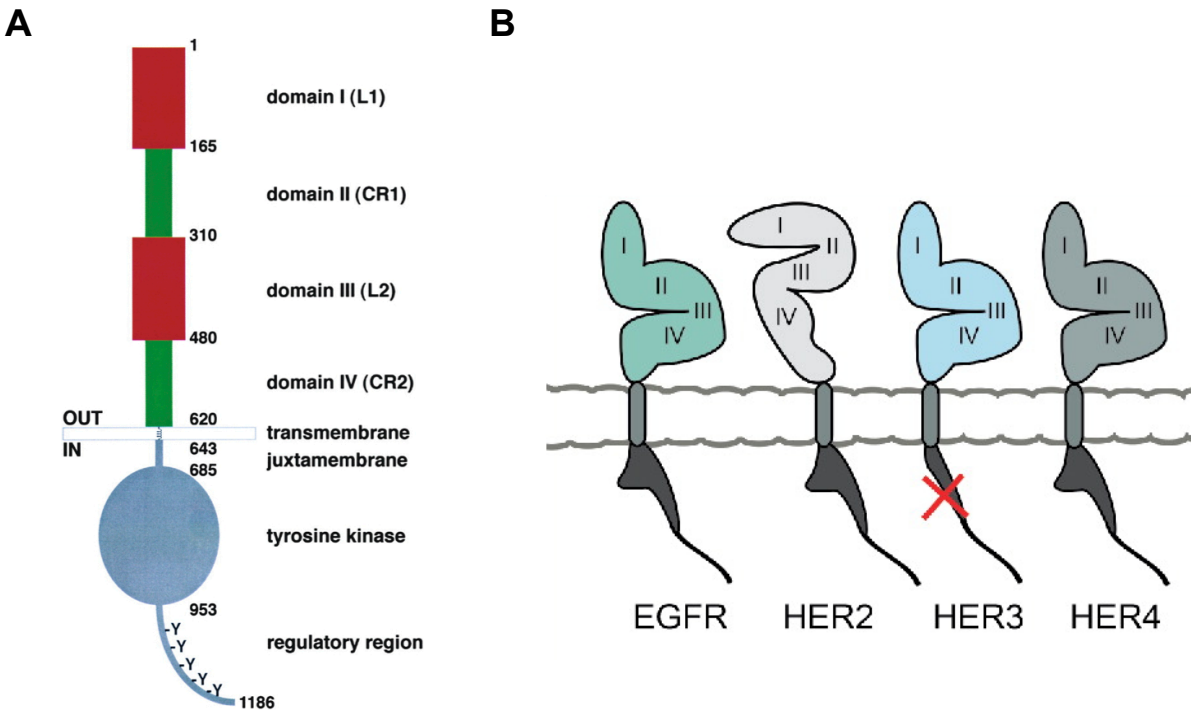

Figure 1-1: Structural commonalities and differences of ErbB receptors

A Common structure of ErbB receptors. Residue numbers for domain boundaries are depicted for EGFR. In this study, the domains are referred to using the I, II, III, IV nomenclature (Lax et al., 1988b). An alternative nomenclature using domain names L1, CR1, L2, CR2 (Ward et al., 1995) is also used in the literature. Figure from: Burgess et al. 2003[14] **B** Overview of the four ErbB receptors and their most prominent differences. The extracellular domain of ErbB2 exhibits an extended conformation, whereas ErbB3 has no active kinase domain. Figure from Malm, 2016[15].

RTKs usually exist as monomers in the cell membrane[16]. Their activities are regulated through ligand-induced hetero- or homooligomerization. Only the binding of a ligand induces dimerization of these receptors resulting in autophosphorylation of their cytoplasmic domains[17]. However, this concept induces a somewhat simplified view. A more complex view assumes that receptor monomers are in equilibrium with receptor dimers. Ligand binding to the extracellular domain stabilizes the formation of active dimers and consequently tyrosine kinase stimulation. Schlessinger also proposed in 2000, that active dimers can exist even in the absence of ligand

binding[16]. This is reasonable, since autophosphorylation of RTKs can be enhanced in the absence of binding ligands by inhibitors of protein tyrosine phosphatases as well as by receptor overexpression. The current model for ErbB receptor activation suggests, that one kinase domain in a dimer allosterically activates its neighbor and, as a consequence, becomes *trans*-autophosphorylated itself [18].

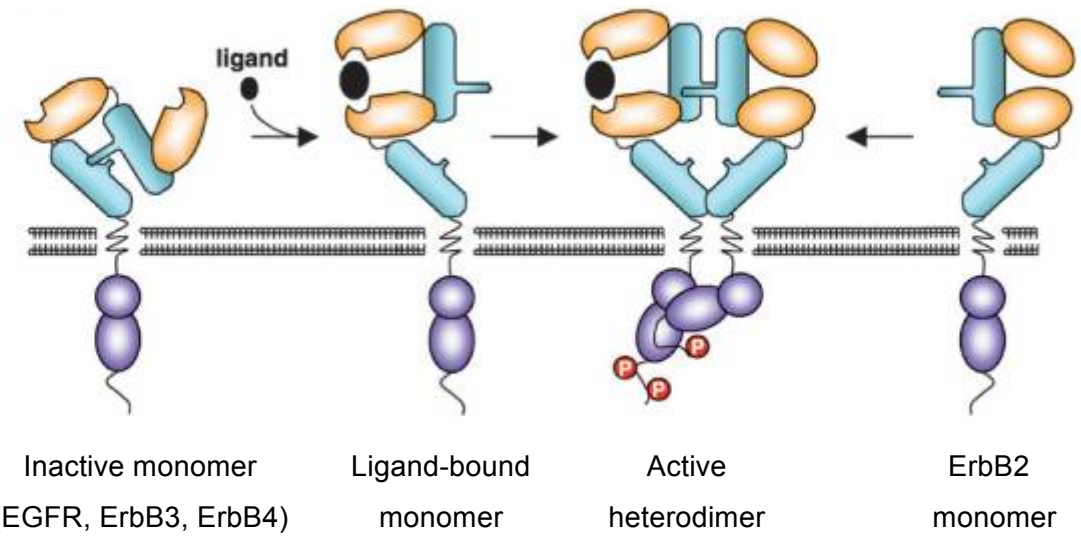

Figure 1-2: Schematic overview of the structural basis for ErbB receptor dimerization and activation

In the ligand-free state, EGFR, ErbB3, and ErbB4 have a tethered conformation stabilized by interaction between the extracellular domains II (CR1) and IV (CR2). Binding of a ligand between the extracellular domain I (L1) and III (L2) creates an extended conformation, which exposes the dimerization loop of domain II (CR1) allowing for receptor homo- and heterodimerization. Receptor dimerization apposes the tyrosine kinase N-lobe of one receptor with the C-lobe of its partner leading to C-terminal tyrosine phosphorylation, creating binding sites for adaptors, signaling molecules and regulatory proteins. ErbB2 is unique in that it is fixed in the extended conformation ready to interact with other ErbB receptors. Figure adapted from Wieduwilt and Moasser, 2008.

Crystal structures of the EGFR extracellular region revealed that in the ErbB family dimerization is entirely mediated by the receptor[19,20]. The bivalent ligand contacts two distinct sites within a single receptor molecule (on Domains I and III) promoting substantial conformational changes in the extracellular region, which unmask a dimerization arm in Domain II[14]. Before the ligand binds, this arm is completely buried by intramolecular interactions with Domain IV that stabilize a 'tethered' conformation in which both ligand binding and dimerization are autoinhibited[19]. In 2007, Dawson et al. confirmed that the tethered and extended conformations are also adopted in solution[21]. Furthermore, they monitored the transition from a tethered to extended configuration in the monomeric extracellular regions of ErbB3.

However, the crystal structure of a truncated ErbB2 ectodomain revealed that this receptor is locked in the extended conformation[22]. This is in consistency with the fact that no ligand for ErB2 could be identified and facilitates interaction with other receptors.

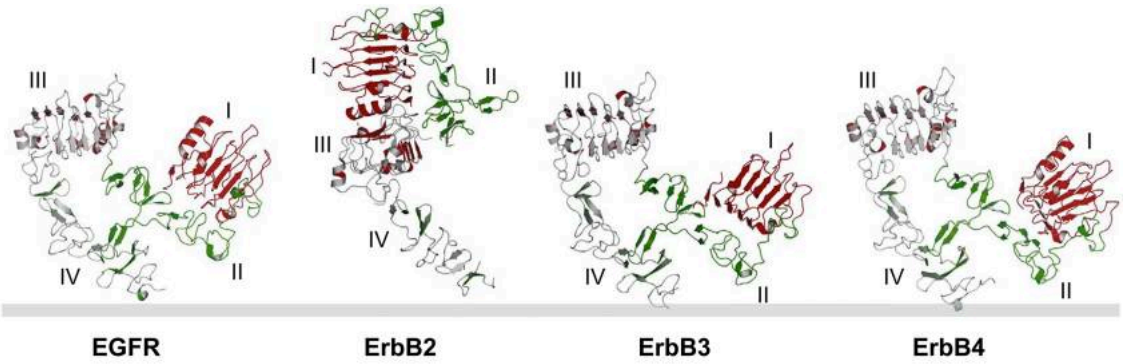

Figure 1-3: Structures of human ErbB receptor extracellular regions without bound ligand.

EGFR, ErbB3 and ErbB4 all adopt the tethered conformation in the absence of ligand, whereas ErbB2 adopts a tethered conformation. Structures are shown in ribbon representation. The sEGFR structure is from Li et al.[23], sErbB2 is from Cho et al.[24], sErbB3 from Cho and Leahy[25], and sErbB4 from Bouyain et al.[26].Figure from Lemmon 2009[27].

1.2 ErbB receptor ligands

ErbB ligands are members of the EGF-like growth factor family. They originate from cell membrane anchored proteins[28]. After proteolytical processing, they are released as soluble molecules[29,30]. Their signaling diversity is achieved by ligand specificity, redundancy, processing and variable tissue expression patterns[1]. Figure 1-4 displays ErbB receptors and their ligands.

EGFR uniquely binds EGF[31,32], transforming growth factor-α (TGF-α)[33,34], and amphiregulin[35]. ErbB3 binds neuregulin-1[36] and neuregulin-2[37-40] and uniquely binds Neuroglycan C[41]. Neuregulin-1 is also known as neu differentiation factor, heregulin, and acetylcholine receptor-inducing activity and glial growth factor[42,43]. ErbB4 is also able to bind neuregulin-1 and neuregulin-2 and uniquely binds neuregulin-3[44], neuregulin-4[45], and tomoregulin[46]. Both EGFR and ErbB4 bind heparin-binding EGF-like growth factor (HB-EGF)[47], betacellulin[48], epiregulin[49] and epigen[50] (all reviewed by Wieduwild and Moasser, 2011[1]).

Ligand-dependent differences in the patterns of ErbB receptor phosphorylation, as first shown for EGFR[51], lead to divers downstream signaling characteristics of the receptors in distinct dimers, modulated by the respective dimerization partner. Moreover, binding of different ligands to ErbB receptors also affects other

characteristic receptor properties, like different exposure times on the outer cellular membrane. For example, EGFR is internalized faster after EGF binding leading to homodimerization, than after activation through NRG binding ErbB4[51] (reviewed by Hynes et al., 2001[3]).

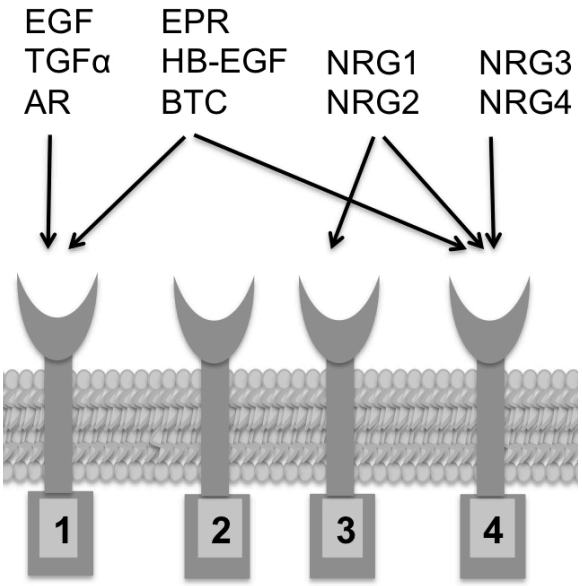

Figure 1-4: Binding specificities of the EGF-related peptide growth factors

Schematic of ErbB receptors and their respective ligands; Hynes et al. proposed a classification of ligands that bind ErbB family receptors in four categories. EGF, AR and TGFα bind ErbB1; BTC, HB-EGF and EPR bind ErbB1 and ErbB4; NRG-1 and NRG-2 bind ErbB3 and ErbB4; NRG-3 and NRG-4 bind ErbB4.

1.3 ErbB receptor downstream signaling cascades

Almost all different homo- and heterodimer combinations of ErbB receptors are possible[12]. Which pathways are activated is determined strongly by the identity of the bound ligand as well as of the dimerization partner. Different dimers have different signaling potencies. Generally, heterodimers are more potent signaling activators than homodimers[12]. Pinkas-Kramarski et al. proposed a specific hierarchy of receptor crosstalk: ErbB2/ErbB3 is the most favored heterodimer, followed by ErbB1/ErbB2 interaction. ErbB1/ErbB1 homodimers are still preferred against ErbB1/ErbB3 heterodimerization[52]. ErbB4, the most recently discovered member of the ErbB family[53,54], is not considered in this study. The hierarchy and selectivity of receptor interactions was also confirmed by others[55,56]. A mathematical model from Shankaran et al furthermore indicated that EGFR-HER2 and HER2-HER3 dimers both contribute to HER2 activation with the EGFR expression level determining the

relative importance of these species, and that the HER2-HER3 dimer is largely responsible for HER3 activation[57]. ErbB2 seems to be the preferred interaction partner[9], and ErbB3 is its major counterpart[55]. Noteworthy, the ErbB2/ErbB3 dimer is also the most mitogenic receptor pair in the ErbB family[58]. However, dimerization partner selection and thereby signal transduction also depend on expression patterns and thereby availability of the different receptors[59]. Taken together, in healthy cells the onset of signaling cascades is controlled by the (tissue-) specific ligand availability, followed by receptor expression with a certain bias towards kinetically favored dimer pairs.

The key event for the activation of ErbB receptors is the binding of a growth factor to their extracellular domain, inducing a conformational change in this domain and thereby allowing receptor dimerization and autophosphorylation of key tyrosine residues within the carboxyterminal tail of the receptors[14]. This provides specific docking sites for cytoplasmic proteins containing Src homology 2 (Sh2) and phosphotyrosine-binding (PTB) domains (reviewed in Yarden & Sliwkowski, 2001[12]). These proteins bind to the specific phosphotyrosine residues and initiate intracellular signaling via several pathways[60]. The enzymatic activity of the tyrosine kinase in the intracellular domain of the receptor is also able to phosphorylate tyrosine residues on different intracellular adaptor proteins[61].

Most of the intracellular second messengers generated when they are activated are shared by all ErbB receptors[42]. On the other hand, different ErbB dimers recruit or activate also different sets of signaling molecules[62]. For example, the p85 subunit of PI3-kinase associates particularly with ErbB3[63]. The two most important pathways induced by ErbB receptors, the MAPK and PI3K/Akt pathways, are described in more detail in the following. A third important ErbB receptor downstream signaling pathway is the phospholipase C (PLCγ) pathway[5].

1.3.1 The MAPK pathway

All ErbB family members couple via Shc and/or Grb2 to the Mitogen activated protein (MAP) kinase pathway[42]. The first step of this cascade occurs in close proximity to the growth factor receptors and involves the activation of a small GTP binding protein (Ras) via the adapter molecule (Grb2) and a guanine nucleotide exchange factor (Sos). This is followed by the sequential stimulation of several cytoplasmic protein kinases[64]. A similar pattern of sequential activation is used by many pathways[64]. However, the pathway leading to activation of extracellular regulated kinase (Erk)

isoforms via mitogen-activated, Erk-activating kinase (MEK) is the principle one in growth factor signaling[64]. In this pathway, Grb2 binds to proline-rich stretches in the Ras-guanine nucleotide exchange factor Sos via its N-terminal SH3 domain[65], enabling the activation of the membrane-associated small GTP binding protein Ras[66]. Activated Ras-GTP promotes the activation of Raf[67] by its recruitment to the plasma membrane[68]. Raf kinase then phosphorylates and activates MEK1/2, which then phosphorylates and activates ERK1/2. After their activation, ERKs in turn are able to phosphorylate various downstream substrates[64]. ERK substrates are numerous and found both in the cytoplasm and in the nucleus and include regulatory proteins as well as transcription factors. Thereby, ERKs serve as important regulators of transcriptional activity[64]. Finally, they regulate important cellular processes such as proliferation, differentiation and cell cycle progression[69].

1.3.2 The PI3K pathway

The phosphoinositide-3-kinase (PI3-kinase)-Akt-mTOR pathway can be activated by receptor tyrosine kinases as well as by G-protein coupled receptors (GPCRs). It is a central signal transduction pathway that regulates many critical physiological aspects, including cell proliferation, differentiation, apoptosis, cell morphology and migration, protein synthesis, and cell metabolism[70].

Class I PI3-kinases consist of a catalytic (p110) and a regulatory subunit (p85). Through binding of the regulatory subunit to activated RTKs or adaptors, PI3K is recruited to the plasma membrane where it catalyzes the phosphorylation of the 3' position of its preferred *in vivo* substrate, the membrane lipid phosphatidylinositol-4,5-bisphosphate (PIP2) to generate the second messenger phosphatidylinositol (3,4,5) trisphosphate (PIP3). PIP3 recruits cytosolic proteins with PIP3-binding pleckstrin homology (PH) domains and thereby localizes them to the plasma membrane. The Serine/Threonine kinase protein kinase B (Akt) appears to be the most notable of the recruited proteins and a major effector of PI3K signaling[71]. The phosphoinositide-dependent kinase Pdk1, also recruited by PIP3, phosphorylates threonine 308 of Akt[70]. The mTOR-containing TORC2 complex mediates Akt phosphorylation on serine 473 that is required for full Akt activation. Akt then phosphorylates several substrates. One of its key downstream targets is the mTOR protein kinase complex. mTOR, the mechanistic target of rapamycin, exists in 2 distinct multiprotein complexes: mTORC1 and mTORC2. Akt phosphorylates tuberous sclerosis complex 2 (TSC2) and PRAS40, which leads to increased

mTORC1 kinase activity. mTORC1 regulates protein synthesis and cellular metabolism via two major substrates: p70 ribosomal protein S6-kinase (p70S6K) and eukaryotic initiation factor 4E binding protein 1 (4EBP1). Akt also catalyzes the inhibiting phosphorylation of BAD[5] which is pro-apoptotic in its unphosphorylated state[72].

The extent and duration of the PI3K/Akt/mTOR pathway is primarily regulated by the tumor suppressor phosphatase and tensin homolog (PTEN), which catalyzes the dephosphorylation of PIP3 back to PI(4,5)P2 (the PI3-kinase pathway is reviewed by Lauring et al.[70], Brown and Toker[73] and by Klempner et al.[74]).

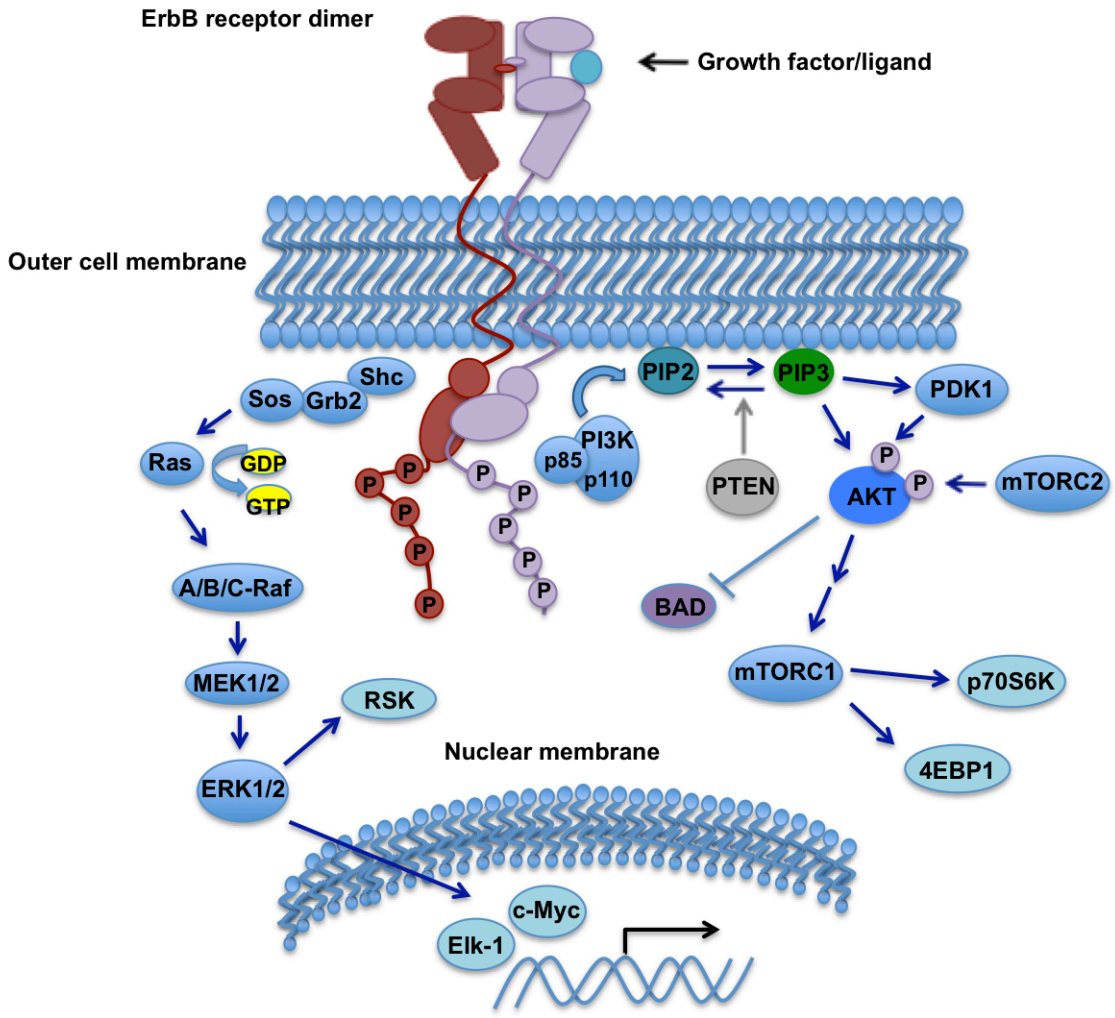

Figure 1-5: ErbB receptor downstream signaling cascades

Simplified illustration of the two major pathways triggered upon ErbB activation. After ligand binding, the extracellular domains of EGFR, ErbB3 or ErbB4 are stabilized in an extended conformation, exposing their dimerization interface and favoring dimerization with for example ErbB2. Autophosphorylation of tyrosine residues in the carboxyterminal tail then provides docking sites for cytoplasmic proteins, leading to the activation of other protein kinases. The key players in the described pathways, Erk and Akt, have multiple targets. They control important cellular processes such as gene expression, proliferation, angiogenesis, protein synthesis, survival, cell cycle control, and apoptosis suppression.

1.4 Alterations of ErbB signaling cascades and their implication in cancer

In 2000, Hanahan and Weinberg proposed six essential alterations in cell physiology that essentially all cancer cells have in common[75]. An update by the same authors in 2011 adjusted the number of typical alterations to ten[76]. According to these reviews, the first "hallmark of cancer" is self-sufficiency in growth signals. It was the first capability of cancer cells clearly described by researchers. Controlling such important cellular processes like proliferation and cell cycle control, it is not surprising that many alterations of growth signaling pathways are found in multiple cancer types. The distinct other five capabilities of cancer cells were specified as "insensitivity to anti-growth signals", "tissue invasion and metastasis", "limited replicative potential", "sustained angiogenesis" and the capability to evade apoptosis. Today, it is clear that ErbB signaling can be involved in most of these hallmarks.

ErbB members have a pivotal role in mammalian development and tissue maintanance[1]. To protect the cells from uncontrolled mitogenic signaling, the pathways are tightly regulated[6]. Besides control through phosphatases and other protein kinases, multiple autoregulatory mechanisms exist[6]. However, aberrant signaling through the ErbB receptors is implicated in many human diseases[1]. Several malignancies are associated with the mutation or increased expression of members of the ErbB family including lung, breast, stomach, colorectal, head and neck, and pancreatic carcinomas and glioblastoma[5].

Since the discovery of EGF in 1962[31], huge progress was made unraveling the role of growth signaling related oncogenes and their role in cancer evolution, homeostasis, progression and treatment resistance. For example, ErbB2 has been identified on the basis of its amplification in a human mammary carcinoma in 1985[77]. Although induced ErbB homodimer formation is unlikely, unphysiological overexpression of ErbB2 leads to the formation of a functional homodimer[78]. *ERBB2* gene amplification occurs in 20-30% of human breast cancers[5] and is associated with adverse outcome[79]. Since breast cancer is the leading cause of female cancer deaths worldwide, this is of great importance and dealing with ErbB driven cellular aberrations is a big challenge of our time. Overexpression is not only common for HER2, but also for EGFR, that is overexpressed in about 40% of glioblastoma multiforme (GBM) and 5-10% of NSCLC, based on gene amplification[80-82].

Besides overexpression of wildtype ErbB receptors, activating mutations are also frequently observed. For example, EGFRvIII, where exons 2-7 are deleted, occurs in lung, breast, ovarian and prostate cancers and GBM[83-85], and activating EGFR tyrosine kinase domain mutations have been observed in 10-20% of NSCLCs[1]. ErbB receptor ligands also are frequently expressed in human carcinomas and play an important role in the pathogenesis of these diseases[61].

1.5 Rising significance of ErbB3

ErbB3 possesses only 1/1000th of the autophosphorylation activity of ErbB1[86]. Due to this impaired kinase activity ErbB3 is active only after transphosphorylation and ErbB3 homodimers are non-functional. Moreover, cancers with driving HER3 amplifications or mutations have not been found at first[87]. These facts led to the long accepted assumption, that the receptor is not crucial in the context of cancer[15,87]. Therefore, unlike its family members EGFR and HER2, that are well-established targets in many different human cancers, the role of HER3 in tumor signaling was elucidated relatively recently[15]. In 2013, Jaiswal et al identified somatic *ERBB3* mutations with transforming potential in ~11% of colon and gastric cancers[88]. Admittedly, this oncogenic activity was dependent on kinase-active HER2. The group also found that anti-ErbB antibodies and small molecule inhibitors could block mutant *ERBB3*-mediated oncogenic signaling and disease progression[88].

Due to the highly interdependent functions of HER proteins, frequently more than one of them are implicated in cancer pathogenesis, and HER3 has been identified as an obligate partner in HER family oncogenesis. Nowadays, its role as an obligate partner is well established in some breast cancers and increasingly suspected in several other cancers[87]. Particularly, it is clear that HER3 plays a critical role in HER2-mediated transformation[89,90] and its expression correlates with proliferation, advanced disease stage and poor prognosis of melanoma[91,92], where it probably activates EGFR and HER4[93]. There is also evidence, that HER3 is implicated in prostate[94], colorectal[95], lung[96] and ovarian[97,98] cancer, glioma[99] and astrocytoma[100]. Moreover, the analysis of drug resistance in several HER family driven cancers highlights a central role for HER3 in mediating treatment failure[87]. In all, it became clear that effective treatment of some cancer types also requires HER3 targeting.

1.6 Monoclonal antibodies as therapeutic agents

ErbB receptors, whose mechanism of action depends on the interaction of their extracellular domains with activating ligands and with the ECDs of their dimerization partners, are accessible to monoclonal antibodies that can disrupt their function if appropriately designed. The first monoclonal antibody (mAb) to enter clinical use for cancer treatment purposes was the ErbB2-targeting trastuzumab (Herceptin®), developed by Genentech (San Francisco, CA, USA) [101]. This humanized version of the murine anti-ErbB2 antibody 4D5 supports ADCC and induces downregulation of ErbB2[102]. Clinical trials have demonstrated, that trastuzumab is active in patients with high levels of ErbB-2 expression[103-105]. Pertuzumab (Perjeta®), another humanized monoclonal antibody, binds to the dimerization arm of HER2, near the center of domain II, which is distinct from the binding site of trastuzumab[106]. The first clinically approved anti-EGFR monoclonal antibody was cetuximab (Erbitux®). This chimeric antibody was developed by chimerization with human IgG1 constant region of the murine 225 antibody[107]. Panitumumab (Vectibix®), a fully human monoclonal antibody also binding the extracellular domain of EGFR and showing activity against colorectal cancer[108], is approved for clinical use too.

Today, many HER3 targeting antibodies are in clinical development. The HER3-targeting agent that has advanced furthest in clinical development is patritumab (U3-1287; U3-pharma GmbH, Amgen, Daiichi-Sankyo), a fully human monoclonal antibody[109]. The HER3-specific seribantumab (MM-121) developed by Merrimack Pharmaceuticals was generated from a phage-displayed antigen-binding fragment (Fab) library. The isolated binder was converted to a full-length human IgG2 format[110] that has been shown to have an anti-proliferative effect in *in vivo* studies with several xenografts[111]. AVEO Oncology's humanized IgG1 AV-203 was shown to block ligand-binding to the receptor and induce HER3 degradation[112]. Kolltan Pharmaceuticals and Medimmune developed KTN3379 by phage display that locks HER3 in an inactive conformation, enabling inhibition of both ligand-dependent and independent signaling[113].

Table 1-1: HER3 targeting monoclonal antibodies. Table adapted from Malm 2016[15].

mAb	Format	Company	Most advanced clinical phase	origin	affinity to human HER3	epitope
Patritumab (U3-1287)[109,114]	Human IgG1	U3-Pharma, Amgen, Daiichi Sankyo	3	XenoMouse® technology	1-3 nM	HER3-ECD
Seribantumab (MM-121)[110,111]	Human IgG2	Merrimack Pharmaceuticals, Sanofi Avantis	2	phage-displayed antigen-binding fragment (Fab) library	0.8 nM	domain I
Elgemtumab (LJM716)[115]	Human IgG1	Novartis Pharmaceuticals, Ariad, Morphosys	1/2	MorphoSys phage-displayed HuCal Fab library	32 pM	interface between domain II and IV
Lumretuzumab (RG7116)[116,117]	Humanized IgG1	Roche, Glycart	1	NMRI mice immunized with recombinant HER3 ECD	0.5 nM	domain I
AV-203[112]	Humanized IgG1	AVEO Oncology, Biogen	1			unknown
KTN3379[113,118]	Human IgG1	Koltan Pharmaceuticals, Medimmune	1	phage-library screen, followed by affinity maturation	166 pM (monovalent)	border between domain 2 and 3
GSK2849330	Humanized IgG1	Glaxo group	1			domain III
TK-A3, TK-A4[119,120]	Humanized IgG	Takis	Preclinical		7.2 nM, 2.2 nM	domain II, conformational
EV20 (MP-RM-1)[121,122]	Humanized IgG	MediaPharma	Preclinical			unknown
Millegen patent anti-HER3[123]	Human IgG	MilleGen Ab Pharma, INSERM	Preclinical			
Sea Lane patent anti-HER3 (SL175 & SL176)[124]	Surrobody	Sea Lane Biotechnologies	Preclinical			
Ablynx patent anti-HER3	Nanobody	Ablynx, Merck Serono	Preclinical			

SGP1	Mouse IgG	University of Kent	Preclinical			unknown
Merck Co patent anti-HER3	NR	Merck & Co	Preclinical			
Immunogen patent anti-HER3	Human-ized IgG	Immuno-Gen	Preclinical			
Symphogen patent anti-HER3	Mouse IgG	Sympho-gen A/S	Preclinical			
KHK patent anti-HER3	Mouse IgG	Kyowa Hakko Kirin Co	Preclinical			
Trellis patent anti-HER3	NR	Trellis Bioscience	Preclinical			
UAB patent anti-HER3	NR	UAB Research Foundation	Preclinical			
Genentech patent anti-HER3	NR	Genentech	Preclinical			
Sorrento patent anti-HER3	NR	Sorrento Thera-peutics	Preclinical			
University of Texas patent anti-HER3	NR	University of Texas	Preclinical			
Roche patent anti-Her3	NR	Roche	Preclinical			
Beijing inst. of basic med. sci anti-HER3	NR	Beijing Institute of basic medical sciences	Preclinical			

In recent years, bispecific antibodies have also become attractive for tumor-targeting purposes. The reason emphasizing the use of this strategy is a potentially enhanced functionality[15]. Different bispecific approaches have been generated to facilitate two-

in-one receptor targeting for improved therapeutic efficiency[125]. For many of them, one specificity is directed against HER3 in order to avoid the development of acquired resistance against single-targeting agents[125-127]. Another clinically validated cancer-targeting strategy of bispecific antibody molecules is the simultaneous binding and engagement of an immune effector cell and a tumor cell to induce cytotoxic activity[128-130].

1.7 Small molecule inhibitors

As the tyrosine kinase function of ErbB members is essential for intracellular signaling and cell transformation, inhibition of this enzymatic function also provides a rational basis for a class of targeted therapies, namely tyrosine kinase inhibitors (TKI)[1]. These compounds competitively bind within the ATP binding region of the kinase domain of ErbB receptors. Therefore, the use of TKIs is an important strategy for the treatment of cancers involving mutated ErbB members with a constitutively activated kinase domain. Well known examples for this class of compounds are the EGFR specific tyrosine kinase inhibitor ZD1839, today known as gefitinib (Iressa®), which was developed around the last turn of the millennium, Erlotinib (Tarceva®) and Lapatinib (Tykerb®), with gefitinib and erlotinib most active against EGFR and lapatinib equally active against EGFR and HER2[131,132]. The TKIs gefitinib and erlotinib are highly active in the treatment of NSCLCs enharbouring activating mutations in the tyrosine kinase domain of EGFR[133] and lapatinib is approved for the use in combination with certain chemotherapies for treatment of breast cancers with HER2 overexpression[134].

However, the impaired kinase activity of HER3 makes it a rather unsuitable target for small molecule inhibitors and appears pointless as therapeutic strategy. Although oncogenic HER3 mutations have been found in a subset of colon and gastric cancers, these mutant receptors still required the activity of HER2 for cell transformation[88].

1.8 Problems and difficulties of targeted therapies

Besides the high costs of targeted therapies, the main problems faced today with targeted therapies are the lack of effectiveness and (intrinsic or acquired) resistance. Although agents directed against the ErbB receptors have shown promising clinical activity, the overall rate of response in cancer patients is generally low[61]. In fact,

clinical responses have been observed in a small percentage of patients as compared with the frequency of expression of the target receptors[61].

Many reasons for resistance mechanisms against ErbB receptor targeting drugs lay in the complexity of the ErbB network. Aberrant signaling due to mutations of receptors and/or downstream effectors, aberrant receptor localization and trafficking or overexpression of ErbB specific ligands can demolish the action of the sophisticatedly designed drugs (as reviewed for cetuximab by Brand et al., 2011[135]). Wheeler et al reported an oncogenic shift in cetuximab-resistant cells through increased activation of different RTKs like HER2, HER3 and cMET and increased heterodimerization[136]. Cordo Russo et al identified nuclear ErbB2 as the major proliferation driver in trastuzumab-resistant breast cancer cells[137]. Another challenge, also effecting targeted cancer therapy, is the heterogeneity of the different tumor cells. Epithelial to mesenchymal transition (EMT) may play a role in resistance to cetuximab[138]. Furthermore, some treatment-resistant cancer cells re-activate pro-angiogenic factors via alternate pathways, for example through increased VEGF production[139]. Prediction of response to targeted therapy is difficult in many cases. For example, early clinical studies did not confirm a correlation between EGFR expression level by immunohistochemistry (IHC) and clinical response to EGFR inhibiting therapy[140]. However, De Roock et al found that KRAS mutation status strongly predicted the effectiveness of cetuximab for irinotecan-refractory metastatic colorectal cancer with a significant increase in overall survival in patients with wild-type KRAS[141].

Regarding side effects, small molecule inhibitors and monoclonal antibodies are specific agents that mostly target tumor cells thereby minimizing unwanted adverse effects, although they also show low side effects on normal cells[142]. For HER2 antagonists like trastuzumab, cardiotoxicity can occur as adverse effect, since these receptors are expressed in the heart, where they play an important role for maintaining physiologic functions[5,143]. Early safety data of some of HER3 targeting antibodies indicate that they are well tolerated, without reported severe adverse effects[109,117]. However, the relatively low expression level of HER3 on tumor cells, along with the expression of this receptor in normal tissues such as liver, lung, small intestine, stomach and salivary gland, may render it a challenging tumor antigen[15]. Several strategies are pursued to strengthen the efficacy of ErbB targeted therapy.

One way to optimize the efficacy of these therapies used in the clinic is to administer these agents in combination with conventional chemotherapy[61]. Furthermore, predictive biomarkers are needed to estimate the potential use of a respective drug. As coexpression of different ErbB receptors can lead to increased drug resistance[144], simultaneous blockade of different signal transduction pathways might result in a more significant anti-tumor effect as compared with monotherapy only blocking a single pathway. Indeed, several reports support this hypothesis[61].

1.9 Aim of the study

Targeting of ErbB family members is of great potential in anti-tumor therapy. Different antibodies vary in multiple aspects. Different isotypes, mutations or other modifications in the constant parts may lead to diverse pharmacokinetics and effector functions. Importantly, the large differences concerning the variable domains do, through specific epitopes and intrinsic capacities such as binding strength and steric issues, affect the mode of action of different antibodies. Regarding the numerous challenges of cancer treatment today, there is a need of multiple different drugs to enrich treatment options. Furthermore, the analysis of different cancer cell targeting antibodies, their intrinsic features and the effects mediated by them implies the potential of better understanding both, the biology of cancer cells and the targeted structures, i.e. receptors, as well as general correlations between specific antibody properties and their clinical benefits.

In this study, multiple antibody binding sites were expressed in the scFv format. A screen of these proteins was performed to extract the clones with good cell binding properties. The chosen clones were used for the construction of potentially therapeutically molecules, i.e. fully human IgG1 antibodies. Analysis of these molecules eventually evidenced their biochemical and functional properties and effects on tumor cells *in vitro*. Importantly, a xenograft model in SCID mice was performed to demonstrate the anti-tumor activity of the novel HER3 targeting antibody *in vivo*.

2 Material and Methods

2.1 Material

2.1.1 Instruments and devices

Balances	440-39N, 440-333N and ALJ 120-4
	(Kern, Balingen, Germany)
Blotter	TransBlot SD, Semidry transfer cell
	(Bio-Rad, Munich, Germany)
Centrifuges	Eppendorf 5415C, 5810R
	(Eppendorf, Hamburg, Germany)
	J2-MC with rotors JA10, JA14, JA20, JA30.5
	(Beckman Coulter, Krefled, Germany)
	Avanti J-30I (Beckman Coulter, Krefeld, Germany)
	Avanti® J-26XP with rotor JLA-8.1000
	(Beckman Coulter, Krefeld, Germany)
CO_2 incubator (eukaryotic cell culture)	Varocell 140 (varolab GmbH, Giesen, Germany)
Electrophoresis systems	Ready Agarose Precast Gel System
	(BioRad, Munich, Germany)
	Mini-PROTEAN 3 Electrophoresis Cell System
	(BioRad, Munich, Germany)
	XCell SureLock® Midi-Cell
	(Thermo Fisher, Waltham, USA)
Film developing machine	Film Processor Curix 60
	(Agfa, Düsseldorf, Germany)
Flow cytometer(s)	MACSQuant® Analyzer 10, MACSQuant® VYB
	(Miltenyi Biotec, Bergisch Gladbach, Germany)
	Cytomics FC 500
	(Beckman Coulter, Krefeld, Germany)
Fluorescence microscope	Axio observer SD
	(Carl Zeiss AG, Oberkochen, Germany)
Gel documentation	Transilluminator, Gel documentation system Felix
	(Biostep, Jahnsdorf, Germany)
Heat block	HBT-1-131
	(HLC BioTech, Bovenden, Germany)

HPLC	Waters 2695 Separation Module, Waters 2489 UV/Visible detector (Waters Cooperation, Milford, USA)
Imager (immunoblots)	FUSION SOLO S (Vilber Lourmat Deutschland GmbH, Eberhardzell, Germany)
Incubator (suspension cells)	Infors HT Multitron Cell (Infors GmbH, Einsbach, Germany)
Incubator for bacteria	Infors HT Multitron (Infors AG, Bottmingen, Switzerland)
Laminar flow cabinet	Variolab Mobilien W90 (Waldner-Laboreinrichtungen, Wangen, Germany)
Magnetic stirrer	MR 3001K 800W (Heidolph Instruments, Nürnberg, Germany
Microplate reader	Tecan infinte M200 (Tecan Austria, Grödig, Austria)
Microscopes	Observation/counting: CKX31 and CK2 (Olympus, Hamburg, Germany);
PCR cycler	RoboCycler 96 (Stratagene, La Jolla, USA) Eppendorf Mastercycler (Eppendorf, Hamburg, Germany)
Quartz crystal microbalance	Attana Cell A200 with C-fast system (Attana AB, Stockholm, Sweden)
Spectrophotometer	NanoDrop Spectrophotmeter ND-1000 (PEQLAB, Erlangen, Germany)
Vortexer	Sky Line (Elmi Ltd., Riga, Latvia)
Western blotting system	iBlot® 2 Dry Blotting System (Thermo Fisher, Waltham, USA)
Zetasizer	ZetaSizer Nano ZS (Malvern Instruments, Herrenberg, Germany)

2.1.2 Consumables and Implements

Laboraty plastics were purchased from Greiner Bio-One (Frickenhausen, Germany). Consumables purchased from different sources are further specified.

Attana sensor chips	Low nonspecific binding-carboxyl chips (Attana AB, Stockholm, Sweden)
Bottle top filter	CA Low Protein binding, 500 ml, 0.2 µm/0.45 µm (Corning Incorporated, Tewksbury, MA, USA)

Centrifuge tubes	13 ml, PP (Sarstedt, Nümbrecht, Germany)
Chromatography columns	Poly-Prep® columns (Bio-Rad, Munich, Germany)
Cell counting chamber	Neubauer 0.0025 mm² (Marienfeld, Lauda-Königshofen, Germany)
Dialysis membrane	23 mm (cut-off 12.4 kDa) (Sigma-Aldrich, St. Louis, Germany)
Dialysis membranes	High retention seamless cellulose tubing, 23 mm, MWCO 12,400 (Sigma-Aldrich, St. Louis, MO, USA); ZelluTrans, MWCO 6,000-8,000, 40 mm; ZelluTrans, MWCO 3,500, 46 mm (Carl Roth, Karlsruhe, Germany)
ELISA plates	Microlon high binding ELISA plate (Greiner Bio-One, Frickenhausen, Germany)
Gradient gels for SDS Page	NuPAGE™ Novex™ 4-12 % Bis-Tris Midi Gels (Thermo Fisher, Waltham, MA, USA)
HPLC columns	Yarra™ 3 µm SEC-2000, Yarra™ 3 µm SEC-3000 (Phenomenex, Torrance, CA, USA); Waters 2695 HPLC (Waters Corporation, Milford, USA)
IMAC affinity beads	Protino Ni-NTA agarose (Macherey-Nagel, Düren, Germany)
Microscopy slides	Chamber slides™
Nitrocellulose membrane (for semidry blotting of purified proteins)	BioTrace™ NT Nitrocellulose Transfer Membrane (Pall Life Sciences, East Hills, USA)
Photo films	BioMax® MR film (Kodak, Stuttgart, Germany)
Protein A beads	TOYOPEARL® AF-rProtein A HC-650F (Tosoh Bioscience, Stuttgart, Germany)
Quartz cuvette	12mm square glass cell for 90 sizing (PCS8501) (Malvern Instruments, Herrenberg, Germany)
Reaction tubes	1.5 ml, 2 ml Safe-Lock (Eppendorf AG, Hamburg, Germany
Syringe filter	Acrodisc® 13 mm, 0.2 µm, HT Tuffryn® Membrane (Pall Corporation, Port Washington, NY, USA)
Triple flask	500 cm, Nunclon™ Delta Surface (Thermo Fisher Scientific, Waltham, MA, USA)
Ultrafiltration spin columns	Vivaspin 500, 30,000 MWCO PES (Sartorius, Göttingen, Germany)
Western blotting membrane stacks	iBlot® NC Regular Stacks

	(Thermo Fisher, Waltham, USA)
Whatman filter paper	Whatman® chromatography paper 3mm (A. Hartenstein Laborbedarf, Würzburg, Germany)

2.1.3 Chemicals

Chemicals were purchased from Carl Roth (Karlsruhe, Germany), Merck (Darmstadt, Germany), Sigma-Aldrich (St. Louis, MO, USA), and Roche (Basel, Switzerland). Chemicals purchased elsewhere are explicitly stated.

Bond-Breaker® TCEP	0.5 M (Thermo Scientific, Rockford, USA)
Coomassie Brilliant Blue G250	SERVA Electrophoresis, Heidelberg, Germany
Propidium Iodide	

2.1.4 Cell culture media and supplements

Ampicillin	100 mg/ml in H2O (Roth, Karlsruhe, Germany)
Choleratoxin (CTX)	Sigma Aldrich, St. Louis, MO, USA
Collagen	PureCol®-S (Advanced Biomatrix, San Diego, CA, USA)
DMEM	+ 4,5 g/L D-Glucose, + L-Glutamine (Thermo Fisher, Waltham, USA)
Doxycycline	Merck, Darmstadt, Germany
DPBS (1x)	GIBCO® Dulbecco's phosphate-buffered saline (Thermo Fisher Scientific, Waltham, MA, USA)
Eosin solution	0.4 % (m/v) eosin G, 0.02 % (w/v) NaN3 in sterile 1x PBS, pH 7.4
Fetal calf serum	HyClone® research grade fetal bovine serum (Thermo Fisher, Waltham, USA) FBS Premium (PAN Biotech, Aidenbach, Germany (PAA Laboratories, Cölbe, Germany)
Freestyle F17-medium	Supplemented with 4mM GlutaMAX-I, 0.1% Kolliphor P188
Freezing medium for eukaryotic cells	10% (v/v) DMSO in FCS
IPTG	1 M isopropyl β-D-1-thiogalactopyranoside as 1000 x stock
LB $_{Amp, Glc}$ agar plates	LB-medium, 2.0 % (w/v) agar, after autoclaving adding of ampicillin to 100 µg/ml and 1 % (w/v) glucose
LB-medium	1 % (w/v) peptone, 0.5 % (w/v) yeast extract, 0.5 % (w/v) NaCl
Liofectamine	Lipofectamine™ 2000 (Thermo Fisher, Waltham, USA)
Matrigel	growth factor reduced matrigel (BD, Franklin Lakes, NJ, USA))

Opti-MEM®	(Invitrogen, Karlsruhe, Germany)
Penicillin/streptomycin	10,000 U/ml / 10,000 µg/ml (100x) GIBCO® (Thermo Fisher, Waltham, USA)
Polyethylenimine (PEI)	(Polisciences, Inc., Hirschberg an der Bergstrasse, Germany)
Puromycin	(Sigma-Aldrich, St. Louis, MO, USA)
RPMI 1640	+ 2 mM glutamine GIBCO® (Thermo Fisher, Waltham, USA)
Trypsin/EDTA	0.5 % (w/v) trypsin, 5.3 mM EDTA (10x) (Thermo Fisher, Waltham, USA)
Trypton N1	(Organo Technie, La Courneuve, France)
TY	1.6 % (w/v) pepton, 1 % (w/v) yeast extract, 0.5 % (w/v) NaCl in H_2O
Zeocin™	100 mg/ml in H2O (Thermo Fisher, Waltham, USA)

2.1.5 Buffers and solutions

Bradford reagent	(5x) Bio-Rad protein assay (Bio-Rad, Munich, Germany)
Competent cell solution 1	0.1 M CaCl2 in 1x PBS
Competent cell solution 2	20 % (v/v) glycerol, 50 mM CaCl2 in 1x PBS
Coomassie staining solution	0.008 % (w/v) Coomassie Brilliant Blue G-250 (SERVA Electrophoresis, Heidelberg, Germany), 35 mM HCl
DNA loading dye (6 x)	10 mM Tris-Hcl pH 7.6, 0.03 % (w/v) xylene cyanol FF, 0.03 % (w/v) bromophenol blue, 60 mM EDTA, 60 % (v/v) glycerol (Thermo Fisher Scientific, Waltham, MA, USA)
ELISA blocking buffer/MPBS	2 % (w/v) non-fat dry milk powder in 1x PBS
ELISA developing substrate solution	100 mM sodium acetate pH 6.0, 0.1 mg/ml TMB, 0.006 % (v/v) H2O2
ELISA stopping solution	1 M H2SO4
ELISA washing buffer/PBST	0.005 % (v/v) TWEEN 20 in 1x PBS
IMAC elution buffer	250 mM imidazole in 1x sodium phosphate buffer
IMAC wash buffer	20 mM imidazole in 1x sodium phosphate buffer
Laemmli sample buffer (5 x)	Non-reducing: 10 % (w/v) SDS, 25 % (v/v) glycerin, 0.05 % (w/v) bromphenol blue in 312.5 mM Tris-Hcl pH 6.8; Reducing: non-reducing buffer, 25 % (v/v) β-mercaptoethanol
PBA	2 % (v/v) FBS, 0.02 % (w/v) NaN3 in 1x PBS
Periplasmic preparation buffer	30 mM Tris-Hcl pH 8.0, 20 % (w/v) sucrose, 1 mM EDTA
Phosphate-buffered saline	80.6 mM Na2HPO4, 14.7 mM KH2PO4, 1.37 M NaCl,

(PBS, 10x)	26.7 mM Kcl; used as 1x PBS pH 7.5
Protease inhibitors	complete protease inhibitors (Roche, Basel, Switzerland)
Protein A elution buffer	100 mM glycine-Hcl pH 3.0
Protein A neutralization buffer	1 M Tris-Hcl, pH 8.0
RIPA buffer	50 mM Tris pH 7.5, 150 mM NaCl, 10 mM NaF, 20 mM β-Glycerophosphate, 1 mM EDTA, 1 % NP-40, 1 mM Na3VO4, 0.5 mM PMSF, 0.25 % DOC, 0.1 % SDS in H2O
SDS running buffer (10 x)	1.92 M glycine, 0.25 M Tris, 1 % SDS, pH 6.8; NuPAGE® MES Running Buffer (Thermo Fisher, Waltham, MA, USA); NuPAGE® Antioxidant (Thermo Fisher, Waltham, MA, USA)
Sodium phosphate buffer (5x, 250 mM)	210 mM Na2HPO4, 40 mM NaH2PO4, 1.25 M NaCl, pH 7.5
TAE (50x)	2 M Tris, 1 M glacial acetic acid, 50 mM EDTA, pH 8.0
Western Blot – blotting buffer	20 % (v/v) methanol, 192 mM glycine, 25 mM Tris, pH 8.3
Western blot washing solution	0.05 % (v/v) Tween 20 in 1x PBS
Blocking reagent	Roche, Basel, Switzerland
Protein A wash buffer	100 mM Tris-Hcl pH 7.5
Western blot solution A	0.1 M Tris, 0.25 mg/ml luminol, pH 8.6
Western blot solution B	0.11 % (w/v) p-coumaric acid in DMSO

2.1.6 Detection antibodies

Table 2-1: Antibodies used for ELISA, FACS analysis, immunoblotting and microscopy.

Antibody	Source	Application
Anti-Akt (pan)	Mouse; #2920, Cell Signaling (Danvers, MA, USA)	WB (1:2000)
Anti-EGFR	Rabbit polyclonal IgG (Santa Cruz Biotechnology, Santa Cruz, USA, #sc-03-G)	WB (1:500)
Anti-Erk1/2	Mouse; #9107, Cell Signaling (Danvers, MA, USA)	WB (1:2000)
Anti-HER2	Mouse mAb (Thermo Fisher, Waltham, USA)	WB (1:1000)
Anti-HER3	#MA5-12675; Thermo Fischer Scientific (Waltham, MA, USA)	WB (1:1000)
Anti-His_6-FITC	Mouse monoclonal IgG1 (dianova, Hamburg, Germany)	FACS (1:200)

Anti-His_6-PE	Mouse IgG1; Miltenyi Biotec;	FACS (1:200)
Anti-human EGFR	AY13; BioLegend (San Diego, CA, USA)	FACS (expression analysis; 1:10)
Anti-human erbB2/HER-2	Clone 24D2; BioLegend (San Diego, CA, USA)	FACS (expression analysis; 1:10)
Anti-human erbB3/HER-3	Clone1B4C3; BioLegend (San Diego, CA, USA)	FACS (expression analysis, 1:10)
Anti-human IgG (F_{ab}-specific)-HRP	Sigma-Aldrich (St. Louis, MO, USA)	WB (1:20000)
Anti-human IgG (Fc specific)-HRP	Polyclonal; Sigma-Aldrich (St. Louis, MO, USA)	ELISA/WB (1:5000)
Anti-human IgG (whole molecule)-HRP	Polyclonal; Sigma-Aldrich (St. Louis, MO, USA)	ELISA/WB (1:20000)
Anti-human IgG (γ-chain specific)-R-PE	Sigma-Aldrich (St. Louis, MO, USA)	FACS (1:500)
Anti-mouse IgG (Fc specific)-HRP	Polyclonal; Sigma-Aldrich (St. Louis, MO, USA)	WB (1:4000)
Anti-phospho-Akt (Thr308)	Mouse; Cell Signaling (Danvers, MA, USA)	WB (1:1000)
Anti-phospho-Akt (Thr308) XP®	Rabbit; #13038, Cell Signaling (Danvers, MA, USA)	WB (1:1000)
Anti-phospho-EGFR (Tyr 1068) XP®	Rabbit mAb #3777, Cell Signaling Technology® (Danvers, MA, USA)	WB (1:1000)
Anti-phospho-Erk1/2 (Thr202/Tyr204)	Rabbit polyclonal; #9101. Cell Signaling (Danvers, MA, USA)	WB (1:1000)
Anti-phospho-HER2 (Tyr1221/1222)	Rabbit mAb, #2243, Cell Signaling Technology® (Danvers, MA, USA)	WB (1:1000)
Anti-phospho-HER3 (Tyr1289)	Rabbit; #4791, Cell Signaling (Danvers, MA, USA)	WB (1:1000)
Anti-rabbit-IgG-Peroxidase	Goat polyclonal; Sigma-Aldrich (St. Louis, MO, USA)	WB (1:5000)
Anti-αTubulin	Mouse; #T6793, Sigma-Aldrich (St. Louis, MO, USA)	WB (1:2000)
His-probe (H3) HRP	Mouse monoclonal; Santa Cruz Biotechnology (Dallas, TX, USA)	ELISA/WB (1:1000)
Purified Mouse IgG1 κ Isotype Control	554121. BD Biosciences	FACS (expression analysis, 1:10)

Purified Mouse IgG2a, κ Isotype Control	Clone MOPC-173, Cat. # 400202 BioLegend (San Diego, CA, USA)	FACS (expression analysis, 1:10)
Purified Mouse IgG2b κ Isotype Control	555740. BD Biosciences	FACS (expression analysis, 1:10)

2.1.7 Proteins and therapeutic antobodies

Annexin V-GFP	kindly provided by Faban Richter, Institue of Cell Biology and Immunology, University of Stuttgart
Atrosab	Baliopharm, Basel, Switzerland
Cetuximab	Erbitux® Merck, Darmstadt, Germany
HER2-Fc	extracellular domain (aa 23-652) fused to the human Fcγ1 chain; kindly provided by Meike Hutt, Institue of Cell Biology and Immunology, University of Stuttgart
HER3-Fc	extracellular domain (aa 20-643) fused to the human Fcγ1 chain; kindly provided by Sina Fellermeier, Institue of Cell Biology and Immunology, University of Stuttgart
HER3-His	extracellular domain (aa 23-652) ; kindly provided by Jonas Honer (Institue of Cell Biology and Immunology, University of Stuttgart) or reproduced for this thesis
Heregulin	PeproTech (Hamburg, Germany) recombinant heregulin-β; Sigma-Aldrich (St. Louis, MO, USA)
His-tagged heregulin	Ser20-Lys241 NRG1, c-Terminal 6-His-tag; R&D systems (Minneapolis, MN, USA)
Mouse HER2	Mouse HER2 (P70424) extracellular domain (Met 1-Thr 653) fused with the Fc region of human IgG1 at the C-terminus. Sino Biological Inc.
Mouse HER3	R&D systems (Minneapolis, MN, USA)
Rituximab	(MABTHERA) Roche, Basel, Switzerland
Trastuzumab	Herceptin® Roche, Basel, Switzerland

2.1.8 Enzymes

Lysozyme	Muramidase from hen egg white; Roche Diagnostics, Mannheim, Germany
Pfu DNA Polymerase	Thermo Fischer, Waltham, MA, USA
Restriction enzymes	Thermo Fischer, Waltham, MA, USA (AgeI, ApaI, BamHI, EcoRI, HindIII, MscI, NcoI, NotI, SfiI)
T4 DNA Ligase	Thermo Fischer, Waltham, MA, USA

2.1.9 Markers

GeneRuler™ DNA Ladder mix	Fermentas, St. Leon-Rot, Germany
PageRuler™	Fermentas, St. Leon-Rot, Germany

2.1.10 Kits

Alanine Transaminase Activity Assay kit	abcam, Cambridge, UK
Amine coupling kit (EDC + sNHS)	Attana AB, Stockholm, Sweden
Cell Counting Kit-8 (CCK-8)	Sigma Aldrich, St. Louis, USA
Cy5 Ab Labeling Kit	GE Healthcare UK eLimited, Buckinghamshire, UK
DC™ Protein Assay	BioRad, Munich, Germany
DreamTaq™ Green PCR Master Mix	Fermentas, St. Leon-Rot, USA
NucleoBond Xtra Maxi	Machery-Nagal, Düren, Germany
NucleoBond® Xtra Midi	Machery-Nagal, Düren, Germany
NucleoSpin® Gel & PCR Clean-up	Machery-Nagal, Düren, Germany
NucleoSpin® Plasmid	Machery-Nagal, Düren, Germany
QIFIKIT®	Dako; purchased from Biozol (Eching, Germany)
REDTaq ReadyMix PCR Reaction Mix	Sigma Aldrich, St. Louis, USA

2.1.11 Bacteria

Escherichia coli TG1	Genotype: *supE thi-1* Δ(*lac-proAB*) Δ(*mcrB-hsdSM*)*5* (rK- mK-) [F' *traD36 proAB lacIqZ*Δ*M15*] (Stratagene, La Jolla, CA, USA)

2.1.12 Eukaryotic cell lines

All eukaryotic cell lines were incubated in a humidified atmosphere of 5 percent CO_2 at 37 °C. A549 cells were obtained from CLS Cell Lines Services (Eppelheim, Germany). FaDu cells were obtained from DSMZ German Collection of Microorganisms and Cell Cultures (Braunschweig, Germany). BT-474 and SKBR-3 cells were originally obtained from Nancy Hynes, Friedrich Miescher Institute, Basel, Switzerland. MCF-7 cells were originally obtained from Cornelius Knabbe, Institute of Clinical Pharmacology, Stuttgart, Germany. Inducible Caco-2 K-Ras^{G12V} cells were originally obtained from Tilman Brummer, Institute for Molecular Medicine and Cell Research, Freiburg, Germany. NCI-N87 cells were kindly provided by TRON, Mainz, Germany.

Table 2-2: Eukaryotic cell lines used in this study.

Cell line	Origin	Culture medium
A431	human epidermoid carcinoma	RPMI 1640 + 10% FCS
A549	human lung carcinoma (NSCLC)	RPMI 1640 + 10% FCS
BT-474	human ductal carcinoma, breast	RPMI 1640 + 10% FCS
Caco-2	human colorectal adenocarcinoma	RPMI 1640 + 10% FCS
Caco2 Tet-on K-Ras	human colorectal adenocarcinoma, inducible K-Ras^{G12V}	DMEM + 10% FCS
Colo205	human colorectal adenocarcinoma	RPMI 1640 + 10% FCS
FaDu	human squamous cell carcinoma (head and neck cancer; pharynx)	DMEM + 10% FCS
HCT-116	human colorectal carcinoma	RPMI 1640 + 10% FCS
HEK293-6E	human embryonic kidney, suspension optimized	F17 Freestyle medium supplemented with L-Glutamine, Kolliphor P-188 and 25 µg/ml G418
HEK293T	human embryonic kidney	RPMI 1640 + 5% FCS
MCF-7	human adenocarcinoma, breast	RPMI 1640 + 10% FCS
NCI-N87	human gastric carcinoma	RPMI 1640 + 10% FCS
SKBR-3	human adenocarcinoma, breast	DMEM + 10% FCS
SKOV-3	human adenocarcinoma, ovary	DMEM + 10% FCS

2.1.13 Mice

SCID® Beige CB17.Cg-Prkdc^{scid}Lyst^{bg}/Crl (Charles River, Wilmington, MA, USA)

2.1.14 Plasmids

Table 2-3: Plasmids used in this study.

Plasmid	Cloned by
pAB1-scFv 2-31	Lisa Schmitt
pAB1-scFv 2-32	Lisa Schmitt
pAB1-scFv 2-33	Lisa Schmitt
pAB1-scFv 2-34	Lisa Schmitt
pAB1-scFv 2-35	Lisa Schmitt
pAB1-scFv 2-36	Lisa Schmitt
pAB1-scFv 2-37	Lisa Schmitt
pAB1-scFv 3-38	Lisa Schmitt
pAB1-scFv 3-39	Lisa Schmitt
pAB1-scFv 3-40	Lisa Schmitt
pAB1-scFv 3-41	Lisa Schmitt

pAB1-scFv 3-42	Lisa Schmitt
pAB1-scFv 3-43	Lisa Schmitt
pAB1-scFv 3-44	Lisa Schmitt
pAB1-scFv 3-45	Lisa Schmitt
pAB1-scFv3M6	Meike Hutt, 2012, Institute of Cell Biology and Immunology
pAB1-scFv4D5	Sina Fellermeier, 2011, Institute of Cell Biology and Immunology
pAB1-scFvGal12	Institute of Cell Biology and Immunology
pAB1-scFvhu225	Anja Nusser, 2008, Institute of Cell Biology and Immunology
pEE14.4-IgG 2-35 SI	Lisa Schmitt
pEE14.4-IgG 3-43 SI	Lisa Schmitt
pEE14.4-IgG 3M6 SI	Lisa Schmitt
pSecTagA-HER2-Fc	Sina Ferrlermeier, 2011, Institute of Cell Biology and Immunology
pSecTagA-HER3-Fc	Sina Fellermeier, 2011, Institute of Cell Biology and Immunology
pSecTagA-HER3$_{DII-IV}$-Fc	Lisa Schmitt
pSecTagA-HER3$_{DIII-IV}$-Fc	Lisa Schmitt
pSecTagA-HER3$_{DIV}$-Fc	Lisa Schmitt
pSecTagA-His-HER3-ECD	Jonas Honer, 2016, Institute of Cell Biology and Immunology
pSecTagAge-scFv 2-31-Fc	Lisa Schmitt
pSEcTagAge-scFv 2-33-Fc	Lisa Schmitt
pSecTagAge-scFv 2-35-Fc	Lisa Schmitt
pSecTagAge-scFv 3-43-Fc	Lisa Schmitt

2.1.15 Primers/Oligonucleotides

Table 2-4: Primer for cloning of scFv-Fc fusion proteins:

#	Name	Sequence
1076	AgeI-Her2-31/32/33-back	aaa accggt caa gtc cag ctg gtg cag tct
1077	AgeI-Her2-34/35-back	aaa accggt caa atg cag ctg gta cag
1078	AgeI-Her3-39/43/44-back	aaa accggt cag gta cag ctg cag cag
1079	NotI-Her2-31-33-Her3-39/43/44-fwd	aaa gcggccgc acc tag gac ggt cag ctt
1080	NotI-Her2-34/35-fwd	aaa gcggccgc acc tag gac ggc cag ttt

Table 2-5: Primer for cloning of HER3-Fc fusion proteins:

#	Name	Sequence
1226	tHer3DII-III-IV-back	aaa g gcc cag ccg gcc tcc gag gtg ggc aac tct cag acc atc

		tgt gct cct cag tgt aat gg
1227	tHer3DIII-IV-back	aaa g gcc cag ccg gcc tcc gag gtg ggc aac tct cag aaa gcc tgt gag gga aca ggc
1228	tHer3DIV-back	aaa g gcc cag ccg gcc tcc gag gtg ggc aac tct cag cac tgc aac ttt ctg aat ggg gag
1229	tHer3-fwd	aaa cgg tgg gca tgt gtg agt ttt gtc

Table 2-6: Primer for Cloning of IgG1 molecules

#	Name	Sequence
1240	MsclVL43 fwd	aaatggccaaa cag cac tgt cag ctt ggt gcc tcc gcc aaa
1241	AgeIVL43IgG back	aaa acc ggt caa gtg cag ctg cag cag
1256	AgeIVL43backneu	aaa accggt caa gcc gga ctg
	MsclVL43forneu	aaa tggcca ca cag cac tgt cag ctt ggt
1291	IgGVL43Msclfor	aaa ctggccaagcactgtcagcttggtgcc
1298	MsclIgGVL3M6for	aaa ctggcca agc acg gtc act ttg gt
1299	AgeIIgGVL3M6back	aaa accggt cag tct gcc ctg aca cag cct gcc agc gtg tcc ggc agc cca ggg cag agc atc aca atc agc
1300	AgeIVIgGH3M6back	aaa acc ggt gaa gtg cag ctg
1301	ApaIIgGVH3M6for	gct ggg gcc ctt ggt gct agc act cga gac tgt gac cag
1258	AgeIVH43back	aaa gag ctc acc ggt caa gtg
1259	ApaIVH43CH1for	aaa ggggcccttggtggaggc aga gga cac tgt gac cat

Table 2-7: Primer for screening and sequencing

#	Name	Sequence
61	LMB4 (pAB1 reverse)	gcaaggcgattaagttgg
82	Lonza-F	gcc acc aga cat aat agc
88	LMB3 (pAB1 forward)	cag gaa aca gct atg acc
89	pET-Seq1/T7-back	taatacgactcactataggg
91	pSec-Seq2	tagaaggcacagtcgagg

2.1.16 Vectors

pAB1	Vector for prokaryotic protein expression and secretion into the periplasm of *E.coli* (R. Kontermann)
pAB1-huCλ	Prokaryotic expression vector comprising the constant region of human IgG lambda light antibody chain
pEE14.4	Glutamine synthetase encoding eukaryotic expression vector (Lonza Biologics, Berkshire, UK)

pEE6.4	Lonza Biologics, Berkshire, UK
pEE6.4-HCg1e*-Acc	pEE6.4 containing human IgG1γ1 heavy chain constant region containing point mutations encumbering ADCC and CDC
pHAL14	phagemid vector derived from pHAL1 (University of Braunschweig[145,146])
pSecTagA	Vector for eukaryotic protein expression and secretion (Thermo Fisher Scientific, Waltham, MA, USA)
pSecTagA-Fc	Eucaryotic expression vector originated from pSecTagA; comprising human IgG Fc-part heavy chain constant regions (hinge, C_H2 and C_H3 of human Fcγ1 chain)
pSecTagA-His	Modification of pSecTagA lacking the *myc* epitope (Gerhard Trunk, 2005, Institute of Cell Biology and Immunology)
pSecTagAge-Fc(lägerer linker)	Modification of pSecTagA-Fc with additional AgeI restriction site and longer linker before the hinge region

2.1.17 Software and online tools

Attana evaluation software 3.3.4	Attana AB (Stockholm, Sweden)
C-Fast Software	Attana AB (Stockholm, Sweden)
Citations	EndNote basic (Thomson Reuters, Stuttgart, Germany)
Data evaluation	GraphPad Prism® 5.00 for windows (GraphPad Software, La Jolla, CA, USA); Microsoft® Excel® für Mac 2011 Version 14.6.9 (Microsoft, Redmont, WA, USA)
Flow cytometry software	MACSQuantify 2.6 (Milteny Biotec, Bergisch Gladbach, Germany); FlowJo 7.6.5 (Tree Star Inc., Ashland, OR, USA)
Microscopy software	ZEN and ZEN lite (Carl Zeiss Microscopy GmbH, Jena, Germany)
Molecular biology software	Serial Cloner 2.6.1 (http://serialbasics.free.fr/Serial_Cloner.html)
Protein database	UniProt (http://www.uniprot.org)
Protein parameter determination	ExPASy ProtParam (http://web.expasy.org/protparam/)
Sequence alignment	BLAST (https://blast.ncbi.nlm.nih.gov/Blast.cgi)
TraceDrawer 1.6	Attana AB (Stockholm, Sweden)
Western blot quantification	FUSION SOLO S software (Vilber Lourmat Deutschland GmbH, Erberhardzell, Germany)
Writing	Microsoft® Word für Mac 2011 Version 14.6.9 (Microsoft, Redmont, WA, USA)

2.2 Methods

2.2.1 Molecular biological Methods

2.2.1.1 Subcloning of scFv proteins

All scFv fragments consisted of the variable domains of an antibody's heavy (V_H) and light chain (V_L) joined by a flexible linker (GSASAPKLEEGEFSEARV) and comprised a C-terminal hexahistidyl (His_6)-tag. For periplasmatic expression, all scFv clones were subcloned from pHAL14 into pAB1. All plasmids and pAB1 vector were digested with NcoI and NotI. Digested scFv sequences were analyzed by electrophoresis, excised, purified and religated into dephosphorylated pAB1 vector.

2.2.1.2 Cloning of scFv-Fc fusion proteins

The scFv sequences were amplified from the pAB1 plasmids with the respective primers (Table 2-4), to introduce an additional AgeI restriction site at the N-terminal site. The resulting PCR products were analyzed by electrophoresis, purified and digested with AgeI and NotI. Then, they were ligated in the parallel digested vector pSecTagAge-Fc (longer linker).

2.2.1.3 Cloning of Fc-fused HER3-ECD fractions

HER3-ECD fractions were amplified by polymerase chain reaction from pSecTagA-HER3-Fc, inserting a SfiI restriction site at the N-terminal site. HER3-ECD fraction sequences were purified and subcloned into pSecTagA-Fc using SfiI and NotI restriction sites.

2.2.1.4 Cloning strategy of IgG molecules

All variable light chain sequences were lambda light chain sequences. For IgG 3-43 and IgG 2-35, variable sequences were codon optimized and synthesized from GeneArt (Regensburg, Germany). Variable light chain sequences were cloned via AgeI and MscI restriction sites into pAB1-huCλ. The resulting signal peptide - V_L - C_Lλ -sequences were subcloned via HindIII and EcoRI restriction sites into pEE14.4.
V_H sequences were subcloned into pEE6.4-huEmp1CH1-CH3 (IgG1e3*; pEE6.4-HCg1e*-Acc, human allotype G1m1,17) using AgeI and ApaI restriction sites. The nucleic acid sequence of human IgG1γ1 heavy chain containing S239D and I332E amino acid exchange inducing mutations was also ordered as ApaI-EcoRI-fragment from GeneArt and subcloned using ApaI and EcoRI restriction sites into V_H

containing pEE6.4 vector. Finally, heavy and light chains were combined via NotI and BamHI restriction sites into pEE14.4.

2.2.1.5 Handling of E. coli strains

E. coli strains were cultured at 37 °C, either in Luria-Bertani (LB) medium with strong agitation or on agar plates (LB medium containing 3 % Agar). Resistant bacteria were selected with media containing 100 mg/l Ampicillin or Kanamycin, according to the respective resistance gene.

2.2.1.6 Chemical competent *E. coli* cells

Calciumchlorid-Methode (Sambrook & Russell, 2001) or (Inoue et al., 1990)
A fresh overnight culture of *E. coli* TG1 was used to inoculate 300 ml of LB medium (dilution 1:100). Cells were grown at 37 °C (shaking at 170 rpm) until an OD_{600} of 0.5 to 0.6 was reached and then chilled on ice for 15 minutes in pre-cooled 50 ml centrifugation tubes. After centrifugation (4000x g, 5 minutes, 4 °C), the supernatant was discarded and the cell pellet was carefully resuspended in 50 ml ice-cold 0.1 M CaCl2 in 1x PBS and incubated for 30 minutes on ice. Cells were centrifuged again (4000x g, 5 minutes, 4 °C) and cell pellet was resuspended in 10 ml ice-cold 20 % (v/v) glycerol/50mM CaCl2 in 1x PBS. Finally, the competent cells were quick-frozen in liquid nitrogen and stored in 300 µl aliquots at -80 °C.

2.2.1.7 Polymerase chain reaction

Polymerase chain reaction (PCR) with pfu-DNA-polymerase was used to amplify desired DNA fragments from vector templates for further cloning steps. A typical PCR mixture contained 50 µl:

10x pfu-polymerase buffer + MgSO4	5 µl
Forward primer (10 pmol/µl)	1 µl
Reverse primer (10 pmol/µl)	1 µl
dNTPs (5 mM each nucleotide)	2 µl
pfu-DNA-polymerase (2.5 U/µl)	1 µl
dH2O	40 µl

2.2.1.8 DNA electrophoresis and gel extraction

Horizontal agarose gel electrophoresis was used to analyze and purify PCR-amplified or digested DNA fragments. Depending on the size of the fragments, 0,8 - 2 % (w/v) agarose was dissolved in 1x TAE buffer by boiling in a microwave oven. Subsequently, ethidium bromide was added to a final concentration of 1 µg/ml. The solution was poured in specialized trays and polymerized by cooling down to room temperature. DNA was mixed 5x DNA loading buffer and applied to the precast gel. Electrophoresis was conducted in 1x TAE buffer at a constant voltage of 80 -100 V for 30-120 minutes. DNA was visualized using ultraviolet light. The relevant bands were excised and purified with a NucleoSpin® Gel and PCR Clean-up kit according to the manufacturer's protocol. The DNA was eluted in 30 µl ddH_20.

2.2.1.9 Restriction digestion

Restriction digestion was performed in a total volume of 50 µl containing 10 µg vector DNA or the complete extracted PCR products from an agarose gel. The digestions were performed consecutively for at least one hour per digestion reaction, with a buffer exchange performed with the NucleoSpin Gel and PCR Clean-up kit in between. The vector DNA was dephosphorylated using 1 U fast alkaline phosphatase after the last digestion step for 1 hour at 37 °C. Either all fragments or only the digested insert DNA were analyzed via agarose gel electrophoresis.

2.2.1.10 Ligation

Insert DNA and 50 - 100 ng linearized dephosphorylated vectors were mixed at a molar ratio of 3:1 or 5:1 and incubated with 1 µl T4 DNA ligase according to the manufacturer's protocol in a total volume of 20 µl 1x ligase buffer in sterile water. If DNA concentrations were not determined, 15 µl of insert DNA were mixed with 2 µl vector DNA, 2 µl Ligase buffer and 1 µl T4 DNA Lidase. For control purposes, a sample without insert DNA was also prepared. Incubation was performed for at least one hour at room temperature. 10 µl of the reaction mixtures were used for the transformation of chemical competent *E. coli* cells.

2.2.1.11 Heat shock transformation of *E.coli* cells

Chemically competent *E.coli* TG1 cells were thawed on ice and mixed with 10 µl of the ligation preparation. The mixture was incubated on ice for 10 minutes, mixed by gentle flipping and incubated for one minute at 42 °C. After another 10 minutes incubation on ice, 1 ml of LB medium was added and the cells were incubated for at

least 30 minutes at 37 °C under agitation. Afterwards, the cells were harvested by centrifugation (1 min, 16,000g) and plated on agar plates containing glucose and ampicillin as selection marker and incubated overnight at 37 °C.

2.2.1.12 Plasmid DNA isolation and sequence analysis

One single clone was inoculated into a 5 ml/100 ml/500 ml LB medium (Mini/Midi/Maxi-preparation) containing 1 % (w/v) glucose and ampicillin, and shaken over night at 37 °C. Cells were harvested the next day and DNA was purified according to manufacturer's protocol with the NucleoSpin Plasmid kit for Mini-preparation or the NuceloBond Xtra Midi or Maxi kit for Midi or Maxi-preparation. The DNA was sequenced by GATC Biotech AG (Konstanz, Germany) using the corresponding primers from Table 2-7.

2.2.2 Cell culture and transfection

All eukaryotic cell lines were cultivated at 37 °C in a humidified 5 percent CO_2 atmosphere in cell culture medium. Cell lines were passaged once, twice or thrice weekly, dependent on the respective confluence and growth rates, by detaching adherent cells with Trypsin/EDTA, centrifugation (1500 rpm, 3-5 minutes) and splitting 1:5 - 1:20. For long-term storage, harvested cells were resuspended in FCS containing 10 % (v/v) DMSO and slowly frozen in isopropanol filled cryoboxes to -80 °C. For thawing, cells were incubated at 37 °C, centrifuged (1500 rpm, 5 min) to remove the residual DMSO and resuspended in the corresponding medium.

For selection of HEK293 cells to express recombinant protein, pSecTagA plasmids were transfected by lipofection. 10^6 cells were seeded in a 6-well tissue culture plate overnight in 2 ml culture medium. The next day, 330 µl of serum free Opti-MEM medium were incubated with 7 µl Lipofectamine 2000 for 5 minutes and subsequently mixed with 3 µg plasmid DNA. The culture medium was withdrawn from the cells and replaced by 1.5 ml Opti-MEM. After 20 min incubation, the lipofectamine-DNA solution was carefully applied to the cells and incubated over night at 37 °C. Supernatant was then removed and cells were detached and transferred to 10 cm tissue culture plates with culture medium. For selection, zeocin was added after 4 hours to a final concentration of 300 µg/ml. Upon successful selection, zeocin concentration was reduced to 50 µg/ml.

2.2.3 Expression and purification of recombinant proteins

2.2.3.1 Periplasmic protein expression in *E. coli* TG1

All scFv analyzed in this study were expressed in *E. coli* TG1 cells. 1 l of TY medium containing ampicillin and 0.1 percent (w/v) glucose were inoculated 1:100 from an overnight culture of pAB1 transformed *E. coli* TG1 and shook at 37 °C until reaching an OD_{600} of 0.8. The protein expression was induced by the addition of IPTG, followed by 3 hours of shaking at room temperature. Cells were harvested (6000 g, 10 minutes, 4 °C) and the cell pellet was resuspended in 100 ml resuspension buffer. From now, all steps were performed on ice and with chilled liquids and centrifuges. Cell wall lysis was accomplished by addition of 10 mg lysozyme and 30 min incubation, followed by the addition of MgSO4 to a final concentration of 10 mM to stabilize the spheroblasts. After centrifugation (10,000 g, 30 minutes), the supernatant was collected and dialyzed over night against 5 l PBS. The dialyzed solution was subjected to purification via IMAC.

2.2.3.2 Protein expression in stably transfected HEK293T cells

All Fc fusion proteins used in this study were expressed in stably transfected HEK293T cells. After selection, stably transfected cells were expanded to triple flasks (Thermo Fisher Scientific, Darmstadt, Germany) in their selection medium. HEK293T cells were incubated in RPMI 1640 with 5 percent FCS and 50 µg/ml zeocin. Upon reaching 80 percent confluence, the medium was changed to serum free Opti-MEM, which was collected every other day for up to two weeks. All further steps were carried out at 4 °C. Proteins from cell free supernatant (centrifugation at 500 g for 5 minutes) were precipitated by addition of 390 g/l ammonium sulfate ($(NH_4)_2SO_4$) addition and stirring for one hour. Consequently, the protein was harvested by centrifugation (11,250 g, 30 min) and the resulting pellet was resuspended in cold PBS. Fc fusion proteins were purified using Protein A chromatography.

2.2.3.3 Transient expression of recombinant proteins in HEK293-6E cells

All IgG molecules as well as his-tagged HER3 were expressed in suspension adapted HEK293-6E cells. HEK293-6E cells were cultured until exponential phase and a density of $1.7 \cdot 10^6$ cells/ml. For production in 100 ml cell suspension, 100 µg plasmid DNA and 200 µl of PEI (1 mg/ml) were each mixed with 5 ml of F17-medium. Both solutions were shortly vortexed and then combined. The resulting mixture was incubated for 15 minutes at room temperature, and carefully added to the cell

suspension. After 24 h incubation at 37 °C and agitation, trypton N1 (TN1) was added to the cells to a final concentration of 0.5 %. After further 96 hours of incubation at 37 °C under agitation, the cell suspension was collected and centrifuged (3000x g, 20 min, 4 °C). The supernatant was sterilized by filtration and proteins were purified as described in the following. To optimize protein purification, cell supernatants were optionally dialyzed against PBS prior to purification.

2.2.3.4 Protein purification via Immobilized Metal Affinity Chromatography (IMAC)

His-tagged proteins were purified via IMAC, using a batch method, where the protein solution is incubated with 0.5 ml of beads for at least 3 hours. All steps were carried out on ice and with chilled liquids. The beads were subsequently collected in a column and unspecifically bound proteins were washed away with at least 40 column volumes of IMAC wash buffer, containing 30 mM imidazole. Protein content of wash fractions as well as following elution fractions was determined using qualitative Bradford assay, where 90 µl of assay solution was mixed with 10 µl of eluted fractions. Blue color identified eluted protein. After washing, the specifically bound protein was eluted with IMAC elution buffer, containing 250 mM imidazole, in 500 µl fractions and main elution fractions (determined by Bradford assay) were pooled for dialysis against 5 l PBS overnight.

2.2.3.5 Protein purification via protein A Affinity Chromatography

All Fc fusion proteins and IgG molecules were purified via Protein A chromatography. All steps were performed on ice and with chilled liquids. The HEK293-6E supernatant or resuspended protein precipitate was incubated with at least 250 µl Protein A beads (considering the capacity of the beads, assumed protein amount and supernatant volume) overnight at 4 °C on a roll mixer and loaded onto a purification column. The beads were washed with 40 column volumes of PBS and protein content of the wash was determined with Bradford reagent as described above. Specifically bound proteins were eluted with Protein A elution buffer (10 mM glycine-HCl pH3) and neutralized with Protein A neutralization buffer (1 M Tris-HCl pH8). Elution fractions were dialyzed against PBS overnight.

2.2.4 Protein characterization

2.2.4.1 Determination of protein concentration

The concentration of all proteins was determined with a spectrophotometer (NanoDrop), based on the absorbance of tryptophan and tyrosine residues at a wavelength of 280 nm. The molar extinction coefficient ε [l/(mol x cm)] and molecular weight (MW [g/mol]) were calculated by the online tool 'ProtParam' and the concentration was computed as follows, where b [cm] represents the path length:

$$c\ [\mu g/ml] = OD280 \times MW / (\varepsilon \times b)$$

2.2.4.2 SDS polyacrylamide gel electrophoresis (SDS-PAGE) analysis of purified proteins

SDS-PAGE was performed to determine integrity and purity of the recombinant proteins. Dependent on the molecular mass of the proteins, gels with 8 - 12 % acrylamide were prepared. Protein samples were mixed with reducing or non-reducing 5x Laemmli sample buffer and boiled for 5 minutes at 95 °C. Protein samples and protein standard were applied to a precast gel, which was run in SDS running buffer for approximately 70 minutes at 40 mA. To remove residual salt and detergent, the gel was washed three times in boiling water. Thereafter, the gel was incubated with Coomassie staining solution for at least 2 hours and destained overnight in water.

Table 2-8: Composition of polyacrylamide gels.

Substances	Stacking Gel	Separating Gel	
	5%	10%	12%
dH2O	2.1 ml	2.95 ml	2.45 ml
30 % Acrylamide	500 µl	2.5 ml	3 ml
1.5 M Tris, pH 8.8	-	1.9 ml	1.9 ml
1.0 M Tris, pH 6.8	380 µl	-	-
10 % SDS	30 µl	75 µl	75 µl
10 % APS	30 µl	75 µl	75 µl
TEMED	3 µl	3 µl	3 µl

2.2.4.3 Size exclusion chromatography

High performance liquid chromatography was performed using size exclusion columns for the determination of purity and integrity of the purified proteins. 25 µl of protein sample with a concentration ranging from 0.3 to 0.5 mg/ml were injected at a PBS mobile phase flow rate of 0.5 ml/min. The following standard proteins were used for calculation of molecular mass and hydrodynamic radius: thyroglobulin (669 kDa, 8.5 nm), apoferritin (443 kDa, 6.1 nm), bovine γ globulin (158 kDa, 5.3 nm), β-amylase (200 kDa, 5.4 nm), bovine serum albumin (67 kDa, 3.55 nm), ovalbumin (44 kDa, 3.2 nm), carbonic anhydrase (29 kDa, 2.35 nm) and cytochrome c (12.5 kDa, 1.77 nm).

2.2.4.4 Thermal stability measurement

The melting point of proteins was determined by thermal denaturation via the ZetaSizer Nano ZS. 100 µg of recombinant protein in 1 ml PBS were sterile-filtered into a quartz cuvette. The temperature at which the protein starts to aggregate was determined by the increase of the mean count rate of dynamic laser light scattering and defined as the melting point. Hereby, the temperature was raised in 1 °C intervals from 35 to 92 °C with 2 minutes of equilibration time.

2.2.5 ELISA

Fc fusion proteins (300 ng/well for all binding studies, 1000 ng/well for epitope mapping) were coated overnight at 4 °C in ELISA plates and remaining binding sites were blocked with 2 percent (w/v) non-fat dry milk/PBS (MPBS). Purified proteins were diluted in MPBS and titrated in duplicates. Plates were washed three times in ELISA washing solution (0.05 % (v/v) Tween20 in 1x PBS) followed by two times washing with PBS. Bound proteins were detected either with HRP-conjugated anti-human IgG (F_{ab} specific) antibody or with HRP-conjugated anti His-tag antibody. Developing was performed using 100 µl of 3,3',5,5'-tetramethylbenzidine (TMB) substrate per well (0.1 mg/ml TMB, 100 mM sodium acetate buffer, pH 6.0, 0.006% H_2O_2). Reaction was stopped with 1 M H_2SO_4 (50 µl/well) and optical density was measured at 450 nm in an ELISA reader.

2.2.6 Flow cytometric analyses

Flow cytometric studies were performed with various human cell lines. Cells were shortly trypsinized at 37 °C, trypsin was quenched with FCS-containing medium and removed by centrifugation. Cells (200.000 cells per probe) were seeded in U-bottom

microtiter plates and incubated with specified protein concentrations for at least one hour at 4 °C. Washing was performed twice with PBA (2 % (v/v) FCS, 0.02 % (w/v) NaN3 in 1x PBS). PE-labeled anti-human Fc antibody or PE-labeled anti-His tag antibody was incubated for another hour to visualize bound molecules. For the analysis of receptor expression, FITC-labeled goat anti-mouse antibody was incubated for 45 minutes, following the manufacturer's instructions. After two further washing steps, the cells were resuspended in PBA and fluorescence was measured with a MACSQuant® Analyzer 10 or MACSQuant® VYB and median fluorescence intensities relative to unstained cells were calculated using the FlowJo software.

2.2.6.1 Analysis of receptor expression

Quantification of receptor expression was performed by indirect immunofluorescence staining using the QIFIKIT (Dako) according to the manufacturer's protocol and anti-EGFR antibody (Clone AY13, diluted 1:10), anti-HER2 antibody (Clone 24D2, diluted 1:10), and anti-HER3 antibody (Clone 1B4C3, diluted 1:10) (all mouse IgG and purchased from BioLegend). In brief, the kit uses beads with specified antigen densities to provide a standard curve, which can then be used to calculate cellular antigen densities. Cellular antigen amounts were detected using mouse antibodies applied in saturation. Comparability of fluorescence intensities is given through the use of the same detection antibody solution. Data analysis was performed using the FlowJo software, Excel and GraphPad Prism.

2.2.6.2 Flow cytometric binding studies

Binding of antibodies or antibody fragments to cell surface-expressed receptors was analyzed by flow cytometry. Target cells (Colo 205, FaDu, MCF-7 or SKBR-3) were treated as described above. After removal of the culture medium, the cells were incubated with serial dilutions of the different antibody proteins (scFv, scFv-Fc, IgG) in 100 µl PBA for 1 h at 4°C. Cells were centrifuged (500 g, 5 min) and washed twice in 150 µl PBA prior to incubating with detection antibody in 100 µl PBA. After three washing steps with 150 µl PBA, cells were resuspended in 150 µl PBA and analyzed. Relative median fluorescence intensities (MFI) were calculated using the formula:

$$\text{relative MFI} = \frac{(\text{MFI}_{\text{sample}} - (\text{MFI}_{\text{detection}} - \text{MFI}_{\text{cells}})}{\text{MFI}_{\text{cells}}}$$

Following a method published by Benedict et al. 1997[147], the concentration corresponding to half-maximal binding (EC_{50}) was calculated from the relative MFI using Graphpad Prism software.

2.2.6.3 Inhibition of heregulin binding

MCF-7 cells were shortly trypsinized at 37 °C, trypsin was quenched with FCS-containing medium and removed by centrifugation. Cells (200.000 cells per probe) were seeded and incubated with 3000 nM of IgG 3-43 or control antibody (cetuximab) at 4 °C. After 30 minutes, 50 nM of recombinant 6His tagged heregulin was added and the cells were mixed and incubated for at least another hour at 4 °C. Washing was performed twice with PBA (2 % (v/v) FCS, 0.02 % (w/v) NaN3 in 1x PBS). PE-labeled anti-His antibody (Milteny Biotec) was incubated for another hour to visualize bound heregulin molecules. After two further washing steps, fluorescence was measured with a MACSQuant® Analyzer 10 and median fluorescence intensities relative to unstained cells were calculated using the FlowJo software.

2.2.7 Quarz crystal microbalance

Affinity of the monomeric receptor ECD of HER3 and dimeric HER3-Fc fusion to IgG 3-43 was determined via quartz crystal microbalance measurements using an Attana Cell 200 instrument. IgG 3-43 was immobilized on the surface of a low nonspecific-binding carboxyl chip using the amine coupling kit (EDC + sNHS, Attana AB, Stockholm, Sweden) in a density that resulted in a frequency change of about 90 Hz. The measurement was performed at 25 °C with a flow-rate of 25 µl/min of PBST (0.1 % Tween) pH 7.4. Regeneration of the binding was performed twice with 3 M $MgCl_2$ for 15 seconds. After every second measurement a buffer injection was performed to determine the baseline, which was subsequently subtracted from the measurements. Soluble His-tagged HER3 was injected in a two-fold dilution series in PBST in random order, with concentrations between 1.25 to 20 nM. Dimeric HER3-Fc was injected in a two-fold dilution series in PBST in random order, with concentrations between 0,625 to 10 nM. Data were analyzed with the Attana evaluation software and TraceDrawer.

Affinity of scFv 2-35 to HER2-Fc was measured using an Attana A200 instrument. HER2-Fc was immobilized on the surface of a low nonspecific-binding carboxyl chip using the amine coupling kit (EDC + sNHS, Attana AB, Stockholm, Sweden) in a density that resulted in a frequency change of about 100 Hz. The measurement was

performed at 25 °C with a flow-rate of 25 µl/min of PBST (0.1 % Tween) pH 7.4. Regeneration of the binding was performed twice with Glycin-HCL pH 3 containing 15 mM NaCl for 12 seconds. After every second measurement a buffer injection was performed to determine the baseline, which was subsequently subtracted from the measurements. ScFv 2-35 was injected in a two-fold dilution series in PBST in random order, with concentrations between 32 to 512 nM. Data were analyzed with the Attana evaluation software and TraceDrawer using a monophasic fit.

2.2.8 Immunoblotting

SDS polyacrylamide gel electrophoresis as first described 1970 by Laemmli[148] was performed to separate the proteins of the cell lysates. Protein samples were mixed with reducing 5x Laemmli sample buffer and boiled for 5 min at 95 °C. Protein samples and protein standard were applied to a gradient gel and let run according to the manufacturer's instructions. Protein bands were transferred to nitrocellulose or PVDF membranes using the iBlot 2 device. Further analysis and sample preparation is described in the following.

For immuno-blotting of purified proteins, the standard procedure and self-made gels as described in 2.2.4.2 were used and protein fractions were transferred to nitrocellulose membrane using a semi-dry blotter. Blocking was performed in 2% MPBS at room temperature for one hour and detection antibodies were incubated in 2% MPBS for at least three hours. Washing was performed twice with western washing solution (PBST) for 5 minutes and once with PBS for another 5 minutes. HRP couple antibodies were detected with ECL substrate and visualized by the FUSION SOLO Imager.

2.2.8.1 Immunoblotting for analyses of signaling pathways

Cells were grown in 6-well plates ($2 \cdot 10^5$ cells per well) overnight and then starved in medium containing 0.2 % FCS for another day. Next, cells were incubated with indicated concentrations of antibodies in starvation medium at 37 °C for 1 hour or the indicated time. Subsequently, cells were stimulated with heregulin (50 ng/ml) for 15 minutes, before being lysed using protease inhibitor containing RIPA buffer (50 mM Tris (pH 7.5), 150 mM NaCl, 1 % Triton-X 100, 0.5 % sodium deoxycholate, 0.1 % SDS, 1 mM sodium orthovanadate, 10 mM sodium fluoride and 20 mM β-glycerophosphate plus Complete protease inhibitors (Roche, Basel, Switzerland) at 4 °C. Lysates were centrifuged (13,200 rpm, 30 minutes, 4 °C) and supernatants

were collected. Protein concentrations in each lysate were assessed using the Bio-Rad DC™ Protein Assay. Lysates were fractionated by SDS-PAGE and transferred onto nitrocellulose membranes (iBlot®Gel Transfer Stacks; Invitrogen) using the iBlot® 2 Dry Blotting System. Membranes were blocked with 0,5 % blocking reagent (Roche) in PBS containing 0.1 % Tween-20 and incubated with indicated primary antibodies overnight at 4 °C, followed by five washing steps with 0.5 % PBST and incubation with HRP-conjugated secondary antibody for 1 hour at room temperature. After washing, activity of HRP was detected with ECL substrate and visualized by the FUSION SOLO Imager. Quantification of band intensities was performed using the FUSION Software and Microsoft Excel. All values were normalized to the corresponding loading control.

2.2.8.1.1 Analysis of concentration dependent protein phosphorylation

Cells were treated as described in 2.2.8.1. Serial antibody dilutions were incubated with the indicated cells in starvation medium at 37 °C for 1 hour. Lysate preparation and analyses was performed as described above (2.2.8.1). The half maximal inhibitory concentration was calculated using GraphPad Prism software.

2.2.8.1.2 Analysis of HER3 degradation

Cells were treated as described in 2.2.8.1. 100 nM IgG 3-43 or control antibody (Atrosab) were incubated with MCF-7 cells in starvation medium at 37 °C for 5 minutes, 1, 2, 4 or 6 hours. Lysate preparation and analyses was performed as described above (2.2.8.1). HER3 receptor was stained with ErbB3 clone 2F12 antibody (Thermo scientific) and detected using HRP-coupled secondary antibody and ECL substrate.

2.2.9 Cy5-Labeling of IgG

For direct protein labeling with fluorescent Cy5 reagent, Amersham Cy5 malemide mono-reactive dye was used according tot he manufacturer's instructions. Briefly, 1 mg of protein was dissolved in 1 ml room tempered degassed PBS and left at room temperature for 30 minutes. A 100 molar excess of TCEP was added (here, 10 µl of an 18 mg/ml TCEP solution in PBS was used). Before and after addition of TCEP, the reaction tube was flushed with nitrogen gas. The vial was capped, mixed and incubated at room temperature for 10 minutes. Meanwhile, the dried labeling dye was dissolved in 50 µl anhydrous Dimethylformamide, also flushed with Nitrogen gas and mixed. The dye solution was then added to the reduced protein. The tube was

flushed with Nitrogen gas again, mixed and incubated at room temperature for two hours while mixing every 30 minutes. The reaction was left over night at 2-8 °C. On the next day, the labeled antibody was separated from unconjugated dye by gel permeation chromatography with a PD-10 Desalting column (also from GE Healthcare). For the estimation of dye to protein ratio, absorbance of dye at 650 nm and protein at 280 nm was measured and divided through the according extinction coefficients. The dye absorbance at 250 nm was assumed to be 5 percent of the absorbance at 650 nm and was subtracted from the protein absorbance.

2.2.10 Receptor internalization

MCF-7 cells were seeded on 8-well glass chamber slides (BD) one day before the experiment to be semi-confluent on the next day (10^4 cells per sample). Cy5 labeled IgG 3-43 was incubated in growth medium at 37 °C for the indicated time periods (5 minutes, 1 hour or 2 hours, or 1 minute at room temperature as binding control (referred to as 0 min sample). The cells were fixed with 4 % PFA in PBS (200 µl/well) for 15 minutes at 37 °C. Fixed cells were washed with PBS and counterstained with Concanavalin A and DAPI for 10 minutes. After three more washing steps with PBS, the cells were mounted with Fluoromunt G and covered with cover slips. Dried slides were stored at 4 °C and the experiment was performed on a Zeiss Axio Observer Spinning Disc microscope equipped with a Plan-Apochromat 10x/0,45 M27 objective and an Axiocam 503 mono CCD camera. The following excitation lasers and emission filters were used: DAPI: 405 diode laser, 450/50 nm filter; GFP: 488 nm diode laser, 525/50 nm filter; RFP: 561 nm (RFP) diode laser, 600/50 nm filter; Cy5: 638 nm, 690/50 nm filter. Images were analyzed with the ZEN software (Zeiss).

2.2.11 Three-dimensional oncogenic K-Ras model

Caco-2tet Ras^{G12V} cells were generated before the start of this thesis as described in Möller et al., 2014[149] and kindly provided by Dr. Tilman Brummer and Prof. Monilola Olayioye. The cells were seeded on a bed of growth factor reduced matrigel (BD) and PureCol-S collagen (Advanced Biomatrix, San Diego, CA, USA) (mixed 1:1) and overlayed with growth medium containing 2 % matrigel. Expression of oncogenic K-Ras^{G12V} was induced one day post seeding with 2 µg/ml doxycycline. 100 nM IgG 3-43 or control antibody (Rituximab) or 200 nM pan-ErbB inhibitor AZD8931 was also applied one day post seeding. Lumen expansion was induced by addition of 100 ng/ml choleratoxin (CTX; Sigma Aldrich) at day 3 post seeding. Five days' post

seeding, the cells were fixed with 4% PFA for 15 min, permeabilized with PBS containing 0.1 % Triton X-100 for 10 minutes and blocked with 5 % goat serum (Invitrogen) in PBS containing 0.1% Tween-20. Cells were then incubated with primary antibodiy (anti-E-cadherin 1:200) in blocking buffer (2 hours at RT), washed with PBS containing 0.1 % Tween-20 and incubated with secondary antibody (anti-rabbit AF 633) in blocking buffer (2 hours at RT). F-Actin and nuclei were counterstained with Alexa Fluor 546-labeled phalloidin and DAPI. Slides were mounted in Fluoromount G and analyzed on a confocal laser scanning microscope (LSM 700; Zeiss, Oberkochen, Germany) using 488, 561 and 633 nm excitation with oil objective lenses Plan-Apochromat 63x/1.40 DIC M27. Images were processed with the ZEN software (Zeiss). To determine the number of cysts with a 'predominant single apical lumen', spheroids were analyzed in terms of roundness, cell-free lumen formation and F-actin staining of the apical surface.

2.2.12 Proliferation assays

$1 \cdot 10^3$ cells per well were grown in 100 µl growth medium containing 10 percent FCS in 96-well plates at 37 °C for one day. Then, cells were incubated with the indicated concentrations of antibodies in reduced serum medium (0.2 % FCS) at 37 °C for 6 days in the presence or absence of 10 ng/ml heregulin. Next, the number of viable cells was determined using the Cell-Counting-Kit-8. The absorbance at 450 nM was measured in an ELISA reader.

2.2.13 *In vivo* assays

Animal care and all experiments performed were in accordance with federal guidelines and have been approved by university and state authorities.

2.2.13.1 Pharmacodynamics

FaDu cells were freshly thawed and expanded in the absence of Penicillin/streptomycin in growth medium. $5*10^6$ cells were injected subcutaneously into both flanks of female SCID Beige mice. For this purpose, adherent cells were detached from the culture flasks using working solution of trypsin/EDTA and resuspended in 50 ml culture medium. The cells were counted and harvested (500x g, 5 minutes, 4 °C), washed with 50 ml 1x PBS and pelleted again. Finally, the cells were resuspended in 1x PBS adjusting cells per ml in 1x PBS. During the injection of the cells, the mice were anesthetized with isoflurane. As soon as the tumors were

palpable, tumor sizes were measured every second day with calipers. Tumor volumes were calculated using the formula

$$\text{Tumor volume} = \frac{a * b^2}{2}$$

with a= longitudinal diameter of tumor and b= transverse diameter of tumor. Treatment started when tumors reached a volume of approximately 80 mm^3 (14 days after tumor cell inoculation). Mice received twice weekly intravenous injections for 3 weeks (q2wx3) at doses of 30, 100, and 300 µg, including PBS as negative control (on day 14, 17, 21, 24, 28 and 31).

2.2.13.2 Pharmacokinetics

Three animals of each treatment group of the pharmacodynamics experiment described in 2.2.13.1 (twice weekly injections with either 30 µg, 100 µg or 300 µg IgG 3-43 for three weeks) were used to determine serum half-life of IgG 3-43. Blood samples (around 50 µl) were collected from the tail in the time intervals of 3 minutes, 1 hour, 1 day, and 3 days after the first (day 14) and 3 minutes, 1 hour, 1 day, 3 days and one week after the last (day 32) antibody injection and incubated on ice for at least 10 minutes. Clotted blood was centrifuged (13,000 g for 30 min at 4 °C) and serum samples were stored at -20 °C. IgG serum concentration was analyzed by ELISA as described above using 300 ng/well HER3-Fc for coating and HRP coupled anti human IgG (Fab-specific) antibody diluted 1:20 000 for detection by interpolation from a standard curve of purified IgG 3-43. Initial and terminal half-lives ($t_{1/2}\alpha$, $t_{1/2}\beta$) and AUC were calculated with Excel. Initial half-lives were calculated over the time interval of 3 min to 24 h. Terminal half-lives were calculated with the last three serum concentrations (1h-72h or 24h -168h).

2.2.13.3 ALT assay

Three animals of each treatment group of the pharmacodynamics experiment described in 2.2.12.1 (twice weekly injections with either 30 µg, 100 µg or 300 µg IgG 3-43 for three weeks) were used to determine potential liver toxicity of IgG 3-43. Blood samples were taken 24 hours after the last injection and incubated on ice for at least 10 minutes. Clotted blood was centrifuged (13,000 g for 30 min at 4 °C) and serum samples were stored at 4 °C. 5 µl of serum and Alanine Transaminase Activity

Assay kit were used according to the manufacturer's instructions to determine ALT activity in the samples.

2.2.14 Statistical analysis

In vitro values are shown as mean with the corresponding standard deviation. The tumor volumes of the *in vivo* experiment are displayed with mean and 95 % confidence interval. Significances were calculated with GraphPad Prism using one-way Anova with Tukey's post-test or unpaired t-test. * represents a p-value below 0.05, ** below 0.01 and *** below 0.001.

3 Results

3.1 Quantitative analysis of ErbB receptor expression

Receptors of the EGFR family are important regulators of cellular growth and are required for the survival of many cancer cells. To assess the therapeutic potential of antagonistic EGFR family receptor-targeting monoclonal antibodies, different cancer cell lines were quantified by indirect immunofluorescence staining for EGFR, HER2, and HER3 expression levels (Table 3-1). The analyzed cell lines express moderate to low levels of HER3, with the highest levels detected in the breast cancer cell lines MCF-7, SKBR-3 and BT-474. In contrast, very high levels of EGFR (A431) and HER2 (BT-474, SKBR-3, NCI-N87) were measured in some cell lines, with values above 1.000.000 receptors per cell, which lies beyond the quantification scale of the used kit (572.000 molecules/cell).

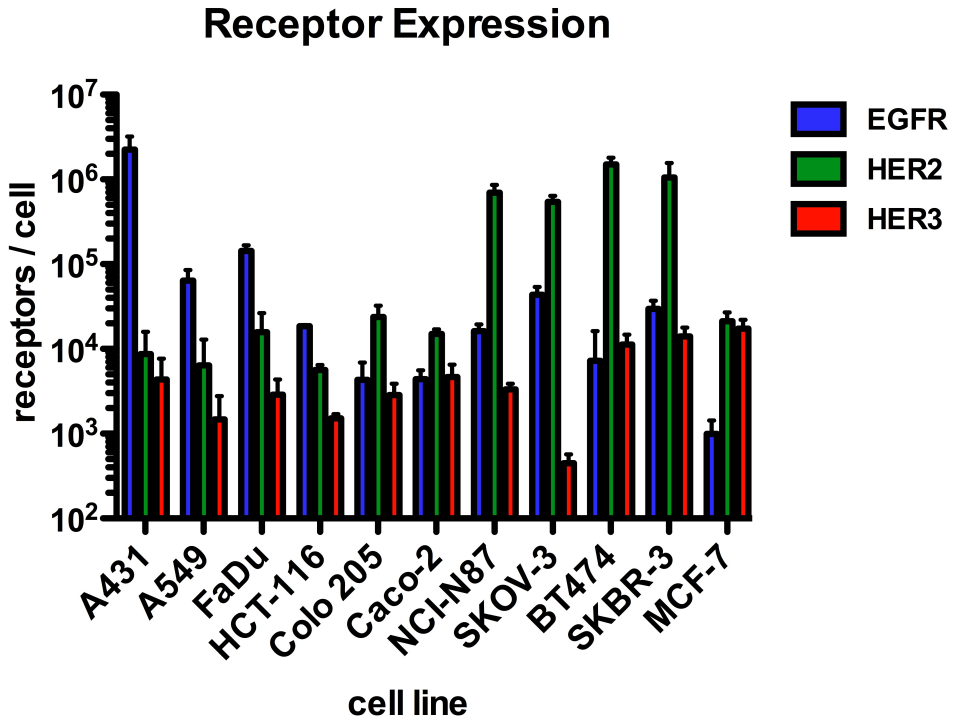

Figure 3-1: ErbB receptor expression of cancer cell lines

Expression of HER receptors was analyzed by FACS using mouse primary antibodies and Dako's QIFIKIT. Mean values of 2-4 independent experiments ± SD are shown.

Table 3-1: Important characteristics of cancer cell lines used in this study

Quantitative expression of the ErbB family members EGFR, HER2 and HER3 was measured using Dako's QIFIKIT. Average numbers of receptors per cell obtained from at least (except BT-474) three independent measurements are listed. Important cancer driving mutations were listed in the last column (mut.). Mutations directly concerning ErbB receptor downstream signaling pathways are shown in bold.

cancer type	cell line	origin	EGFR	HER2	HER3	mut.
breast	**BT-474**	ductal carcinoma (mammary gland)	7,200	>572,000	11,200	**PIK3CA**, TP53
	MCF-7	adenocarcinoma (mammary gland)	<1,900	21,200	17,300	CDKN2A, **PIK3CA**
	SKBR-3	adenocarcinoma (mammary gland)	29,800	>572,000	14,100	TP53
colon	**Caco-2**	colorectal adenocarcinoma	4,400	15,100	4,700	APC, SMAD4
	Colo 205	colorectal adenocarcinoma	4,300	23,800	2,900	APC, **BRAF**, SMAD4, TP53
	HCT-116	colorectal carcinoma	18,600	5,700	<1,900	CDKN2A, **KRAS**, **PIK3CA**,
epithelial	**A431**	epidermoid carcinoma	>572,000	8,700	4,400	TP53
gastric	**NCI-N87**	stomach	16,200	>572,000	3,300	SMAD4, TP53
head and neck	**FaDu**	squamous cell carcinoma (pharynx)	143,300	15,800	2,900	CDKN2A, SMAD4, TP53
lung	**A549**	lung carcinoma	64,100	6,400	<1,900	CDKN2A**,** **KRAS**
ovarian	**SKOV-3**	adenocarcinoma (ovary, ascites)	43,500	54,400	<1,900	SMAD4, TP53

3.2 Screening of newly isolated HER2 receptor antibody binding sites for potential drug components

HER2 is a potent oncogene[150] overexpressed in many human cancer types. In order to generate new antibody binding sites targeting and preferably also inhibiting this receptor, a panel of anti-HER2 scFv (2-31 – 2-37) was isolated from a human antibody phage library by selection against a human $HER2_{ECD}$-Fc fusion (aa 23-652) protein prior to this thesis. After production in TG1 *E. coli* cells and purification via IMAC, the proteins were analyzed with respect to productivity, purity and antigen and cell binding capacity. The obtained results are listed in Table 3-2.

Table 3-2: Yields and binding data of the 7 selected scFvs.

Binding to human HER2-Fc was analyzed by ELISA (n=3; mean ± SD). Binding to SKBR-3 cells was analyzed by flow cytometry (n=1).

scFv	yield (in mg/l)	ELISA (EC_{50} in nM)	cell binding (EC_{50} in nM)
4D5	N/A	2,6 ± 1,1	3.0
2-31	0,2	28,6 ± 21,3	20.9
2-32	1,3	384,3 ± 523,1	n/a
2-33	0,2	24,9 ± 17,0	4.0
2-34	0,2	11,1 ± 2,9	7.3
2-35	0,2	4.2 ± 2.8	5.5
2-36	0,3	12,3 ± 17,3	-
2-37	0,2	91,3 ± 127,4	-

All scFv proteins migrated in good correlation to the calculated molecular weight of around 30 kDa through polyacrylamide gels during electrophoresis (Figure 3-2 A, B). The antigen binding capacities were analyzed via ELISA using immobilized Fc fusion protein of the extracellular domain of HER2 (Figure 3-2 C). The proteins bound to HER2-Fc with EC_{50}-values in the nanomolar range. The lowest determined EC_{50} of 4.2 nM was revealed by scFv 2-35. Five of the seven clones bound to cellular HER2 on SKBR-3 cells, as analyzed by flow cytometry (Figure 3-2 D). Sequence analysis revealed a high similarity between scFv 2-34 and scFv 2-35. To further examine weather this sequence similarity, which was observed in all HER2 binding clones, albeit to a lesser extend, translates in biological consistency in terms of epitope similarity, another flow cytometric experiment was performed using the dimeric scFv-Fc fusion proteins of scFv 2-31, 2-33 and 2-35 (further analysis of the produced scFv-Fc fusion proteins is described in chapter 3.3). SKBR-3 cells were preincubated with the HER2 binding scFv proteins or a HER3 binding scFv as control (scFv 3-43, described in chapter 3.5), and binding of the prebound cellular HER2 by scFv 2-35-Fc was analyzed. This experiment is shown in Figure 3-3 and revealed, that scFv 2-31, scFv 2-33 and scFv 2-35 competed for closely located, overlapping or even the same epitopes on HER2. Therefore, only scFv 2-35, which had the highest affinity for HER2 as analyzed via ELISA, flow cytometry using SKBR-3 cells and quartz crystal microbalance, was chosen for further analysis and IgG construction.

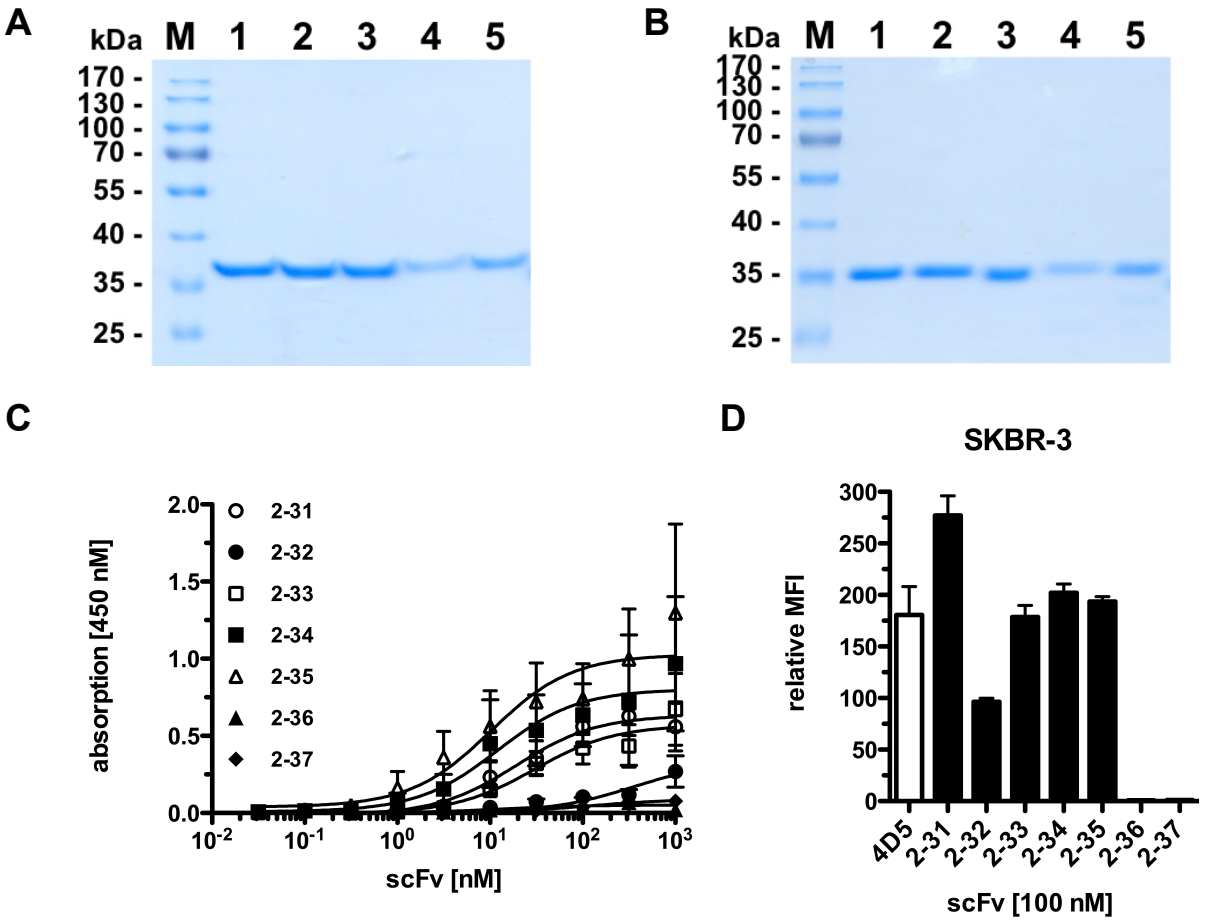

Figure 3-2: Analysis of HER2 binding scFv proteins

A, B SDS-PAGE analysis of the purified HER2 binding scFv proteins 2-31 (1), 2-32 (2), 2-33 (3), 2-34 (4) and 2-35 (5) under reducing (A) and non-reducing (B) conditions. **C** Binding of the scFv proteins to recombinant HER2 was investigated by ELISA. Serial dilutions of the scFv proteins were applied to immobilized Fc tagged HER2 on ELISA plates. The scFv proteins were detected via HRP coupled anti-His-tag antibody (n=3 ; mean ± SD). **D** Binding to cellular HER2 was analyzed by Flow cytometry. 100 nM of the scFv proteins were incubated with detached SKBR-3 cells for two hours in the dark at 4°C. The cells were washed twice before the bound scFv protein was detected with PE coupled anti-His-tag antibody.

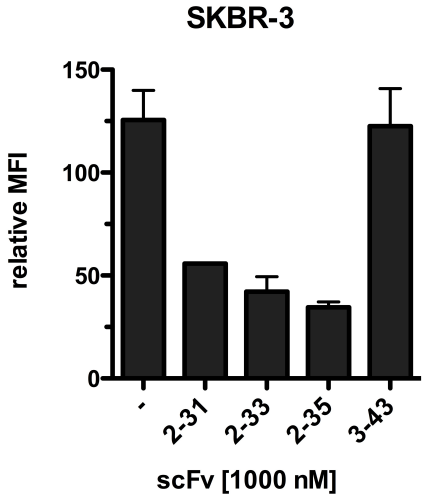

Figure 3-3: Epitope redundancy of scFv 2-32, scFv 2-33 and scFv 2-35.

Overlapping epitopes of the three scFv proteins 2-31, 2-33 and 2-35 were demonstrated by Flow cytometry. SKBR-3 cells were incubated with the indicated scFv antibodies and washed twice before incubation with scFv 2-35-Fc fusion protein. Detection of bound scFv 2-35-Fc was performed using PE coupled anti-human Fc antibody. One representative of two independent experiments is shown with mean of double values ± SD.

Size exclusion chromatography was performed to determine the hydrodynamic radius and protein integrity of scFv 2-35 under native conditions (Figure 3-4 A). The main peak eluted at 19.1 minutes, which corresponds to an estimated molecular mass of 35.5 kDa. An earlier peak with a main fraction eluted at 16.8 minutes, corresponding to an estimated molecular mass of 65.1 kDa and most likely accounting to protein dimer was also observed. The aggregation point of scFv 2-35 was determined by dynamic light scattering to 44 °C (Figure 3-4 B). ScFv 2-35 did not bind to the extracellular domain of mouse HER2 as analyzed via ELISA using recombinant protein consisting of the extracellular domain of mouse HER2 fused to a human Fc part (Figure 3-4 C). Affinity measurements employing quartz crystal microbalance revealed a K_D of 24.8 nM for the binding of scFv 2-35 to dimeric HER2-Fc (Figure 3-4 D). Titration of scFv 2-35 on HER2 overexpressing SKBR-3 cells and further flow cytometric analysis revealed an EC_{50} of 5.5 nM for the binding of cellular HER2 (Figure 3-4 E).

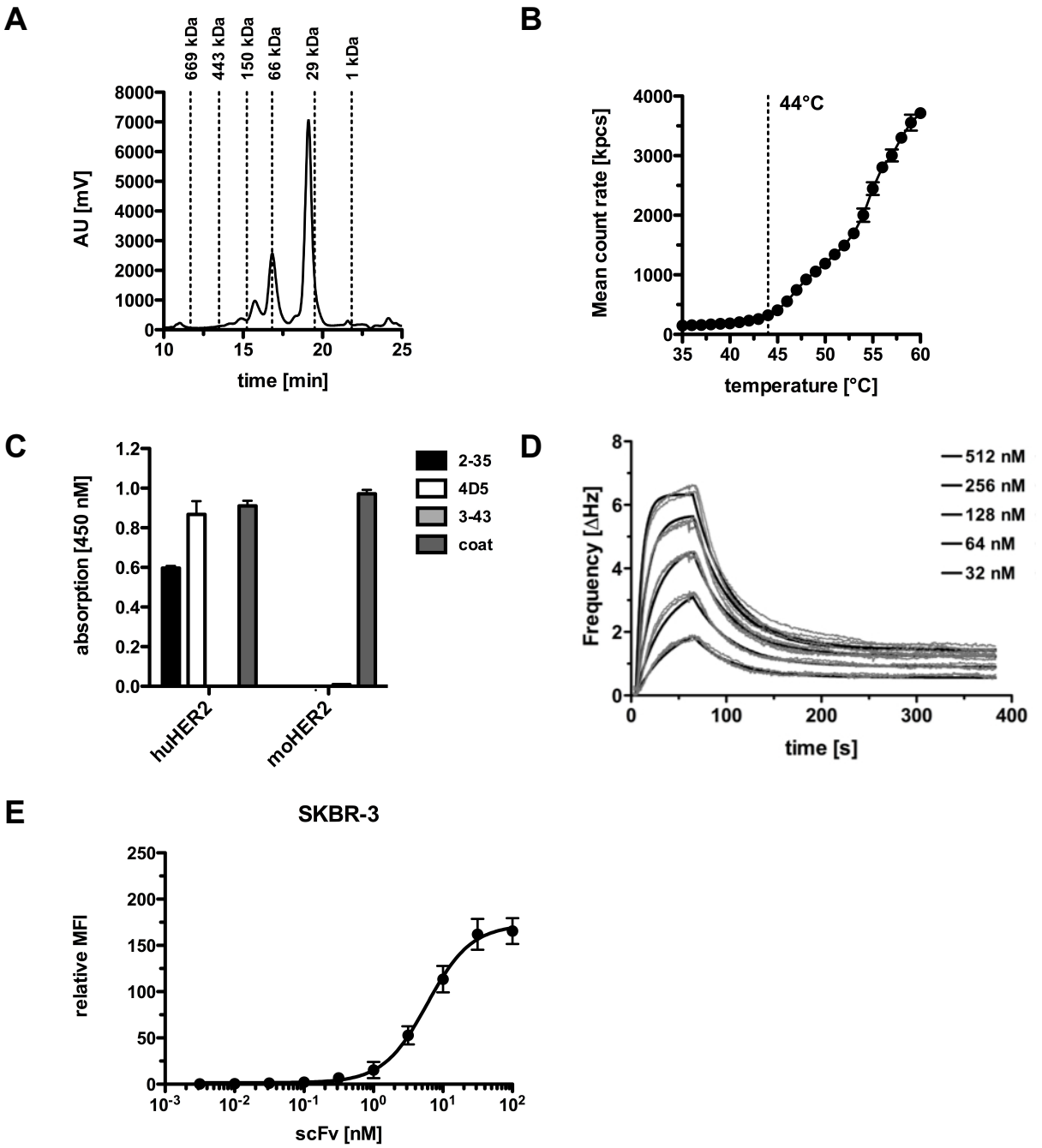

Figure 3-4: Analysis of biochemical integrity and binding characteristics of scFv 2-35

A Purity and integrity of scFv 2-35 was analyzed via size exclusion chromatography using a Yarra SEC-2000 column. Dashed lines represent the retention time of standard proteins with their molecular masses indicated above the lines. Main peek: 19,4 min **B** The aggregation point of scFv 2-35 was determined via dynamic light scattering. The measured aggregation point is indicated by a dotted line. **C** Binding to mouse HER2 was measured using ELISA technique. Recombinant mouse HER2 or human Fc tagged HER2 were immobilized to ELISA plates. 100 nM of scFv 2-35, scFv 4D5 (reference) or HER3 binding scFv 3-43 (negative control) were added and detected with HRP coupled anti-His-tag antibody. Coating was detected using HRP coupled anti-Fc antibody. Shown are means of double values with standard deviations. **D** Affinity of scFv 2-35 to HER2-Fc was measured in a QCM approach. Two-fold serial dilutions of scFv 2-35 starting from 512 nM were injected in random order into the Attana system. The measurement was performed at pH7.4. Three binding curves were measured for each concentration and fitted using TraceDrawer software (black). **E** Binding to cellular HER2 was analyzed by Flow cytometry using the HER2 overexpressing breast cancer cell line SKBR-3. Serial dilutions of scFv 2-35 were added to the detached cells. Binding of scFv 2-35 was detected with PE conjugated anti-His-tag antibody. Mean values of three independent experiments with standard deviations are shown.

3.3 Dimeric scFv-Fc fusion proteins comprising the new HER2 antibody binding sites

The four scFv proteins scFv 2-31, scFv 2-33, scFv 2-35 all showed high affinity to their cellular expressed antigen HER2. However, scFv proteins are very small and unstable. In order to create dimeric proteins of higher molecular mass and stability, scFv-Fc fusion proteins were established from the respective scFv plasmids. ELISA using HER2-Fc, and flow cytometry using SKBR-3 cells for the anti-HER2 scFv-Fc fusion proteins revealed EC_{50} values for antigen and cell binding in the low nanomolar range (Table 3-3) confirming an avidity effect for dimeric antibody molecules comprising the selected binding domains.

Table 3-3: Production yields and binding data of HER2 binding scFv-Fc fusion proteins

Half maximum binding in ELISA was measured using immobilized HER2-Fc protein and HRP coupled anti-His tag antibody for detection; n=2. Cell binding of scFv-Fc fusion proteins to SKBR3 was measured using flow cytometric analysis. Binding was detected via PE conjugated anti-human-Fc antibody; n=3.

scFv-Fc	yield (in mg|l)	ELISA (EC_{50} in nM)	cell binding (EC_{50} in nM)
2-31	6.4	1.4	1.9
2-33	3.0	1.8	0.9
2-35	4.2	0.9	0.7

The scFv-Fc fusion proteins migrated through polyacrylamide during electrophoresis with speeds corresponding to the calculated molecular weights. The double bands seen in Figure 3-5 B most likely refer to the glycosylated and unglycosylated forms of the fusion proteins. However, although the proteins looked pure and integer on SDS-PAGE analysis and bound specifically to their respective antigen as seen in Figure 3-5 D, size exclusion chromatography revealed no exclusive peaks for all of these fusion proteins (Figure 3-5 C). To get one integer antibody with not only high affinity cell binding properties, but also good effector functions enabling immune cell recruiting, the V_H and V_L domains of scFv 2-35 were in the next part of the thesis used for generation of IgG1 molecules.

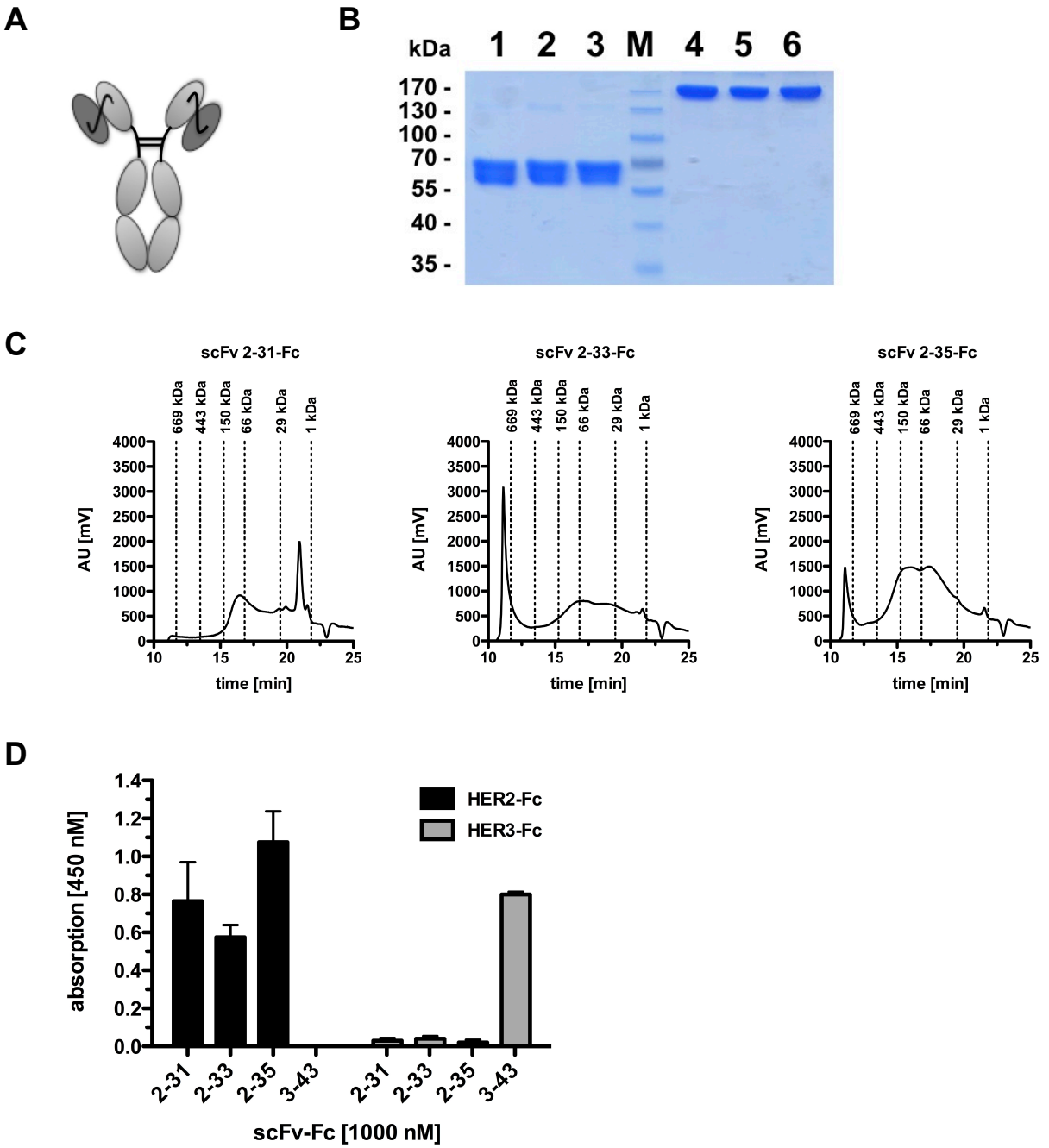

Figure 3-5: ScFv-Fc fusion proteins derived from selected HER2 and HER3 binding scFv

A Schematic illustration of the scFv-Fc fusion proteins. Dimerization is achieved by the Fc part. **B** Coomassie stained SDS-PAGE analysis of scFv-Fc proteins under reducing (left, 1-3) and non-reducing (right, 4-6) conditions. 1,4: scFv 2-31-Fc. 2,5: scFv 2-33-Fc. 3,6: scFv 2-35-Fc. M: protein standard marker. **C** Size exclusion chromatography of HER2 binding scFv-Fc proteins. **D** ELISA using immobilized HER2-Fc and HER3-Fc (receptor specificity control) to investigate antigen binding of the scFv-Fc proteins. Bound scFv-Fc proteins were detected via HRP coupled anti-His tag antibody. HER3 binding scFv 3-43-Fc served as negative control; n=1 (double values, mean ± SD).

3.4 Fully humanized IgG 2-35

To create a potent anti-cancerous drug candidate, scFv 2-35 was converted into IgG1. As a reference, IgG 2-35 was compared with the clinically well-established

antibody Trastuzumab. To improve ADCC of IgG 2-35, two amino acid substitutions (S239D/I332E) were introduced into the human Fc domain (referred to as SI) as described by Horton et al. in 2008[151]. From one liter of HEK293-6E supernatant 66 mg IgG 2-35 could be purified by protein A chromatography. In the following, IgG 2-35 was analyzed in respect of its purity, integrity, and thermal stability. Functional analysis included binding to HER2 expressing cancer cells as well as the examination of its growth inhibiting potential.

3.4.1 Biochemical analysis of IgG 2-35

SDS-PAGE analysis of IgG 2-35 under non-reducing conditions exhibited a single band at a height being in good correlation to the calculated molecular weight of 149.2 kDa, corresponding to the dimeric whole antibody. Under reducing conditions, two bands occurred, corresponding to the monomeric single heavy chain around 50 kDa and the smaller light chain around 25 kDa. In size exclusion chromatography, IgG 2-35 appeared as a single narrow peak eluted shortly after the 200 kDa standard protein. The weight estimated from the hydrodynamic radius revealed in this measurement was 186.6 kDa. This slightly bigger hydrodynamic radius was also observed for other IgG molecules and presumably accounts to glycosylation. Trastuzumab, which was run on the same day on the same column was estimated to have a molecular weight of 202.5 kDa. Dynamic light scattering measurement revealed that the protein was stable up to a temperature of 68 °C.

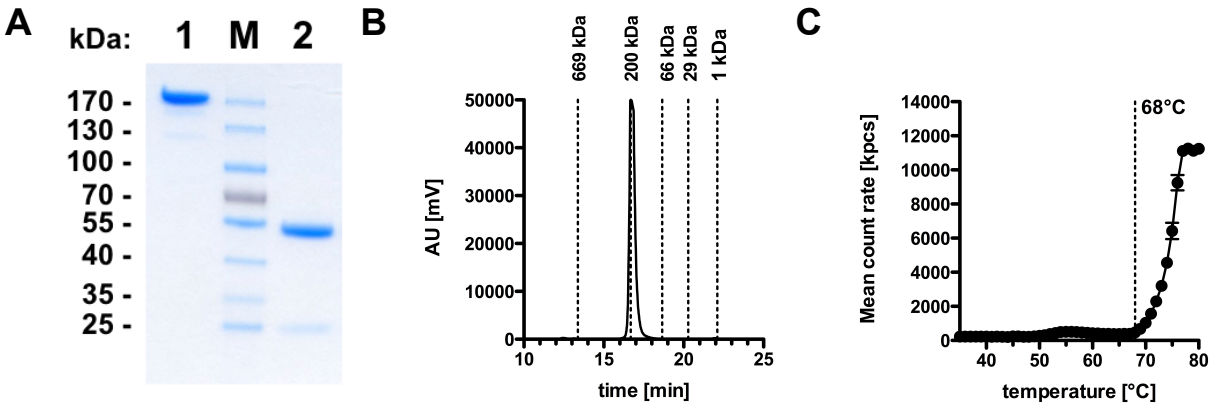

Figure 3-6:Biochemical characterization of IgG 2-35

A SDS-PAGE analysis of IgG 2-35 under non-reducing (line 1) and reducing (line 2) conditions. **B** Size exclusion chromatography of IgG 2-35 using a Yarra SEC-2000 column. (186,6 kDA hydrodynamic radius) **C** Determination of the aggregation point of IgG 2-35 was performed using dynamic light scattering. The measured aggregation point is indicated with a dotted line.

3.4.2 Binding property of IgG 2-35

ELISA using HER2-Fc revealed an EC_{50} of 350 pM for HER2-ECD binding of IgG 2-35. In flow cytometric analysis, IgG 2-35 bound with EC_{50} of 330 pM and 200 pM to SKBR-3 and Colo 205 cells, respectively. According to these measurements, binding capacity of IgG 2-35 is superior to Trastuzumab, which bound in the same assays with EC_{50} of 490 pM, 2.5 nM and 500 pM, respectively (not shown).

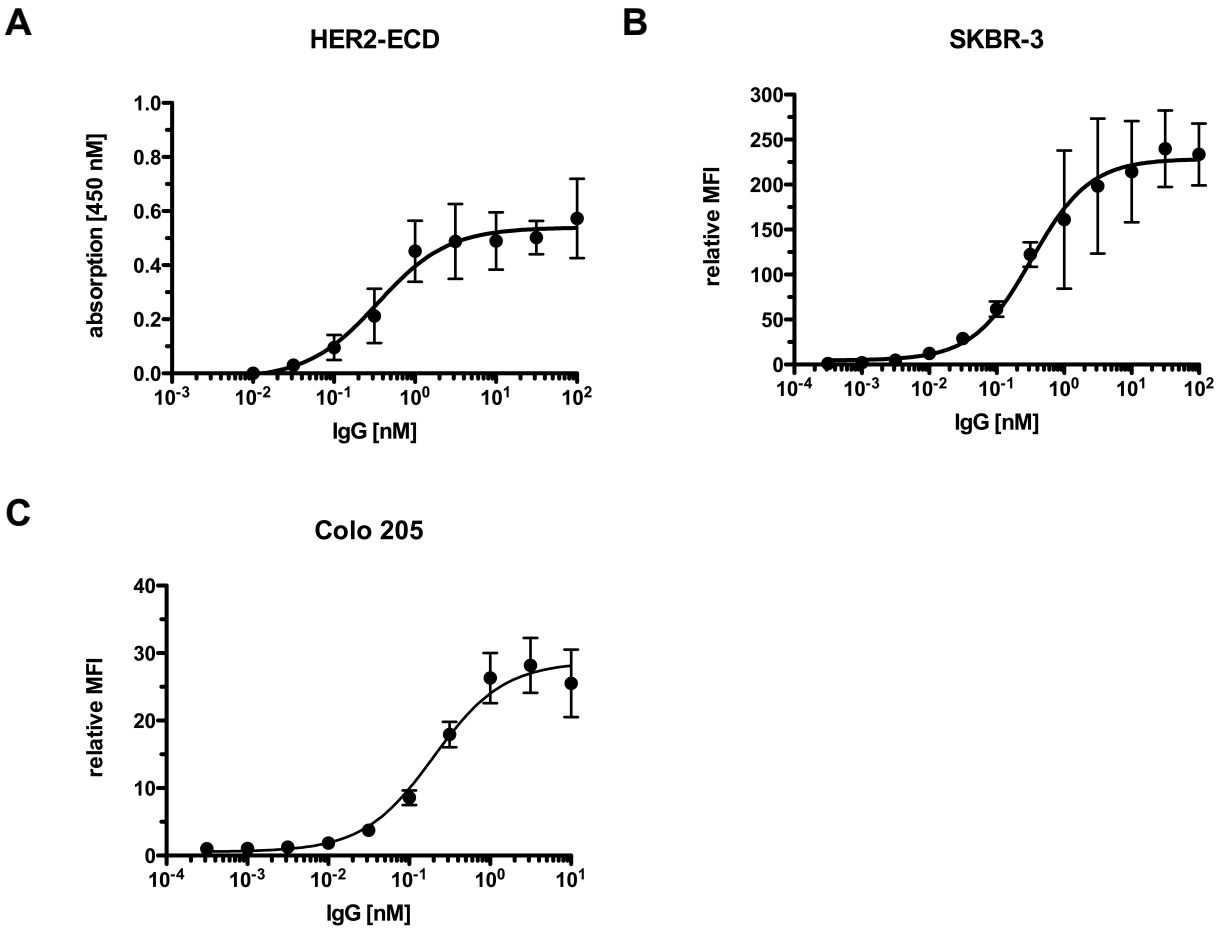

Figure 3-7: Binding characteristics of IgG 2-35

A Binding of IgG 2-35 to recombinant HER2 was analyzed by ELISA using HRP coupled F_{ab}-specific anti-human IgG antibody for detection of the bound IgG. (EC_{50}: 346 pM) **B, C** Binding of IgG 2-35 to cellular HER2 was analyzed by Flow cytometry using HER2 overexpressing SKBR-3 (B) cells (EC_{50}: 327 pM) and Colo 205 (C) (EC_{50}: 200 pM). Bound IgG was detected using PE conjugated anti-human Fc antibody. A,B,C: n=3, ± SD.

3.4.3 IgG 2-35 decelerates growth of HER2 expressing cancer cell lines *in vitro*

A good binding capacity is a favored characteristic of therapeutic antibodies. However, strong binding to growth receptors does not necessarily translate in antiproliferative activity. To monitor the growth inhibiting potential of IgG 2-35,

proliferation assays using the HER2 overexpressing breast and gastric cancer cell lines BT-474 and NCI-N87 were performed. For BT-474, presence of IgG 2-35 reduced the EGF stimulated growth and led to reduction of 40 % in cell count. Trastuzumab also led to a reduction in cell count after six days, but only about 20 %. EGFR binding cetuximab served as positive reference and also led to reduced proliferation of BT-474 cells in the presence of EGF. For NCI-N87, both Trastuzumab and cetuximab led to a 20 % reduction of living cells after six days. Here, IgG 2-35 was significantly superior with only less than 60 percent of the cell amount in the control antibody incubated wells present. However, for SKBR-3 cells incubated in normal growth medium in the absence of EGF, no growth inhibiting effect of IgG 2-35 (up to 3 µg/ml) could be observed, while the same amount of trastuzumab inhibited SKBR-3 proliferation (data not shown).

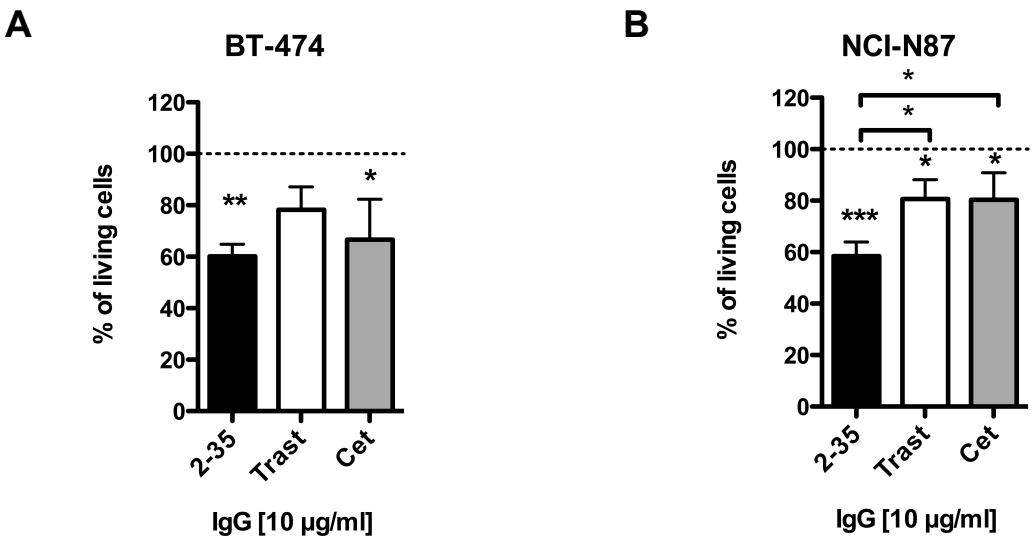

Figure 3-8: Proliferation inhibiting function of IgG 2-35

A Semi confluent proliferating BT-474 breast cancer cells were detached and diluted to 10.000 cells per ml. 100 µl of the cell suspension was pipetted in the wells of a 96 well cell culture plate. After 24 hours' adhesion time 10 µg/ml of the indicated IgG molecules were added to the cells in low FCS but 10 ng/ml EGF containing culture medium. After seven days, the experiment was stopped and the amount of viable cells was measured using CCK-8 cell viability kit. The obtained absorbance values were normalized to cells treated with an irrelevant control IgG (Atrosab). **B** The same experiment like in A was performed using the gastric cancer derived cell line NCI-N87. A, B: n=3, mean ± SD.

3.5 Screening of scFv proteins for a high affinity HER3 binder

A panel of anti-HER3 scFv was isolated from a human antibody phage library by selection against a human HER3-Fc fusion protein (aa 20-643) prior to this study. The production yields were located between 0.2 and 2.9 mg per liter cell suspension. In SDS-PAGE analysis, all scFv proteins appeared as single bands at heights corresponding to the calculated molecular weights (around 30 kDa for all scFv proteins) (Figure 3-9). All eight clones showed binding to HER3-Fc in ELISA with EC_{50} in the nanomolar range (shown in Figure 3-10 and Table 3-4) and were further analyzed for binding to HER3-expressing MCF-7 cells by flow cytometry. Here, one of the clones showed particularly strong cell binding. This clone, scFv 3-43, also depicted the best production yields and lowest EC_{50} in ELISA between the analyzed clones. Furthermore, it also showed better binding performance than scFv 3M6, which was derived from the variable domains of the currently clinically tested Seribantumab (MM-121), comprising one stabilizing mutation (Cys89Ser) and connected via a flexible G_4S-linker, and served as reference. Therefore, scFv 3-43 was chosen as candidate for further development and was thoroughly analyzed in the following.

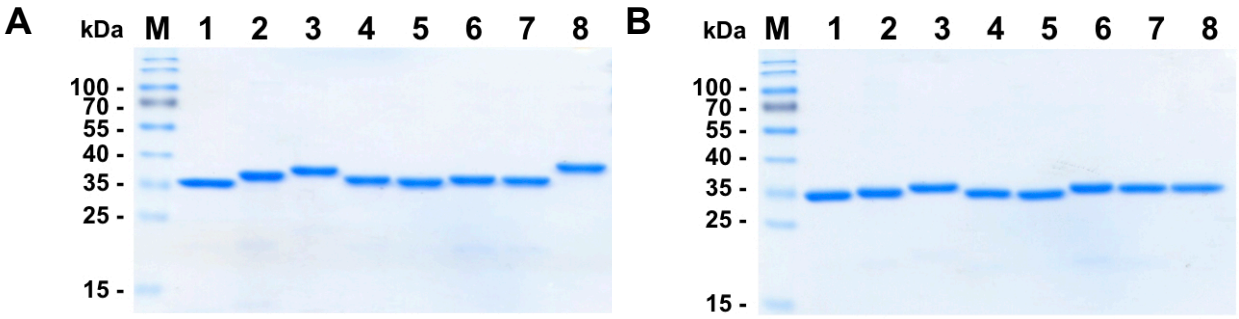

Figure 3-9: SDS-PAGE analysis of the purified HER3 binding scFv proteins

SDS-PAGE (Coomassie stained) under reducing (A) and non-reducing (B) conditions analyzing scFv 3-38 (lane 1), scFv 3-39 (lane 2), scFv 3-40 (lane 3), scFv 3-41 (lane 4), scFv 3-42 (lane 5), scFv 3-43 (lane 6), scFv 3-44 (lane 7) and scFv 3-45 (lane 8) (M, protein standard marker).

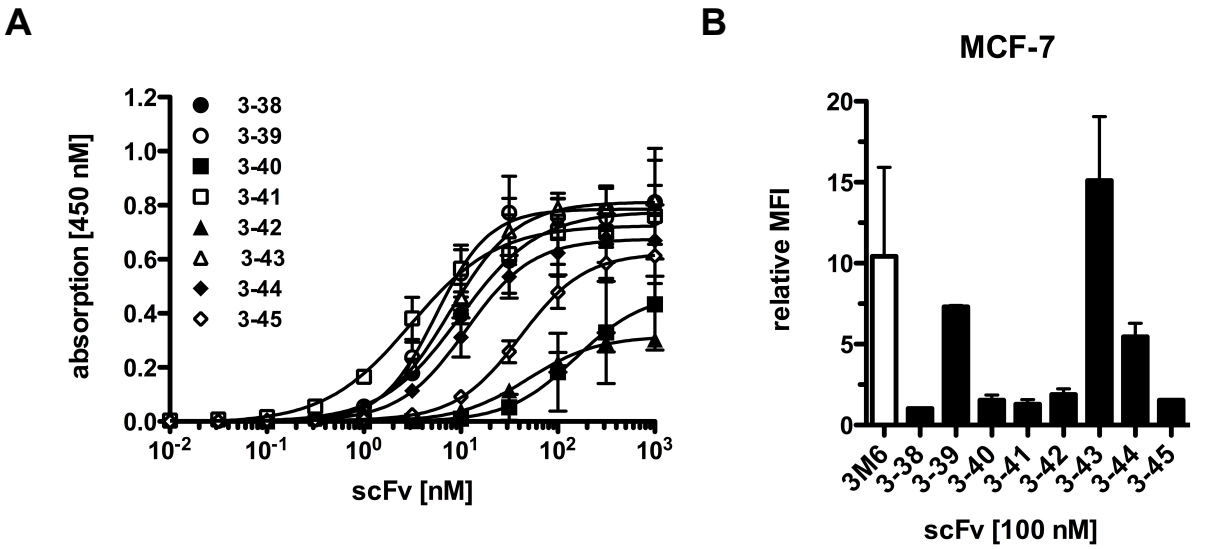

Figure 3-10: HER3 binding of scFv proteins

A Binding of the scFv proteins to HER3 was investigated by ELISA. Serial dilutions of the scFv proteins were added to immobilized Fc tagged HER3 on ELISA plates. The scFv proteins were detected by HRP coupled anti-His-tag antibody. Shown are mean values of n=3 ± SD. **B** Binding of the scFv proteins to cellular HER3 was analyzed by Flow cytometry using HER3 expressing MCF-7 human breast cancer cells. 100 nM of the indicated scFv proteins were incubated with the detached cells and bound scFv was detected via PE conjugated anti-His-tag antibody (mean of double values ± SD).

Table 3-4: Yields and binding data of the 8 selected scFvs.

Binding to human HER3-Fc was analyzed by ELISA. Binding to MCF-7 cells was analyzed by flow cytometry.

scFv	yield (in mg|l)	ELISA (EC_{50} in nM ± SD)	cell binding (EC_{50} in nM ± SD)
3M6	0.4	7.6 ± 3.5	3.3 ± 1.3
3-38	1.3	9.9 ± 1.1	n/a
3-39	1.2	5.8 ± 1.6	8.5
3-40	0.4	88.4 ± 1.7	n/a
3-41	0.5	3.4 ± 1.3	n/a
3-42	0.5	56.8 ± 22.3	n/a
3-43	2.9	3.5 ± 2.8	0.7 ± 0.3
3-44	2.4	11.4 ± 0.6	7.6
3-45	0.2	42.4 ± 8.8	n/a

ScFv3-43 showed a clearly dominating peak in HPLC-SEC at 18.9 minutes, corresponding to a hydrodynamic radius that correlated to an estimated molecular weight of 38.7 kDa, which is in good accordance to the calculated MW of 31.1 kDa. An aggregation temperature of scFv 3-43 of 58 °C was determined by dynamic light scattering. Moreover, scFv3-43 bound in addition to human HER3-Fc also to its mouse counterpart, however, with a slightly reduced EC_{50} value, meaning that scFv

3-43 binds to a conserved epitope on HER3 (Figure 3-11 C). Human HER3, expressed on the surface of MCF-7 cells was bound by scFv 3-43 with an EC_{50} value of 700 pM as determined by Flow cytometry (Figure 3-11 D).

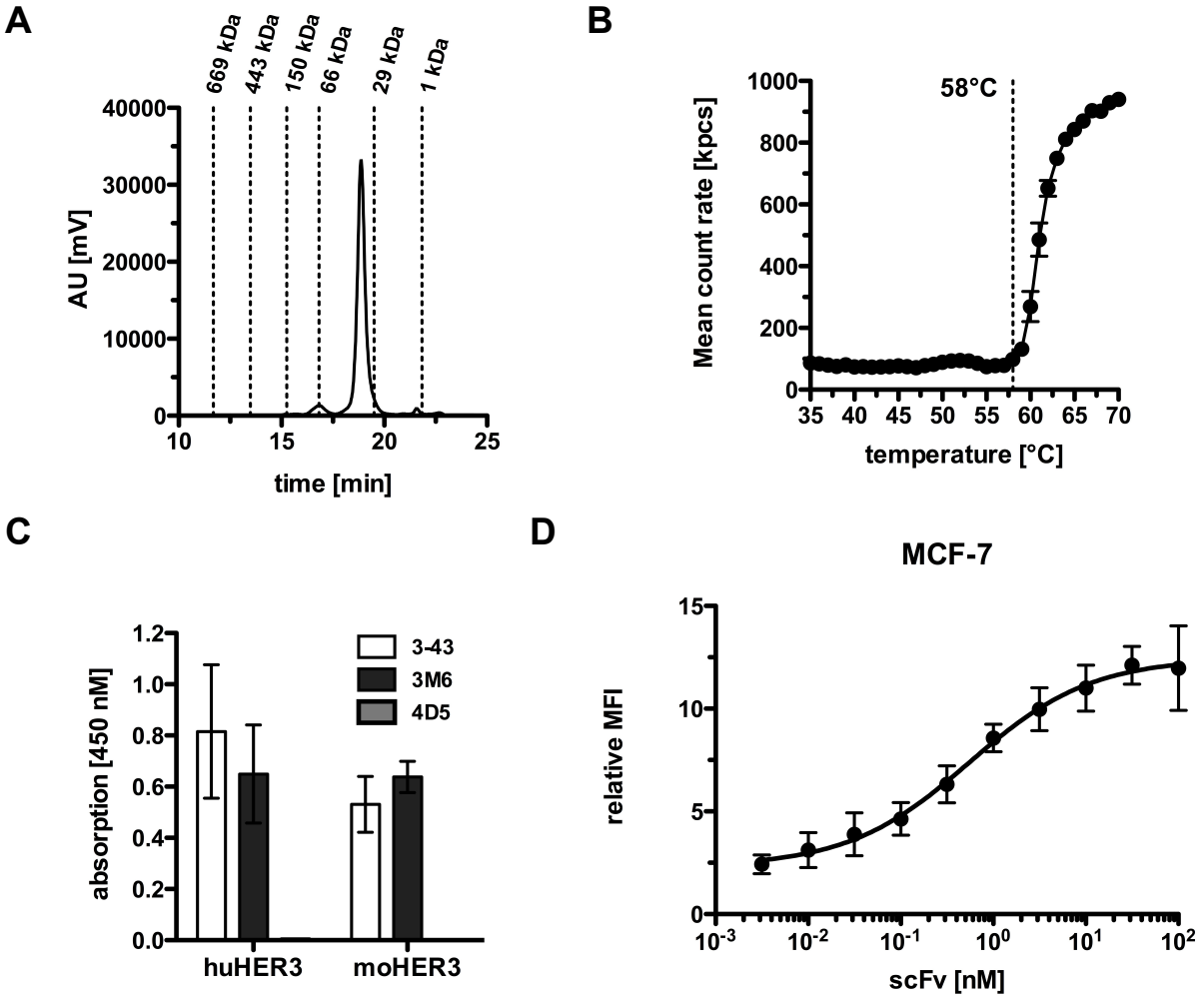

Figure 3-11: Characterization of scFv 3-43

A 25 µl of scFv 3-43 was analyzed for its purity and integrity via size exclusion chromatography on a Yarra SEC-2000 column, with PBS as liquid phase. Dashed lines represent the retention time of standard proteins with their molecular masses indicated above the lines. Main peek: 18,9 min. **B** The aggregation point of scFv 3-43 was determined via dynamic light scattering. The measured aggregation point is indicated by a dotted line. **C** Binding to mouse HER3 was tested by ELISA. Recombinant mouse HER3 or human Fc tagged HER3 were immobilized to ELISA plates. 100 nM of scFv 3-43, scFv 3M6 (reference) or HER2 binding scFv 4D5 (negative control) were added and detected with HRP coupled anti-His-tag antibody. n=2. Shown are double values of one representative experiment ± SD. **D** Binding to cellular HER3 was analyzed by Flow cytometry using the HER3 expressing breast cancer cell line MCF-7. Serial dilutions of scFv 3-43 were added to the detached cells. Binding of scFv 3-43 was detected with PE conjugated anti-His-tag antibody; n=3, mean ± SD.

The scFv 3-43 was further analyzed in immunoblotting experiments for binding to reduced and non-reduced HER3-Fc. The experiment shown in Figure 3-12 indicated a complex epitope for scFv 3-43 on HER3 that is reduction sensitive, meaning that it

does not recognize only the primary amino acid sequence, but needs a correct spatial conformation for binding.

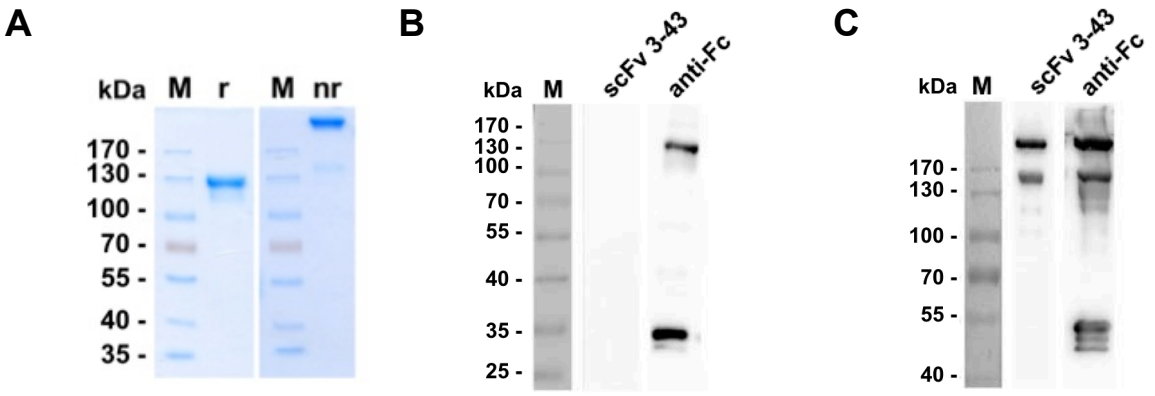

Figure 3-12: Analysis of scFv 3-43 for binding to reduced and non-reduced HER3-Fc.

A Coomassie stained SDS-PAGE of HER3-Fc under reducing (r) and non-reducing (nr) conditions. **B** Immunoblot analysis of reduced HER3-Fc (5 µg per lane) for binding of scFv 3-43. An anti-Fc antibody was included as a positive control. ScFv 3-43 was detected via HRP coupled anti-His antibody. HER3-Fc was detected via HRP coupled anti-Fc antibody. **C** Immunoblot analysis of non-reduced HER3-Fc (5 µg per lane) for binding of scFv 3-43. An anti-Fc antibody was included as a positive control. ScFv 3-43 and HER3-Fc were detected as in (B).

For being able to locate this complex conserved binding epitope of scFv 3-43, the extracellular domain of HER3 was subdivided in its four domains and truncated versions of HER3-Fc were produced, each lacking one more extracellular domain. The truncated versions of HER3-Fc (aa 20-643), namely $HER3_{DII-IV}$-Fc (aa 208-643), $HER3_{DIII-IV}$-Fc (aa 329-643) and $HER3_{DIV}$-Fc (aa 532-643), were produced in stably transfected HEK293 cells and purified from the supernatant via protein A chromatography. SDS-PAGE analysis shown in figure 3-7 A depicts bands in the expected size ranges for all constructs. Due to glycosylation, the bands appeared a bit smeared or as double bands. These constructs were coated in ELISA plates and binding of scFv 3-43 was examined. The experiment revealed that the extracellular domain III of HER3 was needed for binding of scFv 3-43, since the scFv bound to all constructs comprising this domain.

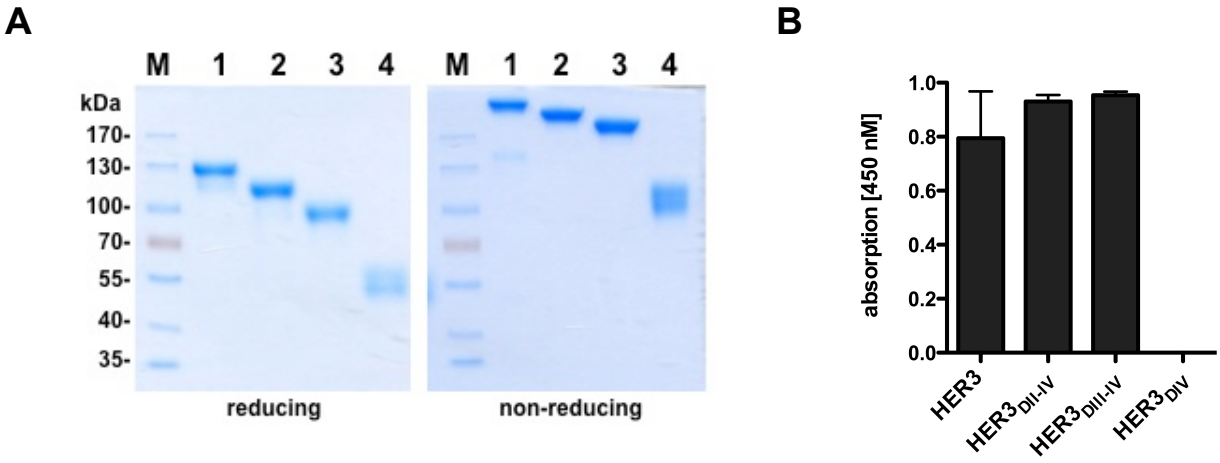

Figure 3-13: Epitope mapping of the 3-43 binding site

A SDS PAGE analysis under reducing and non-reducing conditions of the full ECD and truncated HER3-Fc fusion proteins. Lane 1: HER3-Fc comprising the full HER3 extracellular domain. Line 2: $HER3_{DII-IV}$-Fc lacking the first extracellular domain. Line 3: $HER3_{DIII-IV}$-Fc lacking the first two extracellular domains of HER3. Line 4: $HER3_{DIV}$-Fc lacking the domains one to three of the HER3 ECD. **B** Mapping of the epitope of scFv 3-43 to the four different HER3 extracellular domains was performed by ELISA. 10 ng of the full and truncated HER3-ECD-Fc fusion proteins were immobilized on ELISA plates. 100 nM of scFv 3-43was applied and detected with HRP coupled anti-His-tag antibody. One representative of two independent experiments is shown with mean of double values ± SD.

Together with the extracellular domain I of HER3, domain III is involved in ligand binding. Binding to this domain therefore can potentially inhibit ligand induced signaling pathway activation. To test the ligand dependent signaling inhibiting potential of scFv 3-43 and of the second best HER3 binding clone scFv 3-39, MCF-7 cells were incubated with the HER3 binding scFv proteins or with an irrelevant scFv as control for 15 or 60 minutes, followed by a 15 minutes lasting heregulin stimulus. Whole cell lysates were substracted to Western blotting and the phosphorylation status of HER3, HER2, Akt and the MAPK Erk (isoforms 1 and 2) was analyzed (fig. 3-8). In the absence of heregulin, HER2, HER3, Akt and Erk(1/2) were hardly phosphorylated. Heregulin stimulation induced strong bands for phosphorylated HER3, Akt and Erk and a weaker band for phosphorylated HER2. Preincubation with scFv 3-43 strongly reduced phosphorylation of HER3, HER2 and Akt. Erk phosphorylation could also be reduced, at least after 15 minutes of scFv preincubation. The scFv control scFv Gal12 did not reduce heregulin induced protein phosphorylation. Preincubation with scFv 3-39 for 60 minutes also reduced HER3 phosphorylation and phosphorylation of Akt also was reduced through preincubation with scFv 3-39. However, heregulin induced Erk phosphorylation could not be

prevented by scFv 3-39. This highlighted the suitability of scFv 3-43 for the development of a fully human antibody to test its supposable anti-cancer effect.

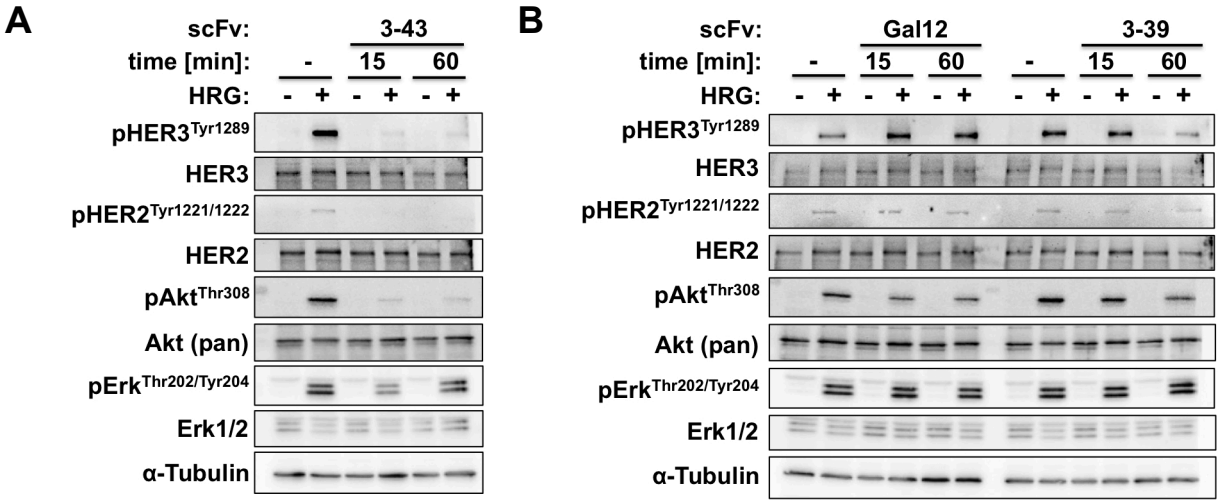

Figure 3-14: scFv 3-43 blocks HRG induced signaling

A Semi confluent MCF-7 cells were incubated at 37°C with 10 µg/ml scFv 3-43 for 15 minutes or one hour before addition of 50 ng/ml heregulin-β. After 15 minutes heregulin stimulation the cells were lysed and subjected to immunoblotting with the indicated antibodies. One representative out of three independent experiments is shown. **B** The same experiment like in A was performed using Gal12 binding scFv as control and the HER3 binding scFv 3-39.

3.6 Dimeric scFv 3-43-Fc

The scFv protein 3-43 showed high affinity to its cellular expressed antigen HER3. However, scFv proteins are very small and unstable. In order to create a dimeric protein of higher molecular mass and stability, a scFv-Fc fusion protein was established from the respective scFv plasmid. ScFv 3-43-Fc was produced in adherent HEK293T cells and purified via protein A chromatography with yields about 1 mg per liter cell supernatant. ELISA using HER3-Fc and flow cytometry using MCF-7 cells revealed EC_{50} values for antigen and cell binding in the low nanomolar range (Table 3-5), confirming an avidity effect for dimeric antibody molecules comprising the selected binding domains.

Table 3-5: Production yields and binding data of scFv 3-43-Fc

scFv-Fc	yield (in mg|l)	ELISA (EC_{50} in nM)	cell binding MCF-7 (EC_{50} in nM)
3-43	1.1	0.8	0.1

The scFv-Fc fusion protein migrated through polyacrylamide during electrophoresis with a migration rate fitting to the calculated molecular weight. The double band seen in Figure 3-15 A most likely refers to the glycosylated and unglycosylated forms of

the fusion protein. However, although the protein looked pure and integer on SDS-PAGE analysis and bound specifically to its antigen as seen in Figure 3-15 C, size exclusion chromatography revealed no exclusive peak (Figure 3-15 B). To get an integer antibody with not only high affinity cell binding properties, but also good effector functions enabling immune cell recruiting, the V_H and V_L domains of scFv 3-43 were in the next part used for generation of IgG1 molecules.

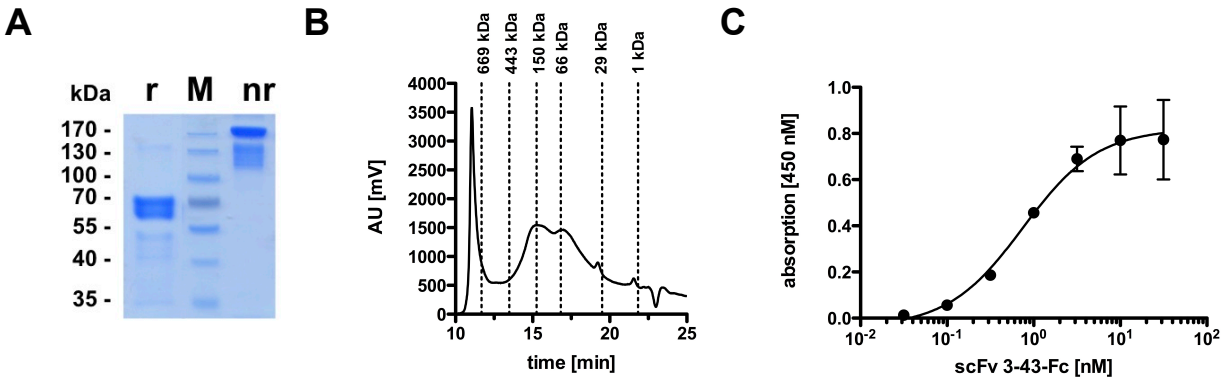

Figure 3-15: Analysis of scFv 3-43-Fc

A Coomassie stained SDS-PAGE of scFv 3-43-Fc **B** SEC of scFv 3-43-Fc **C** ELISA of scFv 3-43-Fc using HER3-Fc for coating and HRP-coupled anti-His tag antibody for detection; n=3 ± SD.

3.7 IgG 3-43

In order to construct a new HER3 binding antibody, scFv 3-43 was converted into a human IgG1 (IgG 3-43). To improve ADCC, two amino acid substitutions (S239D/I332E) were introduced into the human Fc domain (referred to as SI) as described by Horton et al. in 2008[151]. Approximately 43 mg IgG 3-43 could be purified from one liter of supernatant.

To be able to compare binding and inhibiting properties of IgG 3-43 to a clinically tested HER3 targeting antibody, the binding sites of Seribantumab were used for cloning of a fully human IgG1 molecule with the same Fc part like IgG 3-43.

3.7.1 Biochemical analysis of IgG 3-43

The calculated molecular weight of IgG 3-43 accounts to 149.2 kDa. SDS-PAGE analysis was performed after purification. IgG 3-43 exhibited one single band under non-reducing conditions in the range of approximately 150 kDa, corresponding to the antibody dimer. Under reducing conditions, two bands in the range of 50 kDa and

25 kDa corresponding to the heavy and light antibody chains were observed. In size exclusion chromatography, IgG 3-43 eluted as one single narrow peak. This experiment estimated the weight of IgG 3-43 to be 213.6 kDa. The bigger hydrodynamic radius presumably accounts to glycosylation. Dynamic light scattering revealed a thermal stability of IgG 3-43 up to a temperature of 69 °C.

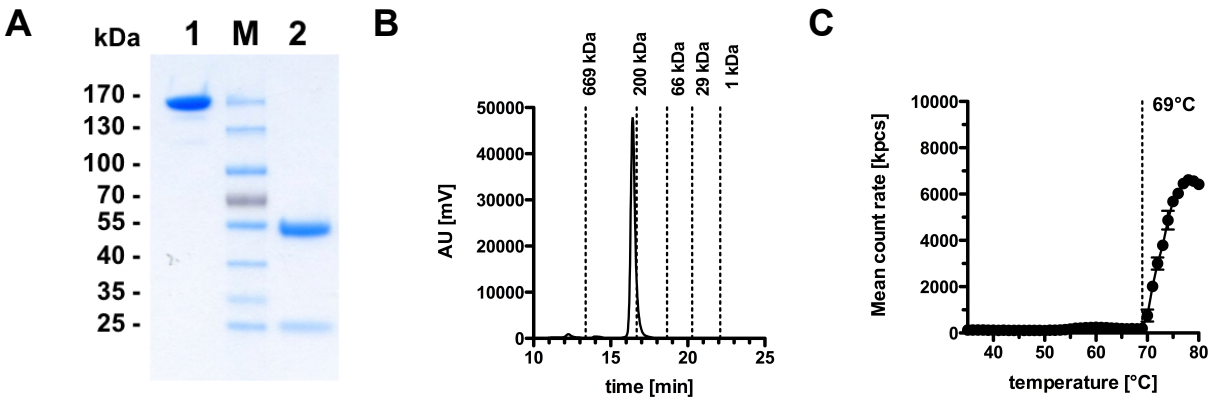

Figure 3-16: Biochemical analysis of IgG 3-43

A Coomassie stained SDS-PAGE analysis of IgG 3-43 under non-reducing (lane 1) and reducing (lane 2) conditions. **B** Size exclusion chromatography of IgG 3-43 using a Yarra SEC-2000 column. **C** The thermal stability of IgG 3-43 was analyzed using dynamic light scattering. The measured aggregation point was indicated by a dotted line.

3.7.2 Binding property of IgG 3-43

IgG 3-43 showed dose dependent binding to HER3-Fc in ELISA with an EC_{50} of 1.1 nM. Cell binding as measured with the HER3 expressing breast cancer cell lines MCF-7 and SKBR-3 revealed EC_{50} values of 30 pM and 20 pM, respectively. EC_{50} of IgG 3-43 binding to FaDu cells, which express only low levels (about 2900 receptors per cell) of HER3, was determined to 3 pM. Compared to IgG 3M6, IgG 3-43 was clearly superior with three to six-fold lower EC_{50} values. IgG 3M6 bound to HER3-Fc in ELISA with EC_{50} of 3.6 nM and to MCF-7 and SKBR-3 cells with 1.1 nM and 1.2 nM, respectively (not shown).

Table 3-6: Binding of 3-43 and 3M6 antobody constructs

Construct	3-43: antigen binding (EC_{50} in nM)	3-43: cell binding (EC_{50} in nM)	3M6: antigen binding (EC_{50} in nM)	3M6: cell binding (EC_{50} in nM)
scFv	1.3	0.6	4.4	3.3
scFv-Fc	0.8	0.1	NA	NA
IgG1	1.1	0.003 - 0.03	3.6	1.1 - 1.2

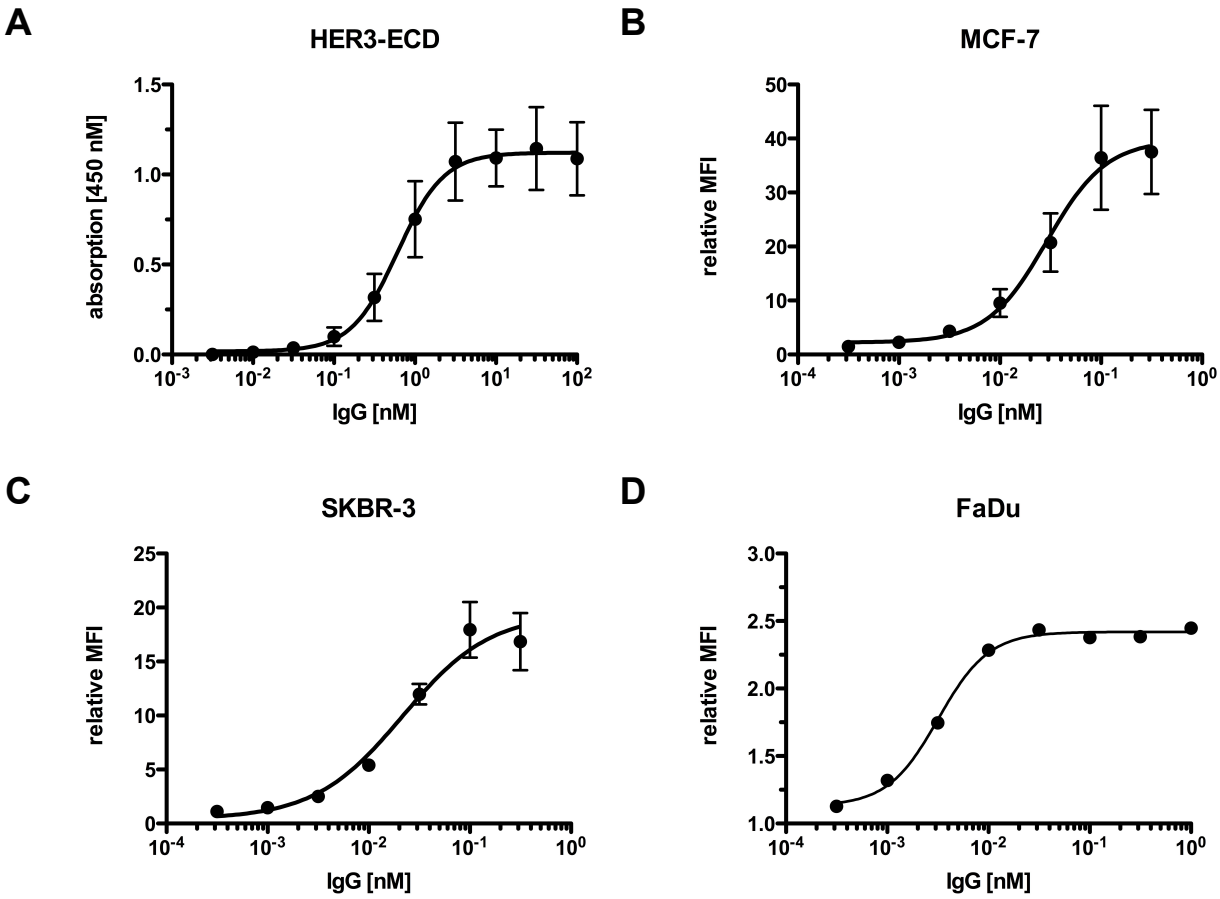

Figure 3-17: HER3 and cell binding characteristics of IgG 3-43

A Binding of IgG 3-43 to recombinant HER3 was analyzed by ELISA using HRP coupled F_{ab}-specific anti-human IgG antibody for detection of the bound IgG. **B, C** Binding of IgG 3-43 to cellular HER3 was analyzed by Flow cytometry using HER3 expressing breast cancer cell lines MCF-7 (B) and SKBR-3 (C). Bound IgG was detected using PE conjugated anti-human Fc antibody. **D** Binding of IgG 3-43 to FaDu cells was analyzed by Flow cytometry. Bound IgG was detected using PE conjugated anti-human Fc antibody. All: n=3, mean values ± SD.

In total, a panel of 12 cell lines was analyzed by flow cytometry for binding of IgG 3-43. For the human non-cancer cell line HEK 293 and for the ovarian cell line SKOV-3, which showed the lowest HER3 expression levels of the cells analyzed in chapter 3.1 (less than 1000 receptors per cell), no binding of 100 pM IgG 3-43 could be detected. The human cancer cell lines A431, A549, BT474, Caco-2, Colo 205, FaDu, HCT-116, MCF-7, NCI-N87 and SKBR-3 all were specifically bound by IgG 3-43.

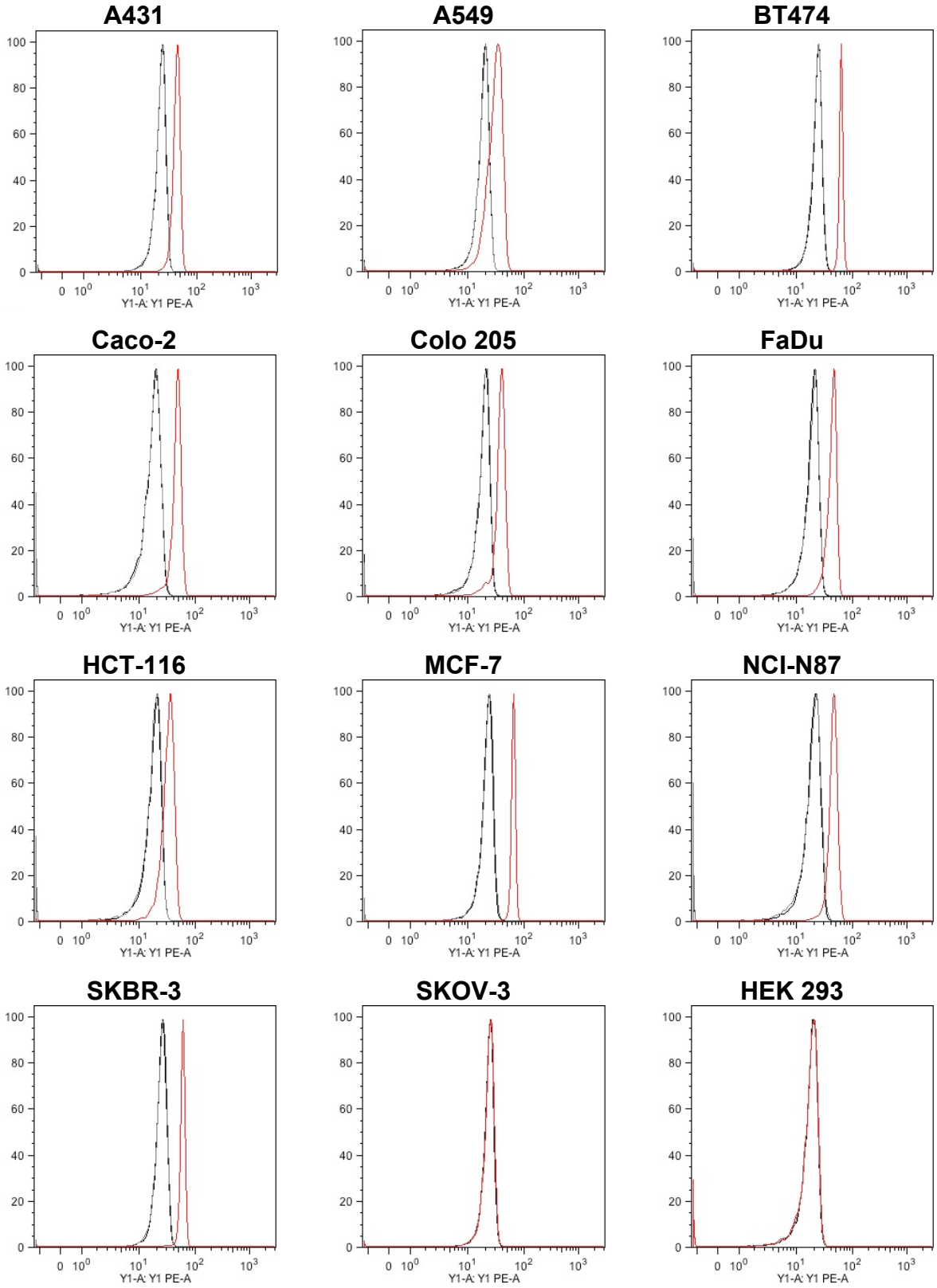

Figure 3-18: IgG 3-43 binds to numerous human cancer cell lines

Binding of 100 pM IgG 3-43 was detected via flow cytometry with PE conjugated anti-human Fc antibody. Human Embryonic Kidney 293 cells (HEK 293, non-cancer) served as negative control. Fluorescence intensities were analyzed using FlowJo software. Black: unstained; grey: detection control (anti hu-Fc PE); red: IgG 3-43.

In order to get more detailed information about the affinity between IgG 3-43 and HER3, quartz crystal microbalance measurements using the Attana system were performed. The affinity of HER3-his to IgG 3-43 was determined to 11.2 nM. The affinity for the probably bivalent interaction between IgG 3-43 and dimeric HER3-Fc was determined to 0.22 nM, highlighting an avidity-strengthened bivalent binding characteristic of IgG 3-43.

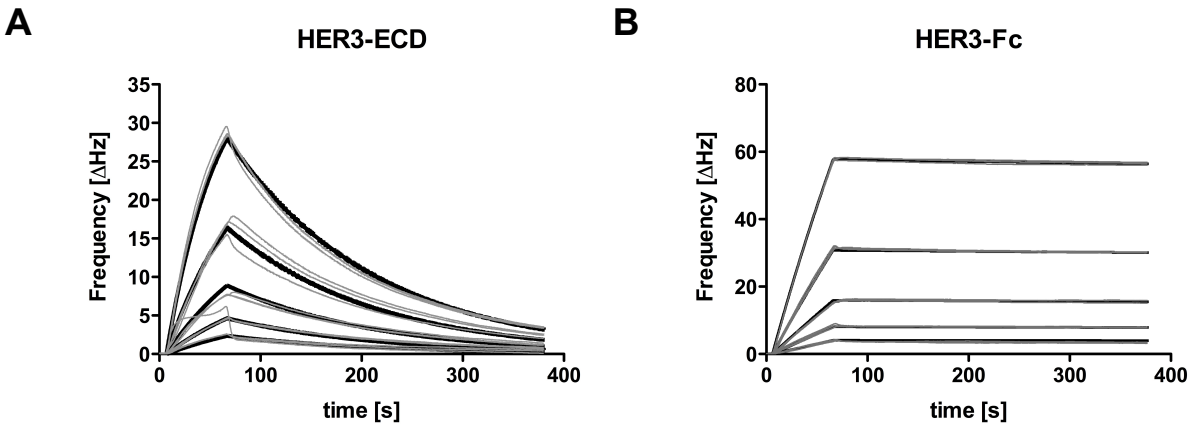

Figure 3-19: HER3 binding kinetics of IgG 3-43

The Attana A200 QCM system was used to analyze the interaction of HER3 and IgG 3-43. All measurements were performed at pH7.4. IgG 3-43 was immobilized on a LNB (low non-specific binding)-Carboxyl chip. **A** Two-fold serial dilutions of His-tagged HER3 were injected in random order into the Attana QCM system. The starting concentration was 20 nM. **B** Two-fold serial dilutions of HER3 fused to a human IgG Fc part were injected in random order into the Attana QCM system. The starting concentration was 10 nM.

Table 3-7: Monovalent and bivalent antigen binding of IgG 3-43 determined by QCM with immobilized IgG 3-43

analyte	Bmax	k_a ($M^{-1}s^{-1}$)	k_d (s^{-1})	K_D (nM)
HER3-His	63,55	$6,22*10^5$	$6,96*10^{-3}$	11.2
HER3-Fc	237,32	$4,68*10^5$	$1,03*10^{-4}$	0.22

3.7.3 Functional characterization of IgG 3-43

A functional analysis of IgG 3-43s influence on HRG binding, HER pathway activation and proliferation of cancer cells was performed in order to monitor possible anti-cancer effects of the antibody.

3.7.3.1 IgG 3-43 blocks HRG binding to HER3 expressing cells and inhibits HRG induced ErbB signaling

Epitope mapping of scFv 3-43 already showed that domain III of the HER3 ECD is crucial for the antibody-receptor interaction. Domains I and III of the HER3 ECD are known to be involved in ligand binding. Thus, it was of interest whether binding of IgG 3-43 to HER3 expressing cells prohibits heregulin binding. MCF-7 cells were incubated with recombinant his-tagged human heregulin-1 and binding was detected via flow cytometry. Preincubation with IgG 3-43 led to a reduction of about 60% of the obtained signal intensity, while preincubation with the anti-EGFR antibody cetuximab, serving as control, only showed marginal effects on heregulin binding.

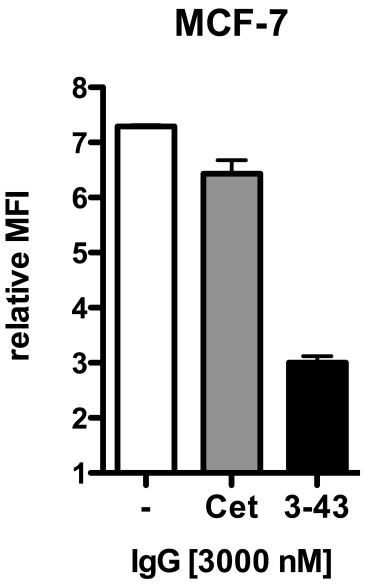

Figure 3-20: IgG 3-43 competes with HRG for binding to HER3 expressing cells

Binding of His-tagged recombinant human heregulin-β1 (50 nM) in the absence and presence of excess of IgG 3-43 (3000 nM) was measured by flow cytometry via PE conjugated anti-His antibody. Preincubation of EGFR binding Cetuximab was performed for IgG control. Mean of double values ± SD of one representative out of two independent experiments are shown.

Since IgG 3-43 inhibits heregulin binding to HER3 expressing cells, it seems obvious that the antibody also may inhibit heregulin induced receptor phosphorylation. Six different cell lines were used to study the influence of IgG 3-43 on constitutively present and heregulin-induced phosphorylation of EGFR family receptors and prominent representative proteins of the downstream signaling pathways. The six cell lines, MCF-7, BT-474, NCI-N87, FaDu, A549 and A431 represent not only different

cancer types, but also different receptor expression patterns and cancer driving mechanisms.

In MCF-7 cells, EGFR phosphorylation could not be detected. HER2 was phosphorylated in all samples. HER2 phosphorylation was not significantly affected from heregulin stimulation or either antibody. HER3 phosphorylation was detected only after heregulin stimulation. IgG 3-43 potently reduced the signal almost to an undetectable level. Total HER3 levels also were strongly reduced after IgG 3-43 incubation. However, HER3 levels seemed slightly weaker as well in the samples treated with the control antibody Rituximab. Phosphorylation of Akt was induced by heregulin stimulation. This was again strongly inhibited through IgG 3-43. Erk1 and Erk2 were already slightly phosphorylated in unstimulated MCF-7 cells. The phosphorylation levels were increased after heregulin stimulation and IgG 3-43 preincubation decreased this heregulin-triggered induction.
Alike for MCF-7, no influence of heregulin stimulation and IgG 3-43 on phosphorylation and expression of EGFR and HER2 could be monitored for the cell lines BT-474 and NCI-N87. However, constitutive phosphorylation of the two receptors appeared more prominent in NCI-N87. HER3 is constitutively phosphorylated in both cell lines. Heregulin induced a powerful increase in HER3 phosphorylation, which could be reduced to the level of unstimulated cell probes by IgG 3-43 preincubation. Akt phosphorylation was also induced by heregulin stimulation in both cell lines and this induction was again reduced after preincubation of IgG 3-43. Both cell lines showed a moderate constitutive phosphorylation of the Erk isoforms 1 and 2. In BT-474 cells, heregulin stimulation induced very strong Erk phosphorylation. Here, IgG 3-43 could reduce the signal almost to a basal level. For NCI-N87, no influence of IgG 3-43 on Erk phosphorylation was observed.

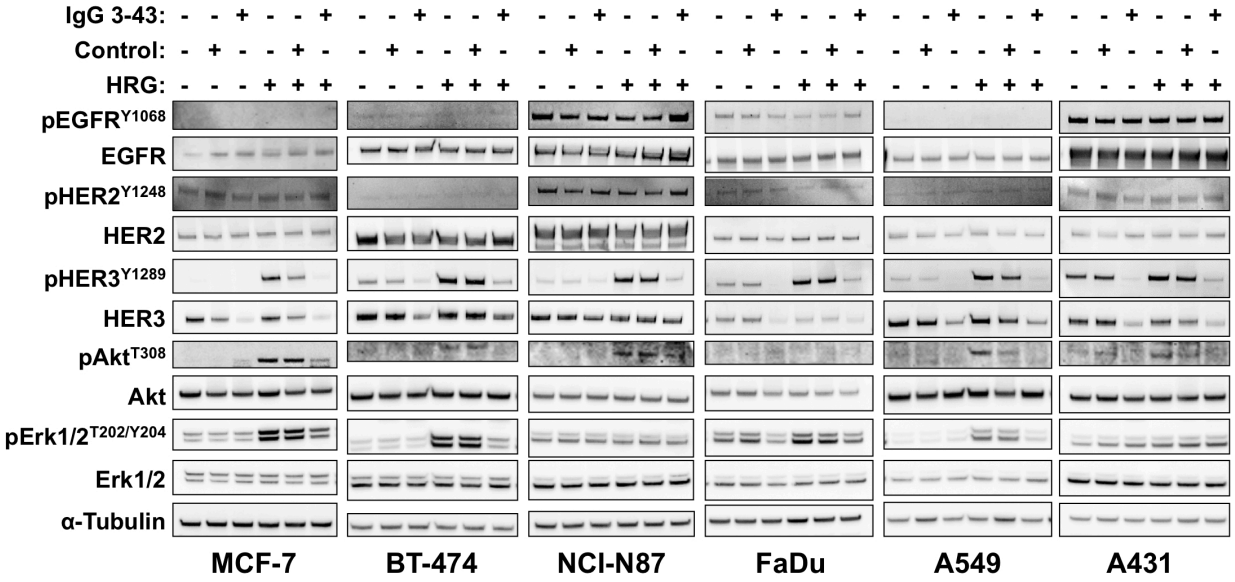

Figure 3-21: IgG 3-43 inhibits HRG mediated signaling in cancer cells

Indicated cells were seeded in 6 well plates to be semi confluent on the day of experiment. After attachment, cells were serum starved overnight and incubated for one hour with 100 nM IgG 3-43 or control (Rituximab) IgG or IgG 3-43 in the absence or presence of 50ng/ml human heregulin-β1 (HRG). Subsequently, cells were lysed with RIPA buffer containing protease inhibitors and cell lysates were analyzed by western blot using the indicated antibodies.

With the high EGFR expressing cell lines FaDu, A549 and A431, again, no influence of short-time heregulin stimulation and IgG 3-43 on EGFR and HER2 phosphorylation was observed. The signal intensities of total EGFR as well as phospho-EGFR correlated with the EGFR expression level (A431 > FaDu > A549). HER3 was constitutively phosphorylated in all three cell lines and signal strength ratios were in accordance with the expression analysis data. Heregulin reinforced HER3 phosphorylation in all three cell lines and IgG 3-43 potently reduced constitutive as well as heregulin induced HER3 phosphorylation. IgG 3-43 also led to a reduction of total HER3 levels. Akt phosphorylation was induced by heregulin stimulation in A549 and A431. This phosphorylation in turn was inhibited by IgG 3-43. Both Erk isoforms were phosphorylated in unstimulated cells to different extend, with a very strong constitutive Erk phosphorylation seen in FaDu cells. Here, IgG 3-43 could reduce the phosphorylation level. Heregulin enforced Erk phosphorylation in A549 and FaDu cells, but not in A431. The heregulin induced Erk phosphorylation could be inhibited with IgG 3-43.

For all six examined cell lines, 100 nM IgG 3-43 were sufficient to block heregulin induced phosphorylation of HER3. To get a better idea of the concentration needed

for this blockade, IgG 3-43 was titrated on MCF-7 cells, which were subsequently stimulated with heregulin. The levels of phosphorylated and total HER3 were analyzed by western blot. 10 nM IgG 3-43 were sufficient to block heregulin induced HER3 phosphorylation in MCF-7 cells. The IC_{50} value of IgG 3-43 was calculated to 108 ± 36 pM (n=3, ± SD). For IgG 3M6, the IC_{50} value was 295 ± 139 pM. The total HER3 levels were also reduced after incubation of IgG 3-43 in a dose-dependent manner.

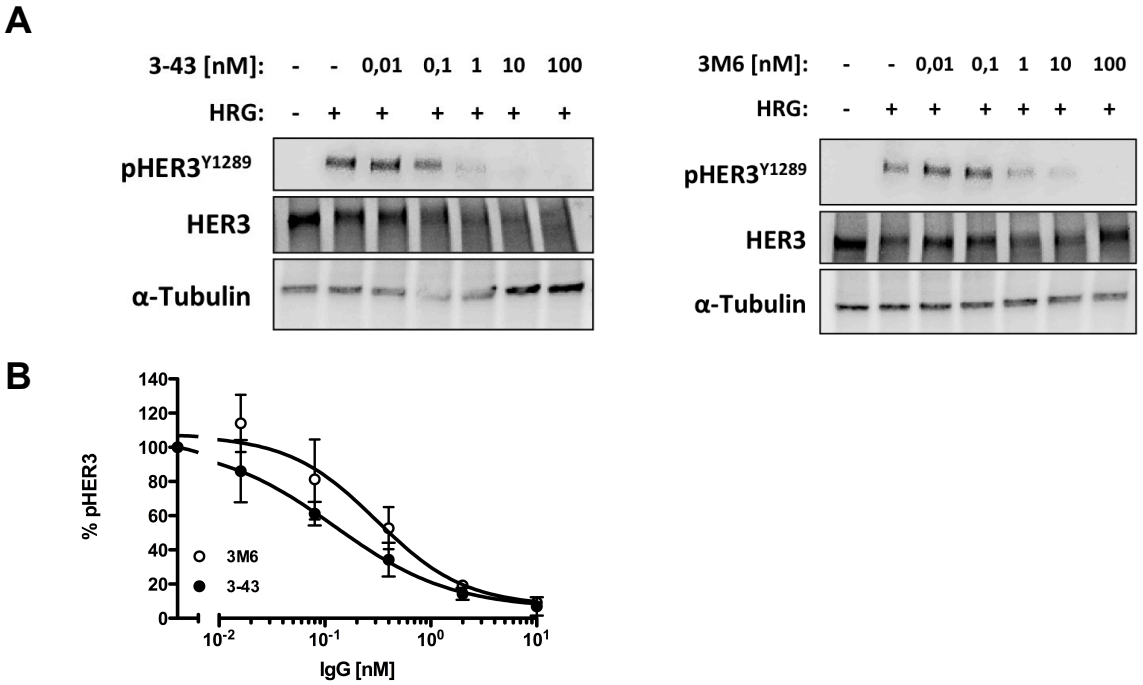

Figure 3-22: Low nanomolar concentration of IgG 3-43 is able to block HER3 phosphorylation

A Semi confluent MCF-7 cells were incubated with the indicated amounts of IgG 3-43 (left) or 3M6 (right) for one hour before HRG stimulation (50 ng/ml) followed by cell lysis. Levels of phosphorylated and total HER3 were analyzed by immunoblotting with the indicated antibodies. One of three independent experiments is shown. **B** Quantification of phospho-HER3 signal; n=2, mean ± SD.

3.7.3.2 IgG 3-43 leads to relocalization of the bound receptor and reduces cellular HER3 levels

Binding of ligands and even some antibodies to their specific receptors may lead to internalization of the respective receptor. For example, cetuximab leads to internalization and degradation of EGFR[152,153]. Mechanistically, this could be one reason for the inhibition of signaling pathway activation after antibody binding. Thus, it is of interest if – and if so, how fast – the respective receptor is internalized and degraded. To examine the velocity of and confirm the degradation of HER3 provoked by IgG 3-43, MCF-7 cells were incubated for different time periods with IgG 3-43 or a

control antibody and HER3 levels were analyzed by western blot. HER3 levels were already reduced to less than 50 percent of the original amount after one hour and decreased further in the following hours. Incubation with a control antibody showed, apart from some fluctuations, no influence on HER3 levels.

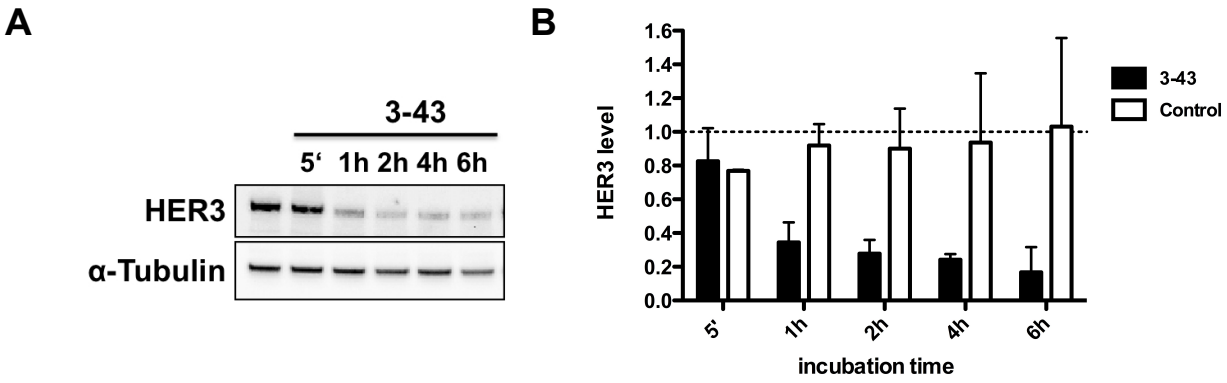

Figure 3-23: IgG 3-43 leads to reduction of cellular HER3 levels.

Cellular HER3 expression levels after incubation of IgG 3-43 were analyzed by immunoblotting. MCF-7 cells were incubated with 100 nM IgG 3-43 or control antibody (Atrosab) for the indicated time points and then lysed immediately. HER3 levels were analyzed by western blot. The HER3 signal rapidly decreased after addition of IgG 3-43, with a reduction already seen after 5 minutes of incubation time. **A** Western blot analysis. One of three independent experiments is shown. **B** Quantification of HER3 signal of three independent experiments relative to tubulin loading control and normalized to untreated cells (mean ± SD).

In order to create a more detailed view on the fate of the receptor and IgG 3-43 after HER3 binding, Cy5 maleimide was coupled to free sulfhydryl groups of the reduced antibody. This enabled microscopic examination of the antibody location after defined incubation times.

A Cy5 labeling kit was used to label IgG 3-43 with the fluorescent dye. Labeled antibody molecules were purified by permeation chromatography. A yield of 0.8 mg labeled IgG was obtained from 1 mg IgG 3-43 used. SDS-PAGE analysis (shown in figure Figure 3-24 A) revealed a major band corresponding to the original weight. Only, a minor portion of the antibody showed a reduced weight band, indicating that a light chain may have been lost during the labeling process. To test the functionality, binding to HER3-Fc in ELISA and to MCF-7 cells of Cy5 labeled IgG 3-43 was measured and compared to the unlabeled protein. The obtained EC_{50} values were quite identical (IgG 3-43-Cy5 vs IgG 3-43: 0.92 nM vs 0.82 nM in ELISA and 35 pM vs 43 pM in FACS analyses), indicating an unimpaired functionality of Cy5 labeled IgG 3-43.

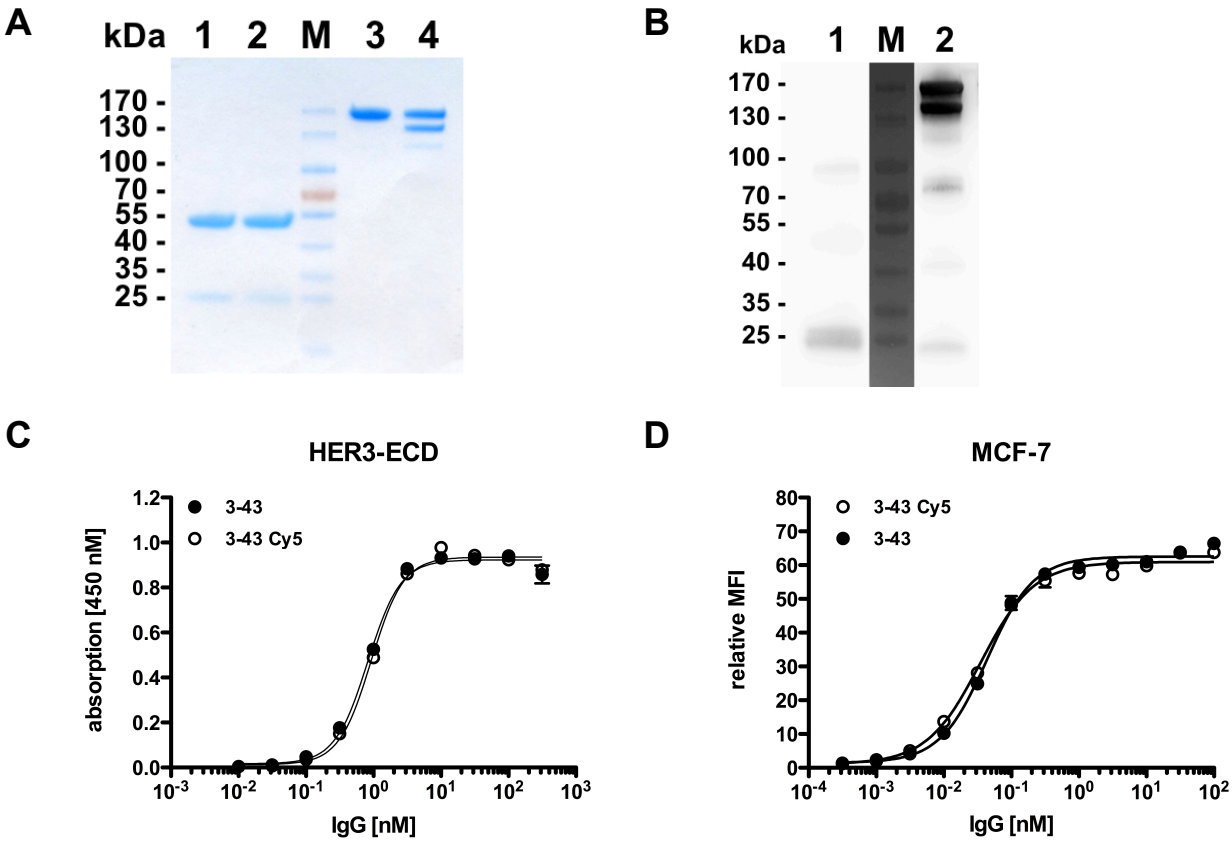

Figure 3-24: Cy5 coupling of IgG 3-43

A Coomassie stained SDS-PAGE analysis under reducing (lane 1, 2) and non-reducing (lane 3, 4) conditions of IgG 3-43 before (lane 1, 3) and after (lane 2, 4) Cy5 coupling. **B** Western blot analysis of Cy5 coupled IgG 3-43 under reducing (lane 1) and non-reducing (lane 2) conditions using HRP coupled anti-human IgG antibody. **C** Binding of IgG 3-43 or Cy5 coupled IgG 3-43 to HER3 (Fc-fusion) was analyzed by ELISA (mean of double values ± SD). **D** Cell binding of IgG 3-43 before and after Cy5 coupling was analyzed by flow cytometry (mean of double values ± SD).

Cy5 labeled IgG 3-43 was then used to study the time-dependent localization of IgG 3-43. MCF-7 cells, which show a good HER3 expression, were used for this analysis. Cy5-labeled IgG 3-43 was added to the cells, which were grown beforehand on microscopic slides. The slides were than either let shortly at room temperature or incubated for a period of 5 minutes, one hour or two hours at 37 °C. The cells were than fixed and stained and analyzed with a fluorescence microscope.

Without incubation at 37°C, IgG 3-43 was located at the outer part of the membrane (Figure 3-25, Figure 3-26). After five minutes of incubation at 37°C, the labeled antibody was still located at the membrane, but also a bit at the inner side of the cell. After one hour, prominent clusters of labeled antibody appeared inside the cell. After two hours of incubation, the main portion of the antibody was located inside the cell. Some cy5 signal also appeared again at the outer membrane or even right outside the cell.

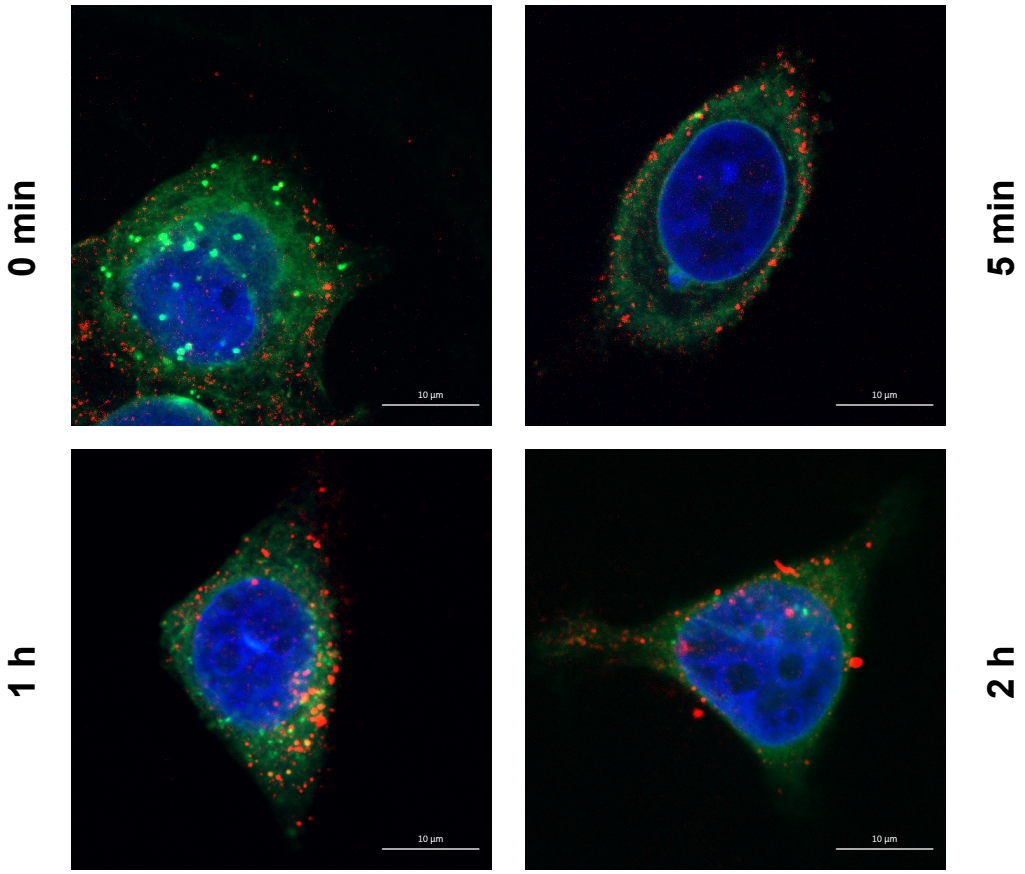

Figure 3-25: Microscopic analysis of IgG 3-43 relocation after binding to MCF-7 cells

Cy5 labeled IgG 3-43 was incubated with MCF-7 cells at 37 °C for the indicated time periods. Cellular membranes were stained with Concanavalin-A and cells were fixed with 4% paraformaldehyde. Pictures of treated and control cells were taken with a spinning disk microscope. Blue: Dapi nuclei staining; green: Con A membrane staining; red: Cy5-labeled IgG 3-43. Scale bar: 10 µm.

The orthogonal representation of the microscopic pictures shown in figure Figure 3-26 allows a more precise impression of the location of IgG 3-43 directly after addition to MCF-7 or after 5 minutes, 1 hour or 2 hours of incubation at 37°C. The sectional planes shown at the image margins clearly identify internalized cy5-labeled IgG 3-43 after 37°C incubation.

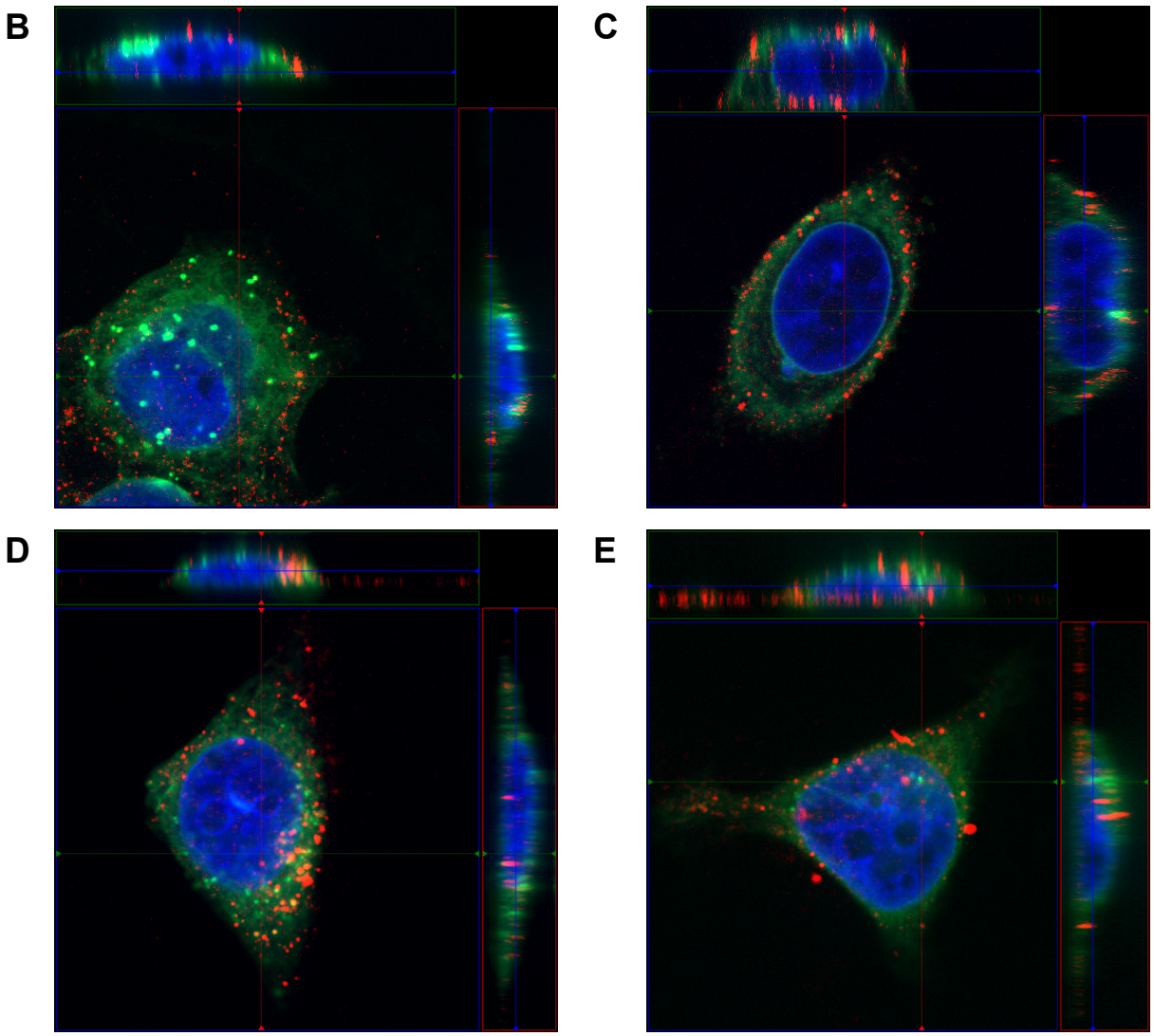

Figure 3-26: Orthogonal representation of microscopic analysis of IgG 3-43 localization

Cy5 labeled IgG 3-43 was incubated with MCF-7 cells at 37 °C for the indicated time periods. Cellular membranes were stained with Concanavalin-A and cells were fixed with 4% paraformaldehyde. Pictures of treated and control cells were taken with a spinning disk microscope. Blue: Dapi nuclei staining; green: Con A membrane staining; red: Cy5-labeled IgG 3-43. **A** <1 minute incubation at RT. **B** 5 minutes' incubation at 37°C **C** One-hour incubation at 37°C **D** Two-hour incubation at 37°C.

3.7.3.3 IgG 3-43 is able to reduce cancer cell growth *in vitro*

Internalization and degradation of a growth factor receptor, accompanied by inhibition of downstream pathway activation, should, in the best case, lead to reduced proliferation of cancer cells. The effect of IgG 3-43 on cancer cell proliferation was assayed with MCF-7, BT-474, NCI-N87, FaDu and A549. To this end, the cells were seeded at low densities in 96 well plates and let grow under low serum conditions in the presence of IgG 3-43 or an irrelevant control IgG. After one week of incubation, the number of viable cells was measured using a colorimetric assay based on the tetrazolium salt WST-8, which is reduced to a formazan dye by dehydrogenase

activities in cells. For the two breast cancer cell lines MCF-7 and BT-474 and the gastric carcinoma cell line NCI-N87, heregulin dependent proliferation was analyzed. Significantly reduced cell numbers after IgG 3-43 incubation compared to the control sample were observed for all of the three cell lines. In some cancer types, heregulin is produced in an autocrine manner. This mechanism is described for example for FaDu and A549. These cell lines were used to study the effect of IgG 3-43 on cancer cell proliferation independent from extrinsic heregulin. FaDu cells were incubated with serial dilutions of IgG 3-43 or control antibody in reduced serum medium. A potent proliferation inhibiting effect of IgG 3-43 was observed at low nanomolar concentrations. The IC_{50} value was calculated to 270 pM. In A549, an about 20 percent reduced cell number was measured after one-week IgG 3-43 incubation.

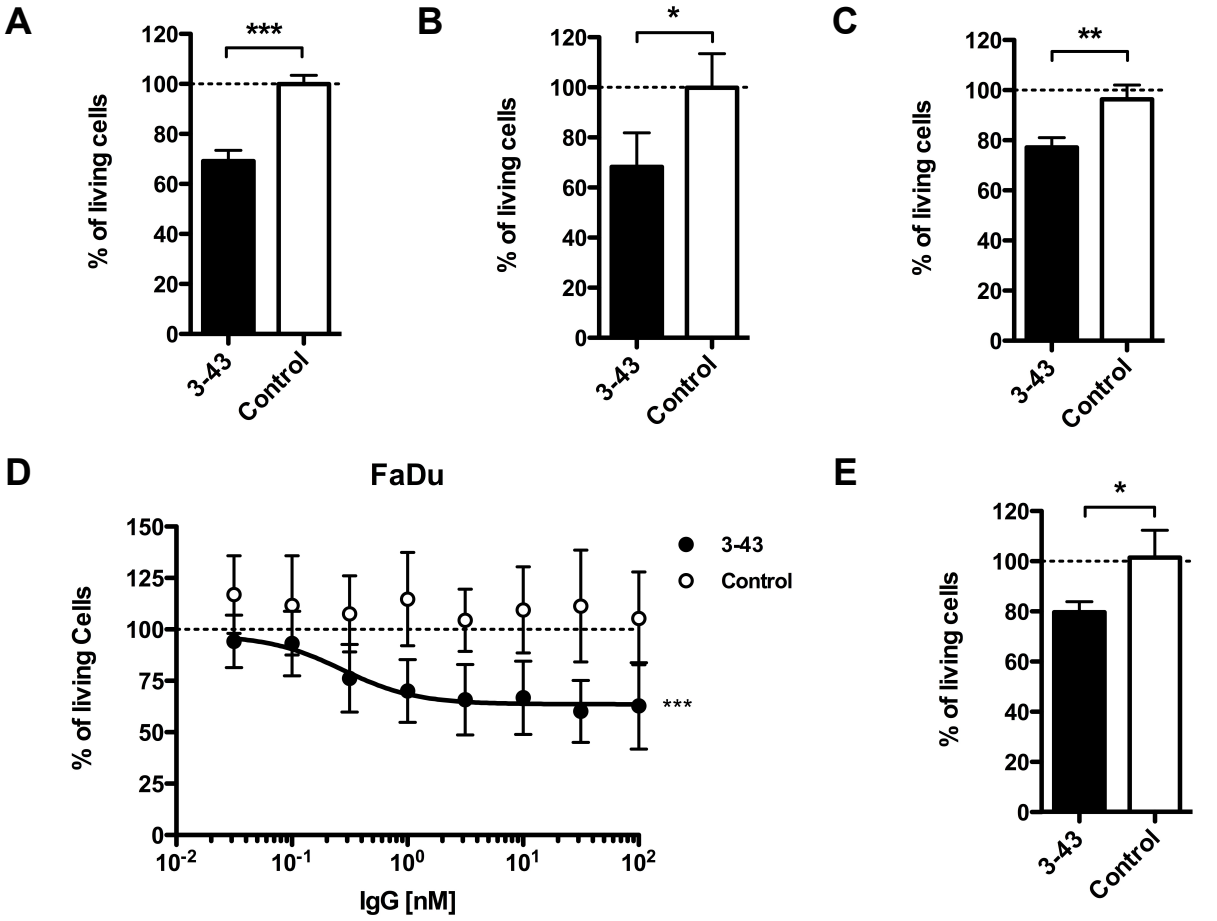

Figure 3-27: IgG 3-43 decelerates proliferation of various cancer cell lines

A, **B**, **C**: MCF-7 (A), BT-474 (B) or NCI-N87 (C) cells were seeded at low densities in 96 well plates, let adhere overnight, and were incubated for one week under low (0,2%) serum concentrations and in the presence of 10 ng/ml heregulin with 10 µg/ml IgG 3-43 or Atrosab as control IgG. N=3, mean ± SD. **D:** FaDu cells, known to produce heregulin in an autocrine manner, were subjected to the same proliferation assay but in the absence of ambient heregulin. Titration of IgG 3-43 revealed a potent growth inhibiting effect even at low nanomolar concentrations. Control: Rituximab. N=3, mean ± SD. **E**: A549 cells were subjected to the same proliferation assay like in D, but as endpoint measurement with 10 µg/ml IgG 3-43. Control: Atrosab. N=3, mean ± SD.

3.7.3.4 *In vivo* Study of IgG 3-43

$5*10^6$ FaDu cells were injected subcutaneously into both flanks of female immunodeficient Fox Chase SCID Beige mice (CB17.Cg-Prkdc^{scid}Lyst^{bg-J}/Crl). Six mice per group received six intravenous injections of 150 µl twice weekly for three weeks on days 14, 17, 21, 24, 28 and 31 after cell injection. Whereas the control group received only PBS, the three treatment groups received either a total of 30 µg, 100 µg or 300 µg IgG 3-43 per injection, dissolved in PBS. Figure 3-28 shows the group means of tumor volumes. Significant differences in tumor volumes could be monitored between the control group and the treated groups. For the IgG 3-43 treated groups, tumors stopped growing or shrank during the treatment time. Approximately two weeks after the treatment ended, the tumors relapsed.

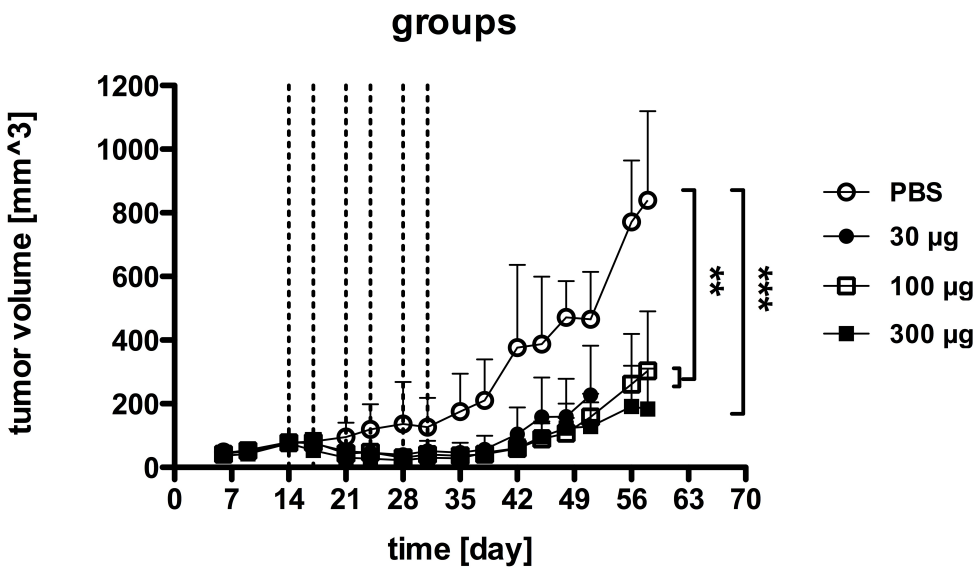

Figure 3-28: Intravenous application of IgG 3-43 inhibits growth of FaDu xenografts in immune-deficient SCID Beige mice

Mean tumor volumes of the groups. Error bars represent 95% confidence intervals. N=3-6 (6 mice per group at start).

Survival of the IgG 3-43 and PBS treated mice was monitored from tumor grafting until the end of the study. A Kaplan-Meier blot illustrating the survival curves of the differently treated groups is shown in Figure 3-29. Median survival of the groups receiving 100 µg IgG 3-43 (59 days) and 300 µg IgG 3-43 (71.5 days) was significantly increased compared to the PBS treated group (51.5 days).

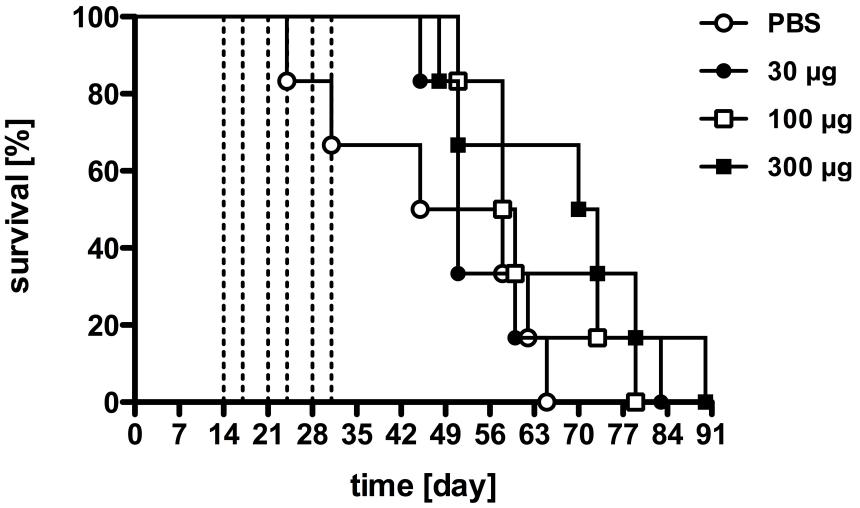

Figure 3-29: Survival of the xenografted mice

Kaplan-Meier blot illustrating the survival curves of the differently treated groups.

At day 42, 11 days after the last treatment, mean tumor volumes of all three treated groups were significantly lower as the mean tumor volume of the control group (Figure 3-30 B). The growth curves of the single tumors shown in Figure 3-30 C-F highlight that, despite a relatively high intra-group diversity accounted by a divers engraftment of the tumors, tumor growth was delayed for almost all treated animals with the longest delay observed for the highest dose.

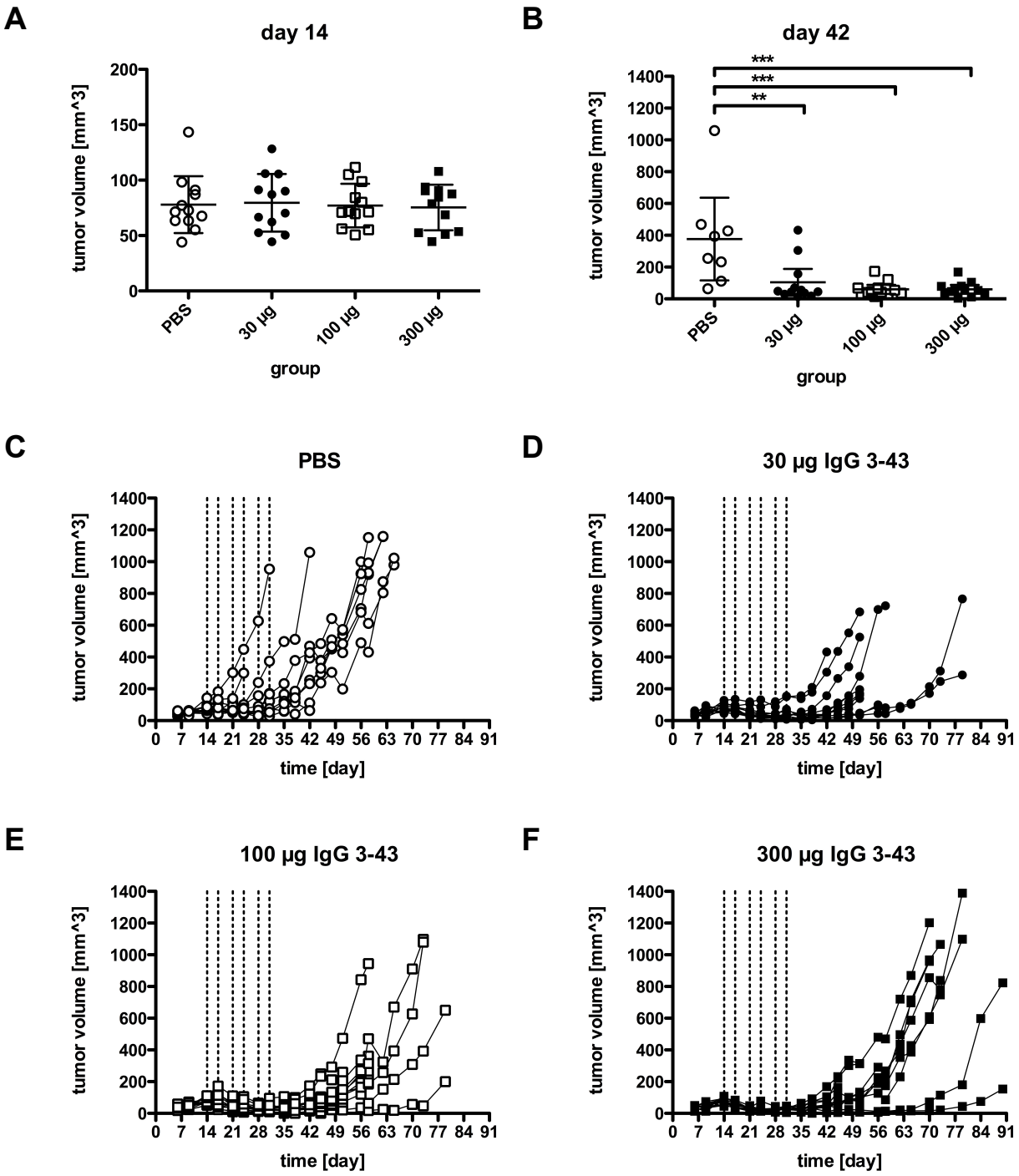

Figure 3-30: Treatment with IgG 3-43 decelerates growth of xenotransplanted FaDu tumors in immunosuppressed SCID/beige mice.

A Tumor volumes and group means before first treatment. Bars indicate mean ± SD. **B** Tumor volumes and group means 11 days after last treatment. Bars indicate mean ± SD **C** Growth curves of single tumors of the PBS placebo treated group. **D** Growth of single tumors of the six times twice weekly 30 µg IgG 3-43 treated group. **E** Growth of single tumors of the six times twice weekly 100 µg IgG 3-43 treated group. **F** Growth of single tumors of the six times twice weekly 300 µg IgG 3-43 treated group.

The pharmacokinetic property of IgG 3-43 was assayed during the *in vivo* study and revealed that serum concentrations of IgG 3-43 were higher after the last injection

than after the first injection for all three groups, indicating an accumulating dose of the antibody. The $AUC_{0\text{-}72h}$ values increased approximately 4- to 9-fold. This resulted also in increased terminal half-lives, while initial half-lives were not affected (Table 3-8).

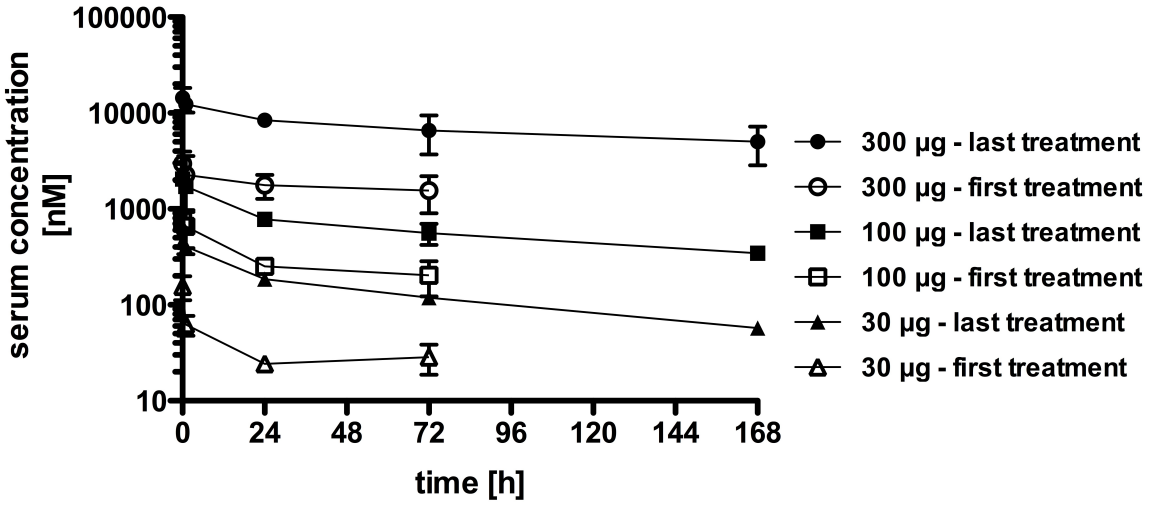

Figure 3-31: Pharmacokinetic property of IgG 3-43

Blood samples of three animals per group were taken at the indicated time points (3 minutes, 1 h, 24 h, 72 h (and 168 h after the last treatment)). IgG serum concentration was analyzed via ELISA. Mean ± SD.

Table 3-8: Pharmacokinetic property of IgG 3-43

amount [µg]	application	$t_{1/2}\,\alpha$ [h]	$t_{1/2}\,\beta$ [h]	$AUC_{0\text{-}72h}$ [nM*h]
30 µg	first	11.7 ± 0.8	59.1 ± 28.4	2,366 ± 84
	last	19.7 ± 4.0	87.1 ± 9.9	14,498 ± 873
100 µg	first	17.3 ± 5.3	47.8 ± 7.2	22,101 ± 5,882
	last	18.7 ± 3.0	126.5 ± 10.1	62,605 ± 5,046
300 µg	first	32.4 ± 9.5	127.9 ± 9.6	151,558 ± 38,462
	last	37.1 ± 9.4	224.2 ± 116.6	610,044 ± 137,488

During the study, the body weight of the mice was measured every other day. No treatment related weight loss was observed for all groups, giving a first indication for a non-toxic behavior of the antibody.

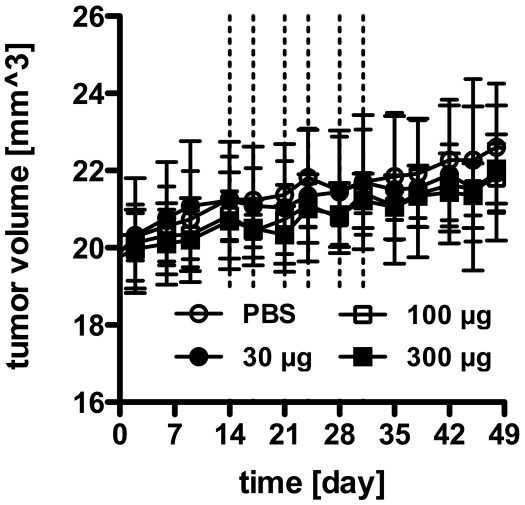

Figure 3-32: IgG 3-43 had no effect on body weight of to SCID beige mice

Body weight was measured twice weekly. Group means ± SD.

3.7.3.5 No apoptosis induction in FaDu cells after IgG 3-43 incubation

To adress the question, weather IgG 3-43 can lead to apoptosis induction in FaDu cells, as it was indicated in the *in vivo* study, FaDu cells were incubated for 48 hours with IgG 3-43, irrelevant control antibody or single chained TRAIL-Fc fusion protein, which is known to induce apoptosis, as positive control. The cells were stained with Annexin V and PI and analyzed by flow cytometry. No increased staining was detected in the antibody treated cells with the tested concentrations (10 nM, 100 nM and 1000 nM) compared to untreated cells after 48 hours.

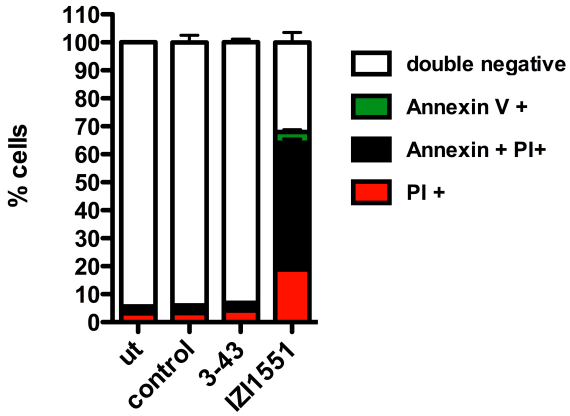

Figure 3-33: Annexin V – PI staining of FaDu cells after 48 hours antibody incubation

FaDu cells were treated for 48 hours with growth medium containing either 1000 nM Rituximab, 1000 nM IgG 3-43 or 10 nM IZI1551 (scTRAIL-Fc). Annexin V and PI staining was analyzed with flow cytometry. Mean of double values ± SD.

3.7.3.6 Presence of IgG 3-43 partially restores lumen formation in oncogenic K-Ras^{G12V} expressing Caco-2 cells

The hitherto obtained data document the suitability of IgG 3-43 for inhibition of HER3 downstream signaling and thereby of cancer cell proliferation. A proliferation inhibiting effect could also be observed in BT-474 and MCF-7 cells, which carry a mutation in the gene encoding for PI3K. In A549, which carry a mutated form of K-Ras, a partial inhibition of proliferation could also be achieved with IgG 3-43. For an application as anti-cancer drug, it is of great interest, weather IgG 3-43 cannot only decelerate proliferation, but also is able to reduce or reverse other carcinogenic characteristics, like aberrant morphogenesis induced by dedifferentiation of the cells. A 3D model of Caco-2 cells with inducible expression of oncogenic K-Ras^{G12V} was used to study the influence of IgG 3-43 on K-Ras^{G12V} driven aberrant morphogenesis in cysts formed by Caco-2 cells in matrigel. The cells harbor a doxycycline (dox)-regulated expression system, described by Herr et al. 2011[154], allowing the conditional expression of K-Ras^{G12V}. AZD8931, a pan HER inhibitor (inhibiting signaling by EGFR, HER2 and HER3), was used as positive control for a partial reversion of the aberrant morphogenic phenotype and Rituximab served as IgG control. Doxycycline induced K-Ras^{G12V} expression is accompanied by expression of GFP. WT K-Ras expressing cells formed round cysts with cell free lumen and F-actin staining of the apical surface. K-Ras^{G12V} expression induced an aberrant phenotype with no cell free lumen or multiple lumens and divergent cell numbers. The ‘normal’ form with one single apical lumen could be restored in some cysts by addition of AZD8931. IgG 3-43 also led to phenotype rescue for a significant number of cysts.

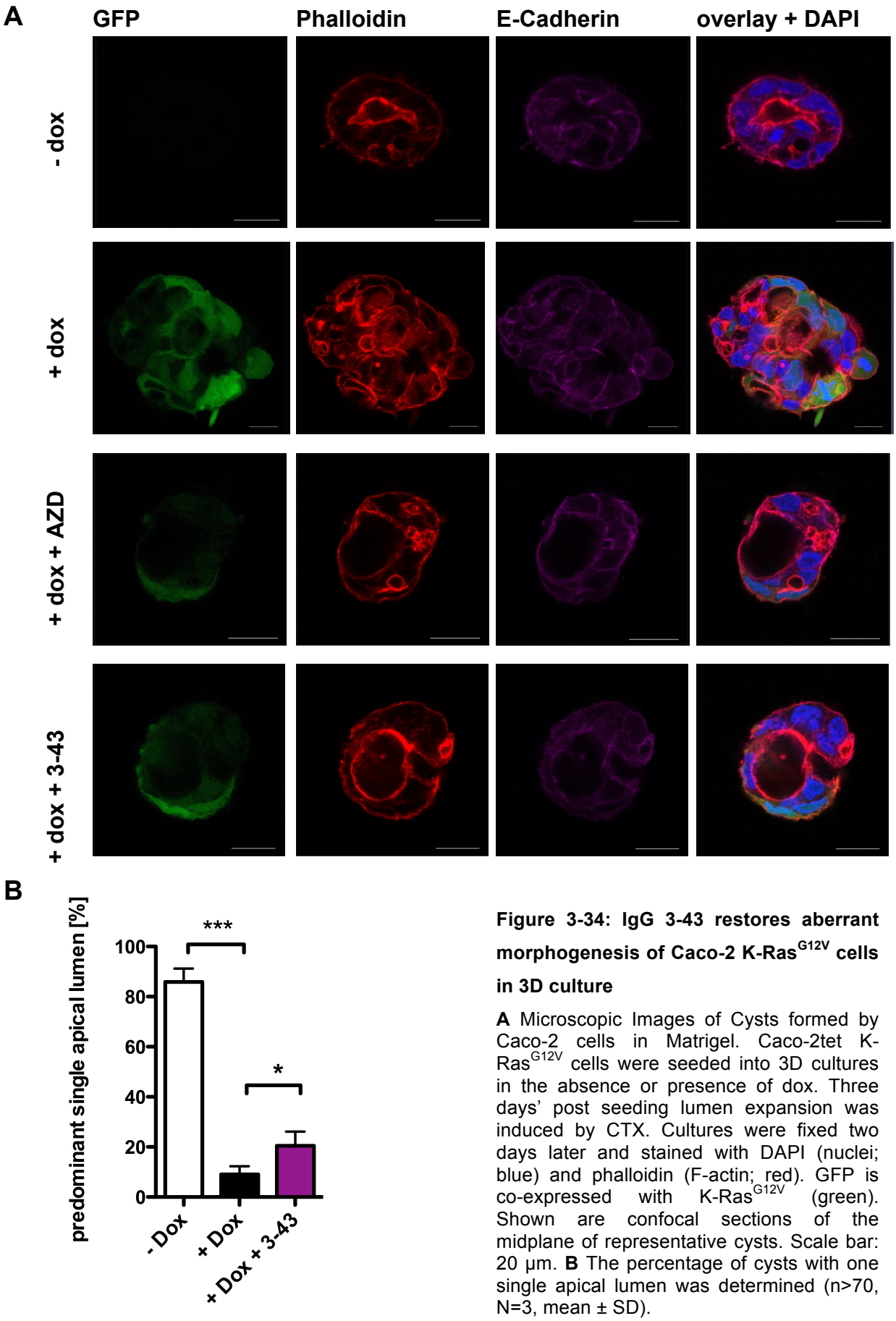

Figure 3-34: IgG 3-43 restores aberrant morphogenesis of Caco-2 K-Ras^{G12V} cells in 3D culture

A Microscopic Images of Cysts formed by Caco-2 cells in Matrigel. Caco-2tet K-Ras^{G12V} cells were seeded into 3D cultures in the absence or presence of dox. Three days' post seeding lumen expansion was induced by CTX. Cultures were fixed two days later and stained with DAPI (nuclei; blue) and phalloidin (F-actin; red). GFP is co-expressed with K-Ras^{G12V} (green). Shown are confocal sections of the midplane of representative cysts. Scale bar: 20 µm. **B** The percentage of cysts with one single apical lumen was determined (n>70, N=3, mean ± SD).

4 Discussion

In this work, fully human IgG molecules with ADCC strengthening constant regions were generated for therapeutic applications. The variable regions were selected from a panel of phage display derived scFv proteins. In one part of the study, HER2 binding IgG 2-35 was generated and analyzed. A strong avidity effect could be achieved with the bivalent IgG format, leading to a three point five times reduced EC_{50} value for cell binding. IgG 2-35 reduced proliferation of HER2 overexpressing NCI-N87 ant BT-474 cells. In the other part of the study, HER3 binding IgG 3-43 was generated. IgG 3-43 was shown to bind to domain III of HER3, thereby impeding heregulin binding, leading to reduced heregulin induced as well as constitutive HER3 and Akt phosphorylation. IgG 3-43 furthermore was internalized into MCF-7 cells and reduced cellular HER3 levels. Most importantly, antitumor activity of IgG 3-43 including tumor regression during the treatment phase and a prolonged survival was demonstrated in a subcutaneous FaDu xenograft tumor model in SCID mice.

4.1 Selection of scFv proteins

The scFv proteins analyzed in this study were selected from the naïve antibody gene libraries HAL7 and HAL8[155] by phage display prior to this thesis. Phage display derived antibodies comprise several advantages compared to more classic techniques such as *in vivo* immunization or infection[156]. Antibodies generated by immunization of a non-human host usually are more immunogenic than a human-derived antibody, even after humanization by replacement of constant or framework regions with human equivalents[157]. Immunogenicity can lead to increased toxicity and reduced clinical efficacy[158]. Furthermore, the technique allows facile post-optimization processes, like affinity maturation[159].

4.2 HER2

HER2 frequently is amplified in human tumors, especially in breast carcinoma[160], and increased expression of the receptor results in cellular transformation and tuzmorigenesis[161]. Since the intracellular kinase domain of HER2 as well is more active than that of EGFR[162], HER2 targeted antibody therapy has great potential, especially for HER2 overexpressing tumors[163]. The first biological drug approved for the treatment of HER2-positive breast cancer, trastuzumab, remains the gold

standard for treatment of this disease[164]. However, about 60% of patients with HER2 positive breast cancer develop de novo resistance to trastuzumab, partially due to the loss of expression of HER2 extracellular domain on their tumor cells due to HER2 cleavage by metalloproteinases (ADAMs and MMPs)[165]. Recent research in breast cancer therapy has therefore focused on dual blockade of HER2, combining trastuzumab and lapatinib or trastuzumab and pertuzumab, or simultaneous blocking of other pathways[166], and more HER2 targeting antibodies with cytostatic effects on tumor cells will enrich the possibility spectrum for combination and monotherapy and possibly broaden the understanding or eventually circumvent resistance mechanisms.

4.2.1 IgG 2-35 shows good binding, but inconsistent inhibiting properties

Affinity measurements against HER2-Fc revealed a K_D of 24.8 nM for scFv 2-35, which is about 20 times weaker than scFv 4D5, the scFv comprising the binding site of the clinically approved Trastuzumab, herein showing a K_D of 1.2 nM. Affinity maturation, which also can be performed by phage display, could increase the affinity of the 2-35 variable domains[167]. Importantly, scFv 2-35 did not compete with trastuzumab for HER2 binding, which is favorable for a possible combination or the generation of bi- or multi-specific antibody constructs, a strategy proven to be meaningful in the past. Tóth et al. demonstrated in 2016 that the combination of trastuzumab (binding to the juxtamembrane region of HER2[24]) and pertuzumab (binding to domain II of HER2[106]) slowed tumor growth of xenografts from intrinsically trastuzumab-resistant JIMT-1 cells[168]. Pedersen et al. demonstrated a synergistic antitumor activity of a tripartite antibody mixture targeting HER2 subdomains I, II, and IV that was superior to trastuzumab *in vitro*[169]. A triparatopic Tribody consisting of 3 noncompeting ErbB2 binders designed by Riccio et al. was more efficient in downregulating ErbB2 and inhibiting tumor cell growth than the control monoparatope tribodies or the combinatorial treatment with the 3 different parental antibodies on tumor cells[170].

IgG 2-35 bound to recombinant HER2 and HER2 expressing cells with EC_{50} values slightly lower than these of trastuzumab, with EC_{50} values for IgG 2-35 of 200 - 300 pM and for trastuzumab of 0.5 – 2.5 nM for cell binding. The binding property of IgG 2-35 was about 3.5 times enhanced compared to the scFv, indicating a strong

avidity effect. In contrast, series of human IgG1 isotype antibodies created from the anti-HER2 C6.5 scFv and its affinity mutants retained the affinities of the scFv from which they were derived[171]. For some anti-EGFR antibodies however, bivalent IgG also had higher observed binding affinity than the cognate monovalent constructs[172]. It is in accordance with literature, that the low affinity scFv 2-35 could benefit more from avidity effects in the IgG format than the trastuzumab derived scFv 4D5, since a work of Nielson et al. indicated that the affinity gain upon conversion from the monovalent to the bivalent format is higher for low affinity binders[173].

In the gastric cancer cell line NCI-N87 and the breast cancer cell line BT-474, IgG 2-35 inhibited proliferation in the presence of EGF with an about 20 percent enhanced effect compared to trastuzumab. The experiments confirm that, although the scFv affinity of 2-35 was inferior to that of trastuzumab, as IgG the antibody is superior to trastuzumab in this setting. Inhibition of EGF induced proliferation with HER2 targeting antibodies is in good accordance to literature, since it was found already in the 90s that HER2 is a potentiator of the EGF signal[174,175] and kinase-deficient HER2 suppresses EGFR function[176]. Interestingly, IgG 2-35 did not inhibit proliferation of SKBR-3 cells in normal growth medium which, however, was observed in the case of trastuzumab. The growth inhibiting effect on SKBR-3 cells was also shown by others for the mouse precursor of trastuzumab 4D5[102]. However, 4D5 did not have any growth inhibiting effect on the mammary carcinoma cell lines MCF-7, MDA-MB-157 and MDA-MB-231, but also on MDA-MB-361 and MDA-MB-175-VII, which express high levels of HER2[177]. In conclusion, IgG 2-35 does not stand alone in provoking diverging effects in different cell lines.

More efforts have to be made to elucidate the mode of function of IgG 2-35. No blockade of HER receptor phosphorylation could be shown in MCF-7 cells with IgG 2-35. This suggests, that IgG 2-35 is no potent inhibitor of HER2 dimerization. Epitope mapping of IgG 2-35 was performed by Jonas Honer in his Master thesis[178] in order to better understand the effects mediated by the antibody. This experiment showed that the epitope of IgG 2-35 is located on domain I of the HER2-ECD, and maybe incorporates parts of domain II. This epitope localization makes a potent and full inhibition of dimerization unlikely. The clinically approved Pertuzumab sterically blocks HER2 dimerization and signaling by binding to ErbB2 near the center of domain II[106], the RTK domain incorporating the dimerization arm[179].

Another possible way to influence cellular processes, such as proliferation, is receptor down-regulation through internalization and degradation[169]. Down-modulation of the targeted receptor is one of the phenotypic changes observed *in vitro* as an effect of trastuzumab[180]. A reduction of HER2 surface levels may be more effective in a setting, where stimulating ligands are available and HER2 could contribute to more efficient signaling dimers. Further studies are necessary to examine the mechanism by which IgG 2-35 inhibits proliferation of HER2 expressing cancer cells and to elucidate predictive biomarkers for a cellular response. The inhibition of EGF driven proliferation in NCI-N87 and BT-474 cells hints on an anti-tumor activity of the antibody. Anyhow, IgG 2-35 may also be suited for the use as targeting unit of antibody drug conjugates or in bispecific antibodies or combinatory settings. Trastuzumab-DM1 for example shows greater anti-proliferative activity compared to unconjugated trastuzumab while maintaining selectivity for HER2-overexpressing tumor cells[181].

4.2.2 Inadequate integrity of scFv-Fc fusion proteins

ScFv-Fc fusion proteins were constructed in order to get bivalent antibody proteins. Although the purity of the proteins seemed adequate in SDS-PAGE analysis, size exclusion chromatography revealed a poor integrity. In contrast, this format showed good integrity in former studies (see e.g. Unverdorben et al. 2016[182]). However, the proteins analyzed in the mentioned studies comprise a different scFv linker, namely $(G_4S)x3$, whereas the linkers of the herein analyzed scFv proteins, which also connect the heavy and light variable chains in the scFv-Fc fusions, consist of the 18 amino acids GSASAPKLEEGEFSEARV. This may be one reason for the different protein integrities.

4.3 HER3

Similar to HER2, HER3 is also often expressed in breast cancer in an elevated manner[183], playing an important role in cancer progression and chemotherapy resistance[184]. ScFv3-43 was chosen for conversion to the IgG format and further development due to potent receptor binding and efficient inhibition of heregulin-induced HER3 phosphorylation. As heregulin induced signaling pathway activation is implicated in cancer growth and progression as well as in resistance to different anti-cancer drugs[185], this characteristic is highly desirable.

4.3.1 Distinguished binding characteristics of IgG 3-43

ScFv 3-43 was primarily chosen for further expression as fully human IgG1 antibody for its good cell binding characteristics. The monovalent antibody molecule bound to cellular HER3 with an EC_{50} value of around 600 pM. Anyhow, it could not be excluded that scFv 3-43 forms dimers, as the estimated corresponding molecular mass of 38.7 kDa for the scFv interpolated after size exclusion chromatography from the protein standard is bigger than the calculated molecular mass of 31,1 kDa. Cell binding was six times enhanced through expression of the antibody's binding sites in a bivalent molecule by –Fc fusion, hinting on a potent avidity effect. The IgG format further enforced the binding strength, what accounted to a 20 times stronger cell binding compared to the scFv. This increase magnitude in binding strength seems to be format specific, because neither the expression as scFv-Fc nor as scDb led to EC_{50} values in the same range as the IgG. Even a tetravalent scDb-Fc fusion molecule bound to FaDu cells with an EC_{50} value of 180 pM, whereas IgG 3-43 bound in the same setting with an EC_{50} value of 6 pM[178]. An approximate 10- to 100-fold increase in binding through avidity effects is in accordance with data obtained for anti-EGFR antibodies with affinities in the nanomolar range[172].

The differences seen between antigen binding in ELISA and cell binding may be due to different antigen densities, as well as different receptor surrounding on cells and different conformation. The antigen binding properties are comparable for all formats, whereas they differ strongly in terms of cell binding. In ELISA, through the high antigen density, monovalent binding is reflected, whereas in cell binding also format specific advantages are reflected. Affinity measurements using quartz crystal microbalance depicted a K_D of the monovalent his-tagged receptor to IgG 3-43 in a range comparable to the EC_{50} values detected for binding of the 3-43 binding site to the receptor. The bivalent HER3-Fc had a higher affinity to the immobilized IgG 3-43. Here, the K_D lay at 220 pM, being more comparable to the bivalent cell binding of the 3-43 constructs. However, cell binding of IgG 3-43 seems to be still stronger. In the QCM setting, IgG 3-43 was immobilized. It may be that the antibody needs its full flexibility to access its complete binding strength.

4.3.2 Mechanistic considerations of IgG 3-43's impact on cancer cell signaling

The effect of a receptor-targeting antibody is to a huge extent determined by its epitope, as binding to different epitopes may lead to divers results. Depending on the bound epitope, antibodies can for example exert conformational effects, such as fixating the receptor in a certain conformation, which in turn can determine the activation status[113]. Inhibition of receptor dimerization through binding at or near the dimerization arm is another possibility to influence receptor activity[186]. Furthermore, binding near the ligand-binding pocket can prevent binding of the natural ligand[110]. The epitope of scFv 3-43 was mapped in this study to domain III of the HER3-ECD. However, further analyses conducted later by Alexander Rau and Jonas Honer defined the epitope more precisely to be located on a fragment formed by aa 329 - 587, containing the entire domain III and 56 amino acids from the N-terminal region of domain IV[187]. To identify the exact epitope of IgG 3-43, further studies, for example using mutational scanning or structural analyses, are necessary. Structural analyses like crystallographic studies would be of advantage though the complex epitope is sensitive to chemical reduction, which complicates easy mapping strategies such as using peptide microarrays or ELISpot techniques.

In this study it was shown that IgG 3-43 binds to domain III of HER3, although, meanwhile, it was pointed out that a small part at the N-Terminal region of domain IV of HER3 also contributes to the epitope. By binding to this receptor area, IgG 3-43 potently prevents ligand binding and thereby also phosphorylation of the receptor. So, the first mode of action of IgG 3-43 is to prevent ligand dependent HER pathway signaling through prevention of ligand binding. This already can inhibit several cancer driving processes through downregulation of two important signaling pathways, the PI3K/Akt and the (Ras – Raf – MEK – Erk) MAPK pathway.

The second effect of the antibody is internalization and degradation of the bound receptor, leading to reduced HER3 receptor levels. Basal HER3 turnover is negatively regulated by the E3 ubiquitin ligases NEDD4[188] and Nrdp1[189]. Antibody induced receptor internalization and degradation was already described for other antibodies. For example, Jaramillo et al. could show that treatment with cetuximab results in a 30-40% decrease in surface EGFR[152]. The same group also showed that endocytosis of the antibody occurred and that it is recycled to the surface[152]. In the in vivo study, accumulation of the doses was observed, despite antigen presence as

well in the FaDu tumors as in healthy tissues of the mice[190]. The mechanism of cetuximab mediated EGFR down-regulation was examined by Dai et al, who found that cetuximab modulates EGFR protein stability through the ubiquitin/proteasome pathway in human oral squamous cell carcinoma cells[153]. However, HER3 degradation induced by IgG 3-43 appears to be much faster than EGFR degradation induced by cetuximab. Besides the biologic differences of the receptors, a possible explanation for the differing internalization velocities, are the distinct differences between the affinities with which the antibodies and the natural ligands bind the receptors. Cetuximab binds to EGFR with a K_D of 200 pM[107,191], whereas TGF-α binds EGFR with a similar affinity of 1 nM[107]. The affinity difference between IgG 3-43 and heregulin (K_D=1.9 nM[192]) are more pronounced. The antibody 9F7-F11, which is directed against domain I of HER3 and also induces rapid internalization of the receptor[123], recently was shown to induce HER3 down-regulation through ubiquitinylation and degradation driven by the itchy E3 ubiquitin ligase (ITCH/AIP4) in a JNK1/2-dependent manner[193].

Another potential mechanism, by which growth factor receptor binding antibodies can alter cellular functions, is by influencing the conformation of the receptor. Cetuximab binds to domain III of the EGFR-ECD. An X-ray crystal structure of the antigen binding (Fab) fragment from cetuximab, in complex with the soluble extracellular region of EGFR, showed that cetuximab interacts exclusively with domain III of sEGFR[23]. The crystal structure was published by Li et al., who also stated that cetuximab thereby partially occludes the ligand binding-region on this domain and also sterically prevents the receptor from adopting the extended conformation. The extended conformation is in turn needed for dimerization. As the extracellular domain of HER3 is to about 40-50% identical with that of EGFR[194,195], and regarding that the epitope of IgG 3-43 is also located on domain III of its receptor, a similar steric blockade is possible. For KTN3379, a HER3 binding antagonistic monoclonal antibody that is currently in clinical development in human cancer patients, a conformation blocking binding mode is highlighted through a crystal structure of the Fab fragment, in complex with the extracellular domain of HER3[113]. Here, extracellular domains III and II of HER3 contribute to the epitope. Weather IgG 3-43 also infers with receptor dimerization, either through a prevention of the extended conformation or through other steric interferences, could be further examined by

crystal structure analyses of the IgG 3-43 Fab fragment in complex with the HER3 extracellular region.

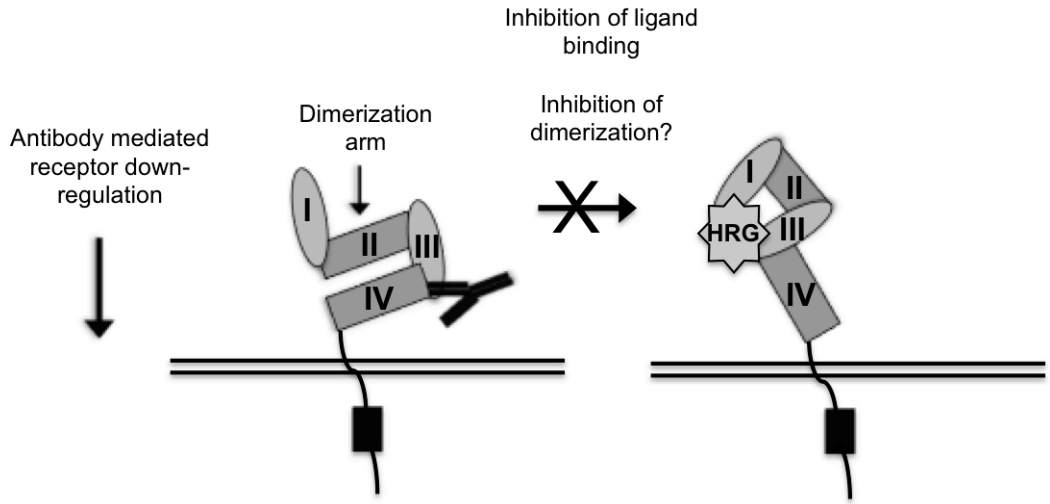

Figure 4-1: Mechanism of IgG 3-43's effect on HER3

IgG 3-43 leads to reduced levels of cellular HER3 and inhibits HRG binding. Impacts on HER3 conformation and dimerization are to prove.

No apoptosis induction of HER3 expressing cells could be seen *in vitro* in 2D with IgG 3-43 after 48 hours. Nonetheless, the size reduction of FaDu tumors seen in the *in vivo* experiment may indicate an apoptosis inducing effect of 3-43 *in vivo*. Apoptosis induction has been described for some anti-HER3 antibodies[123], whereas Seribantumab did not induce apoptosis on its own but enhanced apoptosis induced by chemotherapeutic drugs[196]. Instead of direct apoptosis induction, inhibition of angiogenesis through receptor cross talk may lead to IgG 3-43-triggered tumor cell death *in vivo*. Since the expression and secretion of VEGF in breast cancer cells is regulated by heregulin[197], angiogenesis inhibition with a HER3 targeting antibody is in accordance with current knowledge. The role of HER3 in angiogenesis was further supported by Yu et al. in 2011 who showed that miR-148a inhibits tumor angiogenesis through downregulation of HER3 and resulting reduced activation of downstream signaling molecules[198]. Tissue analysis of treated tumors could provide more hints untangling this issue.

4.3.3 IgG 3-43 potently inhibits cancer cell proliferation and seems applicable as anti-cancer drug

In this study, it was shown that IgG 3-43 inhibits heregulin binding to HER3 expressing cells, downregulates cellular HER3 levels through antibody mediated

receptor internalization and, most importantly, leads to reduced proliferation of multiple human cancer cell lines. Reduced proliferation was monitored in heregulin dependent settings, as well as in heregulin independent settings. This is of special importance, as in some cancers autocrine heregulin loops exist[98,199]. Expression of heregulin by the cancer cells is an often observed resistance mechanism implicated in resistance to other HER receptor targeting drugs, for example cetuximab[200] or trastuzumab[200-202]. Ebbing et al. lately demonstrated with esophageal cancer cells that upregulation of HER3 is the most important response of HER2 inhibition with trastuzumab, that was accompanied with HER2 decrease. The group furthermore showed that HER3 mediated trastuzumab resistance was dependent on autocrine NRG-β shed by upregulated ADAM10[201].

In the *in vivo* study, a long serum availability of IgG 3-43 was observed, fulfilling already one desired drug characteristic of long bioavailability[203]. The magnitude of the time-period of availability in the body can influence drug responses. In a study dealing with infliximab treatment of rheumatoid arthritis, low infliximab serum levels at an early stage often were associated with treatment failure[204]. Furthermore, no loss of body weight was observed in the *in vivo* study, indicating good tolerability of the antibody. IgG1 molecules are well approved for clinical use. However, a more precise examination of IgG 3-43 tolerability might be advantageous. Importantly, a size reduction of FaDu xenografts treated with IgG 3-43 was demonstrated in the *in vivo* study. During the treatment period, tumor outgrowth was prohibited for all mice receiving 300 μg IgG 3-43 q2w3. The median half-life of the tumor bearing mice was prolonged about 20 days for the group twice weekly receiving 300 μg IgG 3-43 compared to the PBS group. This prolongation is in good correlation to the time span of the treatment period, indicating that IgG 3-43 is able to protect from tumor expansion in a dose-dependent manner.

Moreover, immune effector cells might contribute to antitumor activity. This was shown for the glycoengineered anti-HER3 antibody RG7116 in an orthotopic lung xenograft model of A549 cells in SCID mice[116]. Antibody-dependent cellular cytotoxicity is believed to be a major antitumor mechanism of some cancer cell targeting antibodies[171]. For IgG 3-43, ADCC was demonstrated *in vitro* with SKBR3 cells and natural killer cell-containing human PBMCs[187]. Here, efficient lysis of tumor cells was observed with an EC_{50} value of 2.4 pM. Compared to IgG 3M6, (also comprising the two mutations (S239D/I332E) in the Fc region to enhance ADCC),

which is derived from Seribantumab, an approximately four-fold stronger ADCC was determined. This could be explained by the higher affinity to HER3 observed for IgG 3-43, since antibody to target affinity was shown by Tang et al. to be a factor influencing ADCC[171].

4.3.4 IgG 3-43 in comparison with other available antibodies

Since it became clear that HER3 might be a promising target for anti-cancer therapy, many HER3 binding antibodies were developed. Over 40 different HER3-targeting agents already are under development[15]. More than half of them are monospecific antibodies in different developmental stages, rising from preclinical up to clinical Phase 3. To judge the usefulness of another new HER3 targeting agent, a comparison with other antibodies in the pipeline is relevant. For none of the HER3 targeting monovalent antibodies that already entered in clinical studies, an epitope to that domain III and IV of HER3 contribute is reported[15], highlighting a unique characteristic of IgG 3-43. This also offers a good opportunity for dual HER3 targeting. Dual targeting of one receptor can be beneficial in some cases. For IGF-1R it was shown that antibodies recognizing different epitopes of the receptor exhibit an increased neutralizing potential[205]. Phillips et al. confirmed in 2014, that dual targeting with the antibody-drug conjugate trastuzumab ematisine (T-DM1) and pertuzumab results in enhanced antitumor activity in models of HER2-amplified cancer[206]. In respect to binding affinities, IgG 3-43 ranks amongst the best binding candidates under development. Concerning the Fc region, IgG 3-43 includes two mutations (SI) for improved ADCC[151]. Other HER3 targeting antibodies also incorporate modifications to enhance ADCC. The Fc-region of Lumretuzumab has been glycoengineered to increase the affinity toward the Fc-gamma receptor (Fcγ RIIIa) on immune effector cells[116].

From the mechanistic view, other antibodies are known to provoke similar cellular effects like IgG 3-43. Seribantumab[110] and Lumretuzumab[116] also prevent heregulin binding to the receptor, inhibiting HER3 phosphorylation. Patritumab and Lumretuzumab also lead to downregulation of HER3. In the case of Patritumab, this was also linked to receptor internalization. The antitumor effect of IgG 3-43 seen in the FaDu xenograft model is in line with literature. LJM716 has been demonstrated to have tumor regression efficacy *in vivo* against the ligand driven model[115]. U3-1287 on the other hand only partially inhibited growth of these tumor cells[207]. In the present

study, the 3-43 binding site was in many analyses compared to the binding site of Seribantumab (MM-121) which showed anti-proliferative effects in *in vivo* studies with several xenografts due to the competition with HRG for HER3 binding, as well as the ability to downregulate HER3 from the cell surface, depending on cancer cell line[111].

4.4 Summary and Outlook

In this study, two ErbB receptor-binding antibodies with high affinities to their antigens and antigen-expressing cells were generated. IgG 2-35 inhibits proliferation of HER2 overexpressing BT-474 and NCI-N87 cells. More *in vitro* and *in vivo* analyses are necessary, to elucidate the effect of IgG 2-35 on HER2 positive cancer cells and to evaluate its anti-tumor activity. ADCC could lead to potent anti-tumor effects of IgG 2-35 and should be addressed in further studies. For trastuzumab, *in vitro* studies have demonstrated effective antibody-dependent cell-mediated cytotoxicity against HER2-overexpressing tumor targets[180]. The high affinity in combination with the ADCC enhancing mutation of the constant region, make IgG 2-35 an interesting candidate for targeted therapy of HER2 positive cancer. Furthermore, the variable domains of IgG 2-35 offer a potent binding module for the use in Bispecific antibody molecules.

In the main part of this study, a fully human monoclonal IgG1 antibody with engineered Fc part in order to promote enhanced ADCC and high affine, avidity strengthened binding to HER3 was established. The antibody was characterized in terms of antigen and cell binding, impact on HRG dependent and HRG independent signaling, and cancer cell proliferation. An excellently high affinity to the dimeric receptor of 220 pM and outstanding cell binding with EC_{50} values between 3 and 30 pM are reported. Mechanistically, it was shown that IgG 3-43 leads to a fast degradation of cellular HER3 and is internalized into the cells. First experiments indicating a rescue from oncogenic K-Ras driven transformation were collected. These experiments strengthen the hypothesis postulated by Möller et al. (2016)[208], that the cancer driving force of oncogenic K-Ras depends, at least partially, on its role in the formation of an autocrine heregulin loop.

The growth reduction of FaDu xenografts observed in the *in vivo* study in this thesis resulted from the growth inhibiting effect of IgG 3-43. To monitor also the immune stimulating effect of the antibody, a syngenic mouse tumor model, such as the 4T1

model, can be used[209,210]. By applying immune-competent mice, the two anti-tumorigenic mechanisms, growth inhibition and immune cell targeting and stimulation, can be studied, which may lead to even stronger effects. Crosstalk between mouse effector cells and human IgG1 Fc-part will in this case trigger ADCC, as described by Overdijk et al. (2012)[209]. As the herein performed *in vitro* experiments implicate a potent inhibiting effect of IgG 3-43 on cancer cell growth driven by HER2 overexpression, another *in vivo* study for example using xenografts formed by N87 gastric cancer cells could be performed. For the anti HER3 antibody KTN3379, Lee et al. could show significant tumor growth reduction in nu/nu athymic mice using the N87 model[113]. HER3 is also postulated to be a potential target in the treatment of gastric cancer[211]. More *in vitro* and *in vivo* studies can examine the use of IgG 3-43 in this cancer type. Furthermore, due to the role of HER3 in resistance to other ErbB member targeting therapies[201,212,213], combination studies using for example trastuzumab or cetuximab resistant models would be interesting[214,215]. Generally, combination of IgG 3-43 with TKIs or other monoclonal antibodies as well as the of bispecific antibodies incorporating the 3-43 binding site would be a promising strategy for the treatment of various cancer types, like HER2 overexpressing gynecological cancers[216], colon cancer[217], lung[218] and head and neck cancer[219]. As HER3 expression correlates with reduced survival of melanoma patients[91], the use of IgG 3-43 in combination with TKI in melanoma may also lead to improved treatment outcomes. A preclinical proof of concept for the application of HER3-targeting antibodies to enhance the efficacy of RAF inhibitors in melanoma was offered by Kugel et al. in 2014[220]. Furthermore, combination of the antibody with cytostatic or cytotoxic drugs in one molecule may be a powerful strategy, supported by the high affine binding capacity of 3-43 as well as the induced fast receptor internalization[221]. In this case, because of the internalization of 3-43, application of intracellular active drugs is possible. However, due to the relatively low HER3 surface expression of many cancer cells, it would be beneficial to combine the antibody with another tumor-selective drug, like for example TRAIL[222,223].

Taken together, a novel human anti-HER3 antibody with the ability for inhibiting heregulin-dependent and ligand-independent receptor activation, downstream signaling and cell proliferation was established in this study, which is a promising candidate for the treatment of various cancer types.

References

1. Wieduwilt MJ, Moasser MM. The epidermal growth factor receptor family: biology driving targeted therapeutics. *Cell Mol Life Sci.* 2008;65(10):1566-1584.

2. Takeuchi K, Ito F. Receptor tyrosine kinases and targeted cancer therapeutics. *Biol Pharm Bull.* 2011;34(12):1774-1780.

3. Hynes NE, Horsch K, Olayioye MA, Badache A. The ErbB receptor tyrosine family as signal integrators. *Endocr Relat Cancer.* 2001;8(3):151-159.

4. Appert-Collin A, Hubert P, Cremel G, Bennasroune A. Role of ErbB Receptors in Cancer Cell Migration and Invasion. *Front Pharmacol.* 2015;6:283.

5. Roskoski R, Jr. The ErbB/HER family of protein-tyrosine kinases and cancer. *Pharmacol Res.* 2014;79:34-74.

6. Hubbard SR, Mohammadi M, Schlessinger J. Autoregulatory mechanisms in protein-tyrosine kinases. *J Biol Chem.* 1998;273(20):11987-11990.

7. Guy PM, Platko JV, Cantley LC, Cerione RA, Carraway KL, 3rd. Insect cell-expressed p180erbB3 possesses an impaired tyrosine kinase activity. *Proc Natl Acad Sci U S A.* 1994;91(17):8132-8136.

8. Arteaga CL, Engelman JA. ERBB receptors: from oncogene discovery to basic science to mechanism-based cancer therapeutics. *Cancer Cell.* 2014;25(3):282-303.

9. Graus-Porta D, Beerli RR, Daly JM, Hynes NE. ErbB-2, the preferred heterodimerization partner of all ErbB receptors, is a mediator of lateral signaling. *Embo j.* 1997;16(7):1647-1655.

10. Citri A, Skaria KB, Yarden Y. The deaf and the dumb: the biology of ErbB-2 and ErbB-3. *Exp Cell Res.* 2003;284(1):54-65.

11. Holbro T, Civenni G, Hynes NE. The ErbB receptors and their role in cancer progression. *Exp Cell Res.* 2003;284(1):99-110.

12. Yarden Y, Sliwkowski MX. Untangling the ErbB signalling network. *Nat Rev Mol Cell Biol.* 2001;2(2):127-137.

13. Brand TM, Iida M, Dunn EF, et al. Nuclear epidermal growth factor receptor is a functional molecular target in triple-negative breast cancer. *Mol Cancer Ther.* 2014;13(5):1356-1368.

14. Burgess AW, Cho HS, Eigenbrot C, et al. An open-and-shut case? Recent insights into the activation of EGF/ErbB receptors. *Mol Cell.* 2003;12(3):541-552.

15. Malm M, Frejd FY, Ståhl S, Löfblom J. Targeting HER3 using mono- and bispecific antibodies or alternative scaffolds. *MAbs.* 2016;8(7):1195-1209.

16. Schlessinger J. Cell signaling by receptor tyrosine kinases. *Cell.* 2000;103(2):211-225.

17. Schlessinger J. Signal transduction by allosteric receptor oligomerization. *Trends Biochem Sci.* 1988;13(11):443-447.

18. Zhang X, Gureasko J, Shen K, Cole PA, Kuriyan J. An allosteric mechanism for activation of the kinase domain of epidermal growth factor receptor. *Cell.* 2006;125(6):1137-1149.

19. Lemmon MA, Schlessinger J. Cell signaling by receptor tyrosine kinases. *Cell.* 2010;141(7):1117-1134.

20. Garrett TP, McKern NM, Lou M, et al. Crystal structure of a truncated epidermal growth factor receptor extracellular domain bound to transforming growth factor alpha. *Cell.* 2002;110(6):763-773.

21. Dawson JP, Bu Z, Lemmon MA. Ligand-induced structural transitions in ErbB receptor extracellular domains. *Structure.* 2007;15(8):942-954.

22. Garrett TP, McKern NM, Lou M, et al. The crystal structure of a truncated ErbB2 ectodomain reveals an active conformation, poised to interact with other ErbB receptors. *Mol Cell.* 2003;11(2):495-505.

23. Li S, Schmitz KR, Jeffrey PD, Wiltzius JJ, Kussie P, Ferguson KM. Structural basis for inhibition of the epidermal growth factor receptor by cetuximab. *Cancer Cell.* 2005;7(4):301-311.

24. Cho HS, Mason K, Ramyar KX, et al. Structure of the extracellular region of HER2 alone and in complex with the Herceptin Fab. *Nature.* 2003;421(6924):756-760.

25. Cho HS, Leahy DJ. Structure of the extracellular region of HER3 reveals an interdomain tether. *Science.* 2002;297(5585):1330-1333.

26. Bouyain S, Longo PA, Li S, Ferguson KM, Leahy DJ. The extracellular region of ErbB4 adopts a tethered conformation in the absence of ligand. *Proc Natl Acad Sci U S A.* 2005;102(42):15024-15029.

27. Lemmon MA. Ligand-induced ErbB receptor dimerization. *Exp Cell Res.* 2009;315(4):638-648.

28. Gullick WJ. The Type 1 growth factor receptors and their ligands considered as a complex system. *Endocr Relat Cancer.* 2001;8(2):75-82.

29. Sanderson MP, Dempsey PJ, Dunbar AJ. Control of ErbB signaling through metalloprotease mediated ectodomain shedding of EGF-like factors. *Growth Factors.* 2006;24(2):121-136.

30. Massague J, Pandiella A. Membrane-anchored growth factors. *Annu Rev Biochem.* 1993;62:515-541.

31. Cohen S. Isolation of a mouse submaxillary gland protein accelerating incisor eruption and eyelid opening in the new-born animal. *J Biol Chem.* 1962;237:1555-1562.

32. Cohen S. ISOLATION AND BIOLOGICAL EFFECTS OF AN EPIDERMAL GROWTH-STIMULATING PROTEIN. *Natl Cancer Inst Monogr.* 1964;13:13-37.

33. Derynck R, Roberts AB, Winkler ME, Chen EY, Goeddel DV. Human transforming growth factor-alpha: precursor structure and expression in E. coli. *Cell.* 1984;38(1):287-297.

34. Marquardt H, Hunkapiller MW, Hood LE, Todaro GJ. Rat transforming growth factor type 1: structure and relation to epidermal growth factor. *Science.* 1984;223(4640):1079-1082.

35. Shoyab M, Plowman GD, McDonald VL, Bradley JG, Todaro GJ. Structure and function of human amphiregulin: a member of the epidermal growth factor family. *Science.* 1989;243(4894 Pt 1):1074-1076.

36. Carraway KL, 3rd, Sliwkowski MX, Akita R, et al. The erbB3 gene product is a receptor for heregulin. *J Biol Chem.* 1994;269(19):14303-14306.

37. Chang H, Riese DJ, 2nd, Gilbert W, Stern DF, McMahan UJ. Ligands for ErbB-family receptors encoded by a neuregulin-like gene. *Nature.* 1997;387(6632):509-512.

38. Carraway KL, 3rd, Weber JL, Unger MJ, et al. Neuregulin-2, a new ligand of ErbB3/ErbB4-receptor tyrosine kinases. *Nature.* 1997;387(6632):512-516.

39. Busfield SJ, Michnick DA, Chickering TW, et al. Characterization of a neuregulin-related gene, Don-1, that is highly expressed in restricted regions of the cerebellum and hippocampus. *Mol Cell Biol.* 1997;17(7):4007-4014.

40. Higashiyama S, Horikawa M, Yamada K, et al. A novel brain-derived member of the epidermal growth factor family that interacts with ErbB3 and ErbB4. *J Biochem.* 1997;122(3):675-680.

41. Kinugasa Y, Ishiguro H, Tokita Y, Oohira A, Ohmoto H, Higashiyama S. Neuroglycan C, a novel member of the neuregulin family. *Biochem Biophys Res Commun.* 2004;321(4):1045-1049.

42. Olayioye MA, Neve RM, Lane HA, Hynes NE. The ErbB signaling network: receptor heterodimerization in development and cancer. *Embo j.* 2000;19(13):3159-3167.

43. Peles E, Yarden Y. Neu and its ligands: from an oncogene to neural factors. *Bioessays.* 1993;15(12):815-824.

44. Zhang D, Sliwkowski MX, Mark M, et al. Neuregulin-3 (NRG3): a novel neural tissue-enriched protein that binds and activates ErbB4. *Proc Natl Acad Sci U S A.* 1997;94(18):9562-9567.

45. Harari D, Tzahar E, Romano J, et al. Neuregulin-4: a novel growth factor that acts through the ErbB-4 receptor tyrosine kinase. *Oncogene.* 1999;18(17):2681-2689.

46. Uchida T, Wada K, Akamatsu T, et al. A novel epidermal growth factor-like molecule containing two follistatin modules stimulates tyrosine phosphorylation of erbB-4 in MKN28 gastric cancer cells. *Biochem Biophys Res Commun.* 1999;266(2):593-602.

47. Higashiyama S, Abraham JA, Miller J, Fiddes JC, Klagsbrun M. A heparin-binding growth factor secreted by macrophage-like cells that is related to EGF. *Science.* 1991;251(4996):936-939.

48. Sasada R, Ono Y, Taniyama Y, Shing Y, Folkman J, Igarashi K. Cloning and expression of cDNA encoding human betacellulin, a new member of the EGF family. *Biochem Biophys Res Commun.* 1993;190(3):1173-1179.

49. Toyoda H, Komurasaki T, Uchida D, et al. Epiregulin. A novel epidermal growth factor with mitogenic activity for rat primary hepatocytes. *J Biol Chem.* 1995;270(13):7495-7500.

50. Strachan L, Murison JG, Prestidge RL, Sleeman MA, Watson JD, Kumble KD. Cloning and biological activity of epigen, a novel member of the epidermal growth factor superfamily. *J Biol Chem.* 2001;276(21):18265-18271.

51. Olayioye MA, Graus-Porta D, Beerli RR, Rohrer J, Gay B, Hynes NE. ErbB-1 and ErbB-2 acquire distinct signaling properties dependent upon their dimerization partner. *Mol Cell Biol.* 1998;18(9):5042-5051.

52. Pinkas-Kramarski R, Soussan L, Waterman H, et al. Diversification of Neu differentiation factor and epidermal growth factor signaling by combinatorial receptor interactions. *Embo j.* 1996;15(10):2452-2467.

53. Carpenter G. ErbB-4: mechanism of action and biology. *Exp Cell Res.* 2003;284(1):66-77.

54. Plowman GD, Culouscou JM, Whitney GS, et al. Ligand-specific activation of HER4/p180erbB4, a fourth member of the epidermal growth factor receptor family. *Proc Natl Acad Sci U S A.* 1993;90(5):1746-1750.

55. Tzahar E, Waterman H, Chen X, et al. A hierarchical network of interreceptor interactions determines signal transduction by Neu differentiation factor/neuregulin and epidermal growth factor. *Mol Cell Biol.* 1996;16(10):5276-5287.

56. Baselga J, Swain SM. Novel anticancer targets: revisiting ERBB2 and discovering ERBB3. *Nat Rev Cancer.* 2009;9(7):463-475.

57. Shankaran H, Zhang Y, Tan Y, Resat H. Model-based analysis of HER activation in cells co-expressing EGFR, HER2 and HER3. *PLoS Comput Biol.* 2013;9(8):e1003201.

58. Zhang Q, Park E, Kani K, Landgraf R. Functional isolation of activated and unilaterally phosphorylated heterodimers of ERBB2 and ERBB3 as scaffolds in ligand-dependent signaling. *Proc Natl Acad Sci U S A.* 2012;109(33):13237-13242.

59. Karamouzis MV, Dalagiorgou G, Georgopoulou U, Nonni A, Kontos M, Papavassiliou AG. HER-3 targeting alters the dimerization pattern of ErbB protein family members in breast carcinomas. *Oncotarget.* 2016;7(5):5576-5597.

60. Scaltriti M, Baselga J. The epidermal growth factor receptor pathway: a model for targeted therapy. *Clin Cancer Res.* 2006;12(18):5268-5272.

61. Normanno N, Bianco C, De Luca A, Maiello MR, Salomon DS. Target-based agents against ErbB receptors and their ligands: a novel approach to cancer treatment. *Endocr Relat Cancer.* 2003;10(1):1-21.

62. Muthuswamy SK, Gilman M, Brugge JS. Controlled Dimerization of ErbB Receptors Provides Evidence for Differential Signaling by Homo- and Heterodimers. *Mol Cell Biol.* 1999;19(10):6845-6857.

63. Fedi P, Pierce JH, di Fiore PP, Kraus MH. Efficient coupling with phosphatidylinositol 3-kinase, but not phospholipase C gamma or GTPase-activating protein, distinguishes ErbB-3 signaling from that of other ErbB/EGFR family members. *Mol Cell Biol.* 1994;14(1):492-500.

64. Seger R, Krebs EG. The MAPK signaling cascade. *FASEB J.* 1995;9(9):726-735.

65. Wöhrle FU, Daly RJ, Brummer T. How to Grb2 a Gab. *Structure.* 2009;17(6):779-781.

66. Wimmer R, Baccarini M. Partner exchange: protein-protein interactions in the Raf pathway. *Trends Biochem Sci.* 2010;35(12):660-668.

67. Kholodenko BN. Four-dimensional organization of protein kinase signaling cascades: the roles of diffusion, endocytosis and molecular motors. *J Exp Biol.* 2003;206(Pt 12):2073-2082.

68. Stokoe D, Macdonald SG, Cadwallader K, Symons M, Hancock JF. Activation of Raf as a result of recruitment to the plasma membrane. *Science.* 1994;264(5164):1463-1467.

69. Yoon S, Seger R. The extracellular signal-regulated kinase: multiple substrates regulate diverse cellular functions. *Growth Factors.* 2006;24(1):21-44.

70. Lauring J, Park BH, Wolff AC. The phosphoinositide-3-kinase-Akt-mTOR pathway as a therapeutic target in breast cancer. *J Natl Compr Canc Netw.* 2013;11(6):670-678.

71. Stephens L, Anderson K, Stokoe D, et al. Protein kinase B kinases that mediate phosphatidylinositol 3,4,5-trisphosphate-dependent activation of protein kinase B. *Science.* 1998;279(5351):710-714.

72. Vanhaesebroeck B, Stephens L, Hawkins P. PI3K signalling: the path to discovery and understanding. *Nat Rev Mol Cell Biol.* 2012;13(3):195-203.

73. Brown KK, Toker A. The phosphoinositide 3-kinase pathway and therapy resistance in cancer. *F1000Prime Rep.* 2015;7:13.

74. Klempner SJ, Myers AP, Cantley LC. What a tangled web we weave: emerging resistance mechanisms to inhibition of the phosphoinositide 3-kinase pathway. *Cancer Discov.* 2013;3(12):1345-1354.

75. Hanahan D, Weinberg RA. The hallmarks of cancer. *Cell.* 2000;100(1):57-70.

76. Hanahan D, Weinberg RA. Hallmarks of cancer: the next generation. *Cell.* 2011;144(5):646-674.

77. King CR, Kraus MH, Aaronson SA. Amplification of a novel v-erbB-related gene in a human mammary carcinoma. *Science.* 1985;229(4717):974-976.

78. Ghosh R, Narasanna A, Wang SE, et al. Trastuzumab has preferential activity against breast cancers driven by HER2 homodimers. *Cancer Res.* 2011;71(5):1871-1882.

79. Ross JS, Fletcher JA. The HER-2/neu oncogene in breast cancer: prognostic factor, predictive factor, and target for therapy. *Stem Cells.* 1998;16(6):413-428.

80. Nicholas MK, Lukas RV, Jafri NF, Faoro L, Salgia R. Epidermal growth factor receptor - mediated signal transduction in the development and therapy of gliomas. *Clin Cancer Res.* 2006;12(24):7261-7270.

81. Shigematsu H, Gazdar AF. Somatic mutations of epidermal growth factor receptor signaling pathway in lung cancers. *Int J Cancer.* 2006;118(2):257-262.

82. Hirsch FR, Varella-Garcia M, Bunn PA, Jr., et al. Epidermal growth factor receptor in non-small-cell lung carcinomas: correlation between gene copy number and protein expression and impact on prognosis. *J Clin Oncol.* 2003;21(20):3798-3807.

83. Moscatello DK, Holgado-Madruga M, Godwin AK, et al. Frequent expression of a mutant epidermal growth factor receptor in multiple human tumors. *Cancer Res.* 1995;55(23):5536-5539.

84. Garcia de Palazzo IE, Adams GP, Sundareshan P, et al. Expression of mutated epidermal growth factor receptor by non-small cell lung carcinomas. *Cancer Res.* 1993;53(14):3217-3220.

85. Wikstrand CJ, Hale LP, Batra SK, et al. Monoclonal antibodies against EGFRvIII are tumor specific and react with breast and lung carcinomas and malignant gliomas. *Cancer Res.* 1995;55(14):3140-3148.

86. Shi F, Telesco SE, Liu Y, Radhakrishnan R, Lemmon MA. ErbB3/HER3 intracellular domain is competent to bind ATP and catalyze autophosphorylation. *Proc Natl Acad Sci U S A.* 2010;107(17):7692-7697.

87. Amin DN, Campbell MR, Moasser MM. The role of HER3, the unpretentious member of the HER family, in cancer biology and cancer therapeutics. *Semin Cell Dev Biol.* 2010;21(9):944-950.

88. Jaiswal BS, Kljavin NM, Stawiski EW, et al. Oncogenic ERBB3 mutations in human cancers. *Cancer Cell.* 2013;23(5):603-617.

89. Holbro T, Beerli RR, Maurer F, Koziczak M, Barbas CF, 3rd, Hynes NE. The ErbB2/ErbB3 heterodimer functions as an oncogenic unit: ErbB2 requires ErbB3 to drive breast tumor cell proliferation. *Proc Natl Acad Sci U S A.* 2003;100(15):8933-8938.

90. Lee-Hoeflich ST, Crocker L, Yao E, et al. A central role for HER3 in HER2-amplified breast cancer: implications for targeted therapy. *Cancer Res.* 2008;68(14):5878-5887.

91. Reschke M, Mihic-Probst D, van der Horst EH, et al. HER3 is a determinant for poor prognosis in melanoma. *Clin Cancer Res.* 2008;14(16):5188-5197.

92. Buac K, Xu M, Cronin J, Weeraratna AT, Hewitt SM, Pavan WJ. NRG1 / ERBB3 signaling in melanocyte development and melanoma: inhibition of differentiation and promotion of proliferation. *Pigment Cell Melanoma Res.* 2009;22(6):773-784.

93. Ueno Y, Sakurai H, Tsunoda S, et al. Heregulin-induced activation of ErbB3 by EGFR tyrosine kinase activity promotes tumor growth and metastasis in melanoma cells. *Int J Cancer.* 2008;123(2):340-347.

94. Soler M, Mancini F, Meca-Cortes O, et al. HER3 is required for the maintenance of neuregulin-dependent and -independent attributes of malignant progression in prostate cancer cells. *Int J Cancer.* 2009;125(11):2565-2575.

95. Lee D, Yu M, Lee E, et al. Tumor-specific apoptosis caused by deletion of the ERBB3 pseudo-kinase in mouse intestinal epithelium. *J Clin Invest.* 2009;119(9):2702-2713.

96. Fujimoto N, Wislez M, Zhang J, et al. High expression of ErbB family members and their ligands in lung adenocarcinomas that are sensitive to inhibition of epidermal growth factor receptor. *Cancer Res.* 2005;65(24):11478-11485.

97. Tanner B, Hasenclever D, Stern K, et al. ErbB-3 predicts survival in ovarian cancer. *J Clin Oncol.* 2006;24(26):4317-4323.

98. Sheng Q, Liu X, Fleming E, et al. An activated ErbB3/NRG1 autocrine loop supports in vivo proliferation in ovarian cancer cells. *Cancer Cell.* 2010;17(3):298-310.

99. Ritch PS, Carroll SL, Sontheimer H. Neuregulin-1 enhances survival of human astrocytic glioma cells. *Glia.* 2005;51(3):217-228.

100. Addo-Yobo SO, Straessle J, Anwar A, Donson AM, Kleinschmidt-Demasters BK, Foreman NK. Paired overexpression of ErbB3 and Sox10 in pilocytic astrocytoma. *J Neuropathol Exp Neurol.* 2006;65(8):769-775.

101. Carter P, Presta L, Gorman CM, et al. Humanization of an anti-p185HER2 antibody for human cancer therapy. *Proc Natl Acad Sci U S A.* 1992;89(10):4285-4289.

102. Hudziak RM, Lewis GD, Winget M, Fendly BM, Shepard HM, Ullrich A. p185HER2 monoclonal antibody has antiproliferative effects in vitro and sensitizes human breast tumor cells to tumor necrosis factor. *Mol Cell Biol.* 1989;9(3):1165-1172.

103. Baselga J, Tripathy D, Mendelsohn J, et al. Phase II study of weekly intravenous recombinant humanized anti-p185HER2 monoclonal antibody in patients with HER2/neu-overexpressing metastatic breast cancer. *J Clin Oncol.* 1996;14(3):737-744.

104. Cobleigh MA, Vogel CL, Tripathy D, et al. Multinational study of the efficacy and safety of humanized anti-HER2 monoclonal antibody in women who have HER2-overexpressing metastatic breast cancer that has progressed after chemotherapy for metastatic disease. *J Clin Oncol.* 1999;17(9):2639-2648.

105. Vogel CL, Cobleigh MA, Tripathy D, et al. Efficacy and safety of trastuzumab as a single agent in first-line treatment of HER2-overexpressing metastatic breast cancer. *J Clin Oncol.* 2002;20(3):719-726.

106. Franklin MC, Carey KD, Vajdos FF, Leahy DJ, de Vos AM, Sliwkowski MX. Insights into ErbB signaling from the structure of the ErbB2-pertuzumab complex. *Cancer Cell.* 2004;5(4):317-328.

107. Goldstein NI, Prewett M, Zuklys K, Rockwell P, Mendelsohn J. Biological efficacy of a chimeric antibody to the epidermal growth factor receptor in a human tumor xenograft model. *Clin Cancer Res.* 1995;1(11):1311-1318.

108. Overman MJ, Hoff PM. EGFR-targeted therapies in colorectal cancer. *Dis Colon Rectum.* 2007;50(8):1259-1270.

109. LoRusso P, Janne PA, Oliveira M, et al. Phase I study of U3-1287, a fully human anti-HER3 monoclonal antibody, in patients with advanced solid tumors. *Clin Cancer Res.* 2013;19(11):3078-3087.

110. Schoeberl B, Pace EA, Fitzgerald JB, et al. Therapeutically targeting ErbB3: a key node in ligand-induced activation of the ErbB receptor-PI3K axis. *Sci Signal.* 2009;2(77):ra31.

111. Schoeberl B, Faber AC, Li D, et al. An ErbB3 antibody, MM-121, is active in cancers with ligand-dependent activation. *Cancer Res.* 2010;70(6):2485-2494.

112. Meetze K, Vincent S, Tyler S, et al. Neuregulin 1 expression is a predictive biomarker for response to AV-203, an ERBB3 inhibitory antibody, in human tumor models. *Clin Cancer Res.* 2015;21(5):1106-1114.

113. Lee S, Greenlee EB, Amick JR, et al. Inhibition of ErbB3 by a monoclonal antibody that locks the extracellular domain in an inactive configuration. *Proc Natl Acad Sci U S A.* 2015;112(43):13225-13230.

114. Li C, Brand TM, Iida M, et al. Human epidermal growth factor receptor 3 (HER3) blockade with U3-1287/AMG888 enhances the efficacy of radiation therapy in lung and head and neck carcinoma. *Discov Med.* 2013;16(87):79-92.

115. Garner AP, Bialucha CU, Sprague ER, et al. An antibody that locks HER3 in the inactive conformation inhibits tumor growth driven by HER2 or neuregulin. *Cancer Res.* 2013;73(19):6024-6035.

116. Mirschberger C, Schiller CB, Schraml M, et al. RG7116, a therapeutic antibody that binds the inactive HER3 receptor and is optimized for immune effector activation. *Cancer Res.* 2013;73(16):5183-5194.

117. Meulendijks D, Jacob W, Martinez-Garcia M, et al. First-in-Human Phase I Study of Lumretuzumab, a Glycoengineered Humanized Anti-HER3 Monoclonal Antibody, in Patients with Metastatic or Advanced HER3-Positive Solid Tumors. *Clin Cancer Res.* 2016;22(4):877-885.

118. Xiao Z, Carrasco RA, Schifferli K, et al. A Potent HER3 Monoclonal Antibody That Blocks Both Ligand-Dependent and -Independent Activities: Differential Impacts of PTEN Status on Tumor Response. *Mol Cancer Ther.* 2016;15(4):689-701.

119. Aurisicchio L, Marra E, Luberto L, et al. Novel anti-ErbB3 monoclonal antibodies show therapeutic efficacy in xenografted and spontaneous mouse tumors. *J Cell Physiol.* 2012;227(10):3381-3388.

120. Belleudi F, Marra E, Mazzetta F, et al. Monoclonal antibody-induced ErbB3 receptor internalization and degradation inhibits growth and migration of human melanoma cells. *Cell Cycle.* 2012;11(7):1455-1467.

121. Sala G, Traini S, D'Egidio M, et al. An ErbB-3 antibody, MP-RM-1, inhibits tumor growth by blocking ligand-dependent and independent activation of ErbB-3/Akt signaling. *Oncogene.* 2012;31(10):1275-1286.

122. Sala G, Rapposelli IG, Ghasemi R, et al. EV20, a Novel Anti-ErbB-3 Humanized Antibody, Promotes ErbB-3 Down-Regulation and Inhibits Tumor Growth In Vivo. *Transl Oncol.* 2013;6(6):676-684.

123. Lazrek Y, Dubreuil O, Garambois V, et al. Anti-HER3 domain 1 and 3 antibodies reduce tumor growth by hindering HER2/HER3 dimerization and AKT-induced MDM2, XIAP, and FoxO1 phosphorylation. *Neoplasia.* 2013;15(3):335-347.

124. Foreman PK, Gore M, Kobel PA, et al. ErbB3 inhibitory surrobodies inhibit tumor cell proliferation in vitro and in vivo. *Mol Cancer Ther.* 2012;11(7):1411-1420.

125. Schaefer G, Haber L, Crocker LM, et al. A two-in-one antibody against HER3 and EGFR has superior inhibitory activity compared with monospecific antibodies. *Cancer Cell.* 2011;20(4):472-486.

126. McDonagh CF, Huhalov A, Harms BD, et al. Antitumor activity of a novel bispecific antibody that targets the ErbB2/ErbB3 oncogenic unit and inhibits heregulin-induced activation of ErbB3. *Mol Cancer Ther.* 2012;11(3):582-593.

127. Huang S, Li C, Armstrong EA, et al. Dual targeting of EGFR and HER3 with MEHD7945A overcomes acquired resistance to EGFR inhibitors and radiation. *Cancer Res.* 2013;73(2):824-833.

128. Müller D, Kontermann RE. Recombinant bispecific antibodies for cellular cancer immunotherapy. *Curr Opin Mol Ther.* 2007;9(4):319-326.

129. Przepiorka D, Ko CW, Deisseroth A, et al. FDA Approval: Blinatumomab. *Clin Cancer Res.* 2015;21(18):4035-4039.

130. Staerz UD, Kanagawa O, Bevan MJ. Hybrid antibodies can target sites for attack by T cells. *Nature.* 1985;314(6012):628-631.

131. Wood ER, Truesdale AT, McDonald OB, et al. A unique structure for epidermal growth factor receptor bound to GW572016 (Lapatinib): relationships among protein conformation, inhibitor off-rate, and receptor activity in tumor cells. *Cancer Res.* 2004;64(18):6652-6659.

132. Stamos J, Sliwkowski MX, Eigenbrot C. Structure of the epidermal growth factor receptor kinase domain alone and in complex with a 4-anilinoquinazoline inhibitor. *J Biol Chem.* 2002;277(48):46265-46272.

133. Jänne PA, Johnson BE. Effect of epidermal growth factor receptor tyrosine kinase domain mutations on the outcome of patients with non-small cell lung cancer treated with epidermal growth factor receptor tyrosine kinase inhibitors. *Clin Cancer Res.* 2006;12(14 Pt 2):4416s-4420s.

134. Geyer CE, Forster J, Lindquist D, et al. Lapatinib plus capecitabine for HER2-positive advanced breast cancer. *N Engl J Med.* 2006;355(26):2733-2743.

135. Brand TM, Iida M, Wheeler DL. Molecular mechanisms of resistance to the EGFR monoclonal antibody cetuximab. *Cancer Biol Ther.* 2011;11(9):777-792.

136. Wheeler DL, Huang S, Kruser TJ, et al. Mechanisms of acquired resistance to cetuximab: role of HER (ErbB) family members. *Oncogene.* 2008;27(28):3944-3956.

137. Cordo Russo RI, Beguelin W, Diaz Flaque MC, et al. Targeting ErbB-2 nuclear localization and function inhibits breast cancer growth and overcomes trastuzumab resistance. *Oncogene.* 2015;34(26):3413-3428.

138. Fuchs BC, Fujii T, Dorfman JD, et al. Epithelial-to-mesenchymal transition and integrin-linked kinase mediate sensitivity to epidermal growth factor receptor inhibition in human hepatoma cells. *Cancer Res.* 2008;68(7):2391-2399.

139. Viloria-Petit A, Crombet T, Jothy S, et al. Acquired resistance to the antitumor effect of epidermal growth factor receptor-blocking antibodies in vivo: a role for altered tumor angiogenesis. *Cancer Res.* 2001;61(13):5090-5101.

140. Chung KY, Shia J, Kemeny NE, et al. Cetuximab shows activity in colorectal cancer patients with tumors that do not express the epidermal growth factor receptor by immunohistochemistry. *J Clin Oncol.* 2005;23(9):1803-1810.

141. De Roock W, Piessevaux H, De Schutter J, et al. KRAS wild-type state predicts survival and is associated to early radiological response in metastatic colorectal cancer treated with cetuximab. *Ann Oncol.* 2008;19(3):508-515.

142. Khamisipour G, Jadidi-Niaragh F, Jahromi AS, Zandi K, Hojjat-Farsangi M. Mechanisms of tumor cell resistance to the current targeted-therapy agents. *Tumour Biol.* 2016;37(8):10021-10039.

143. Dias A, Claudino W, Sinha R, Perez CA, Jain D. Human epidermal growth factor antagonists and cardiotoxicity-A short review of the problem and preventative measures. *Crit Rev Oncol Hematol.* 2016;104:42-51.

144. Chen X, Yeung TK, Wang Z. Enhanced drug resistance in cells coexpressing ErbB2 with EGF receptor or ErbB3. *Biochem Biophys Res Commun.* 2000;277(3):757-763.

145. Hust M, Dübel S. Phage display vectors for the in vitro generation of human antibody fragments. *Methods Mol Biol.* 2005;295:71-96.

146. Kirsch M, Zaman M, Meier D, Dübel S, Hust M. Parameters affecting the display of antibodies on phage. *J Immunol Methods.* 2005;301(1-2):173-185.

147. Benedict CA, MacKrell AJ, Anderson WF. Determination of the binding affinity of an anti-CD34 single-chain antibody using a novel, flow cytometry based assay. *J Immunol Methods.* 1997;201(2):223-231.

148. Laemmli UK. Cleavage of structural proteins during the assembly of the head of bacteriophage T4. *Nature.* 1970;227(5259):680-685.

149. Möller Y, Siegemund M, Beyes S, et al. EGFR-targeted TRAIL and a Smac mimetic synergize to overcome apoptosis resistance in KRAS mutant colorectal cancer cells. *PLoS One.* 2014;9(9):e107165.

150. Moasser MM. The oncogene HER2; Its signaling and transforming functions and its role in human cancer pathogenesis. *Oncogene.* 2007;26(45):6469-6487.

151. Horton HM, Bernett MJ, Pong E, et al. Potent in vitro and in vivo activity of an Fc-engineered anti-CD19 monoclonal antibody against lymphoma and leukemia. *Cancer Res.* 2008;68(19):8049-8057.

152. Jaramillo ML, Leon Z, Grothe S, Paul-Roc B, Abulrob A, O'Connor McCourt M. Effect of the anti-receptor ligand-blocking 225 monoclonal antibody on EGF receptor endocytosis and sorting. *Exp Cell Res.* 2006;312(15):2778-2790.

153. Dai W, Li Y, Zhou Q, et al. Cetuximab inhibits oral squamous cell carcinoma invasion and metastasis via degradation of epidermal growth factor receptor. *J Oral Pathol Med.* 2014;43(4):250-257.

154. Herr R, Wöhrle FU, Danke C, Berens C, Brummer T. A novel MCF-10A line allowing conditional oncogene expression in 3D culture. *Cell Commun Signal.* 2011;9:17.

155. Hust M, Meyer T, Voedisch B, et al. A human scFv antibody generation pipeline for proteome research. *J Biotechnol.* 2011;152(4):159-170.

156. Chan CE, Lim AP, MacAry PA, Hanson BJ. The role of phage display in therapeutic antibody discovery. *Int Immunol.* 2014;26(12):649-657.

157. Hwang WY, Foote J. Immunogenicity of engineered antibodies. *Methods.* 2005;36(1):3-10.

158. Tovey MG, Lallemand C. Immunogenicity and other problems associated with the use of biopharmaceuticals. In: *Ther Adv Drug Saf.* Vol 2.2011:113-128.

159. Knappik A, Ge L, Honegger A, et al. Fully synthetic human combinatorial antibody libraries (HuCAL) based on modular consensus frameworks and CDRs randomized with trinucleotides. *J Mol Biol.* 2000;296(1):57-86.

160. Liu E, Thor A, He M, Barcos M, Ljung BM, Benz C. The HER2 (c-erbB-2) oncogene is frequently amplified in in situ carcinomas of the breast. *Oncogene.* 1992;7(5):1027-1032.

161. Hudziak RM, Schlessinger J, Ullrich A. Increased expression of the putative growth factor receptor p185HER2 causes transformation and tumorigenesis of NIH 3T3 cells. *Proc Natl Acad Sci U S A.* 1987;84(20):7159-7163.

162. Di Fiore PP, Segatto O, Lonardo F, Fazioli F, Pierce JH, Aaronson SA. The carboxy-terminal domains of erbB-2 and epidermal growth factor receptor exert different regulatory effects on intrinsic receptor tyrosine kinase function and transforming activity. *Mol Cell Biol.* 1990;10(6):2749-2756.

163. Nuciforo P, Thyparambil S, Aura C, et al. High HER2 protein levels correlate with increased survival in breast cancer patients treated with anti-HER2 therapy. *Mol Oncol.* 2016;10(1):138-147.

164. Maximiano S, Magalhaes P, Guerreiro MP, Morgado M. Trastuzumab in the Treatment of Breast Cancer. *BioDrugs.* 2016;30(2):75-86.

165. Nami B, Wang Z. HER2 in Breast Cancer Stemness: A Negative Feedback Loop towards Trastuzumab Resistance. *Cancers (Basel).* 2017;9(5).

166. Zanardi E, Bregni G, de Braud F, Di Cosimo S. Better Together: Targeted Combination Therapies in Breast Cancer. *Semin Oncol.* 2015;42(6):887-895.

167. Steinwand M, Droste P, Frenzel A, Hust M, Dubel S, Schirrmann T. The influence of antibody fragment format on phage display based affinity maturation of IgG. *MAbs.* 2014;6(1):204-218.

168. Tóth G, Szöor Á, Simon L, Yarden Y, Szöllosi J, Vereb G. The combination of trastuzumab and pertuzumab administered at approved doses may delay development of trastuzumab resistance by additively enhancing antibody-dependent cell-mediated cytotoxicity. *MAbs.* 2016;8(7):1361-1370.

169. Pedersen MW, Jacobsen HJ, Koefoed K, et al. Targeting Three Distinct HER2 Domains with a Recombinant Antibody Mixture Overcomes Trastuzumab Resistance. *Mol Cancer Ther.* 2015;14(3):669-680.

170. Riccio G, Da Fonseca-Ricardo AR, Passariello M, Cunnah P, Mertens N, De Lorenzo C. Superior Suppression of ErbB2-positive Tumor Cells by a Novel Human Triparatopic Tribody. *J Immunother.* 2017.

171. Tang Y, Lou J, Alpaugh RK, Robinson MK, Marks JD, Weiner LM. Regulation of antibody-dependent cellular cytotoxicity by IgG intrinsic and apparent affinity for target antigen. *J Immunol.* 2007;179(5):2815-2823.

172. Zhou Y, Goenaga AL, Harms BD, et al. Impact of intrinsic affinity on functional binding and biological activity of EGFR antibodies. *Mol Cancer Ther.* 2012;11(7):1467-1476.

173. Nielsen UB, Adams GP, Weiner LM, Marks JD. Targeting of bivalent anti-ErbB2 diabody antibody fragments to tumor cells is independent of the intrinsic antibody affinity. *Cancer Res.* 2000;60(22):6434-6440.

174. Graus-Porta D, Beerli RR, Hynes NE. Single-chain antibody-mediated intracellular retention of ErbB-2 impairs Neu differentiation factor and epidermal growth factor signaling. *Mol Cell Biol.* 1995;15(3):1182-1191.

175. Wada T, Qian XL, Greene MI. Intermolecular association of the p185neu protein and EGF receptor modulates EGF receptor function. *Cell.* 1990;61(7):1339-1347.

176. Qian X, Dougall WC, Hellman ME, Greene MI. Kinase-deficient neu proteins suppress epidermal growth factor receptor function and abolish cell transformation. *Oncogene.* 1994;9(5):1507-1514.

177. Hudziak RM, Lewis GD, Shalaby MR, et al. Amplified expression of the HER2/ERBB2 oncogene induces resistance to tumor necrosis factor alpha in NIH 3T3 cells. *Proc Natl Acad Sci U S A.* 1988;85(14):5102-5106.

178. Honer J. *Multivalent and bispecific antibodies targeting ErbB family members*. Stuttgart: Institute of Cell Biology and Immunology, University of Stuttgart; 2016.

179. Ogiso H, Ishitani R, Nureki O, et al. Crystal structure of the complex of human epidermal growth factor and receptor extracellular domains. *Cell.* 2002;110(6):775-787.

180. Sliwkowski MX, Lofgren JA, Lewis GD, Hotaling TE, Fendly BM, Fox JA. Nonclinical studies addressing the mechanism of action of trastuzumab (Herceptin). *Semin Oncol.* 1999;26(4 Suppl 12):60-70.

181. Lewis Phillips GD, Li G, Dugger DL, et al. Targeting HER2-positive breast cancer with trastuzumab-DM1, an antibody-cytotoxic drug conjugate. *Cancer Res.* 2008;68(22):9280-9290.

182. Unverdorben F, Richter F, Hutt M, et al. Pharmacokinetic properties of IgG and various Fc fusion proteins in mice. *MAbs.* 2016;8(1):120-128.

183. Lemoine NR, Barnes DM, Hollywood DP, et al. Expression of the ERBB3 gene product in breast cancer. *Br J Cancer.* 1992;66(6):1116-1121.

184. Huang X, Gao L, Wang S, et al. Heterotrimerization of the growth factor receptors erbB2, erbB3, and insulin-like growth factor-i receptor in breast cancer cells resistant to herceptin. *Cancer Res.* 2010;70(3):1204-1214.

185. Kawakami H, Yonesaka K. HER3 and its Ligand, Heregulin, as Targets for Cancer Therapy. *Recent Pat Anticancer Drug Discov.* 2016;11(3):267-274.

186. Adams CW, Allison DE, Flagella K, et al. Humanization of a recombinant monoclonal antibody to produce a therapeutic HER dimerization inhibitor, pertuzumab. *Cancer Immunol Immunother.* 2006;55(6):717-727.

187. Schmitt LC, Rau A, Seifert O, et al. Inhibition of HER3 activation and tumor growth with a human antibody binding to a conserved epitope formed by domain III and IV. *MAbs.* 2017:0.

188. Huang Z, Choi BK, Mujoo K, et al. The E3 ubiquitin ligase NEDD4 negatively regulates HER3/ErbB3 level and signaling. *Oncogene.* 2015;34(9):1105-1115.

189. Mujoo K, Choi BK, Huang Z, Zhang N, An Z. Regulation of ERBB3/HER3 signaling in cancer. *Oncotarget.* 2014;5(21):10222-10236.

190. Camprecios G, Lorita J, Pardina E, Peinado-Onsurbe J, Soley M, Ramirez I. Expression, localization, and regulation of the neuregulin receptor ErbB3 in mouse heart. *J Cell Physiol.* 2011;226(2):450-455.

191. Vincenzi B, Schiavon G, Silletta M, Santini D, Tonini G. The biological properties of cetuximab. *Crit Rev Oncol Hematol.* 2008;68(2):93-106.

192. Sliwkowski MX, Schaefer G, Akita RW, et al. Coexpression of erbB2 and erbB3 proteins reconstitutes a high affinity receptor for heregulin. *J Biol Chem.* 1994;269(20):14661-14665.

193. Le Clorennec C, Lazrek Y, Dubreuil O, et al. The anti-HER3 (ErbB3) therapeutic antibody 9F7-F11 induces HER3 ubiquitination and degradation in tumors through JNK1/2- dependent ITCH/AIP4 activation. *Oncotarget.* 2016;7(24):37013-37029.

194. Jiang N, Saba NF, Chen ZG. Advances in Targeting HER3 as an Anticancer Therapy. *Chemother Res Pract.* 2012;2012:817304.

195. Coussens L, Yang-Feng TL, Liao YC, et al. Tyrosine kinase receptor with extensive homology to EGF receptor shares chromosomal location with neu oncogene. *Science.* 1985;230(4730):1132-1139.

196. Wang S, Huang J, Lyu H, et al. Therapeutic targeting of erbB3 with MM-121/SAR256212 enhances antitumor activity of paclitaxel against erbB2-overexpressing breast cancer. *Breast Cancer Res.* 2013;15(5):R101.

197. Kumar R, Yarmand-Bagheri R. The role of HER2 in angiogenesis. *Semin Oncol.* 2001;28(5 Suppl 16):27-32.

198. Yu J, Li Q, Xu Q, Liu L, Jiang B. MiR-148a inhibits angiogenesis by targeting ERBB3. *J Biomed Res.* 2011;25(3):170-177.

199. Wilson TR, Lee DY, Berry L, Shames DS, Settleman J. Neuregulin-1-mediated autocrine signaling underlies sensitivity to HER2 kinase inhibitors in a subset of human cancers. *Cancer Cell.* 2011;20(2):158-172.

200. Yonesaka K, Zejnullahu K, Okamoto I, et al. Activation of ERBB2 signaling causes resistance to the EGFR-directed therapeutic antibody cetuximab. *Sci Transl Med.* 2011;3(99):99ra86.

201. Ebbing EA, Medema JP, Damhofer H, et al. ADAM10-mediated release of heregulin confers resistance to trastuzumab by activating HER3. *Oncotarget.* 2016;7(9):10243-10254.

202. Hurrell T, Outhoff K. The in vitro influences of epidermal growth factor and heregulin-beta1 on the efficacy of trastuzumab used in Her-2 positive breast adenocarcinoma. *Cancer Cell Int.* 2013;13(1):97.

203. Wang W, Wang EQ, Balthasar JP. Monoclonal antibody pharmacokinetics and pharmacodynamics. *Clin Pharmacol Ther.* 2008;84(5):548-558.

204. Bendtzen K, Geborek P, Svenson M, Larsson L, Kapetanovic MC, Saxne T. Individualized monitoring of drug bioavailability and immunogenicity in rheumatoid arthritis patients treated with the tumor necrosis factor alpha inhibitor infliximab. *Arthritis Rheum.* 2006;54(12):3782-3789.

205. Dong J, Demarest SJ, Sereno A, et al. Combination of two insulin-like growth factor-I receptor inhibitory antibodies targeting distinct epitopes leads to an enhanced antitumor response. *Mol Cancer Ther.* 2010;9(9):2593-2604.

206. Phillips GD, Fields CT, Li G, et al. Dual targeting of HER2-positive cancer with trastuzumab emtansine and pertuzumab: critical role for neuregulin blockade in antitumor response to combination therapy. *Clin Cancer Res.* 2014;20(2):456-468.

207. Gala K, Chandarlapaty S. Molecular pathways: HER3 targeted therapy. *Clin Cancer Res.* 2014;20(6):1410-1416.

208. Möller Y, Morkel M, Schmid J, et al. Oncogenic Ras triggers hyperproliferation and impairs polarized colonic morphogenesis by autocrine ErbB3 signaling. *Oncotarget.* 2016.

209. Overdijk MB, Verploegen S, Ortiz Buijsse A, et al. Crosstalk between human IgG isotypes and murine effector cells. *J Immunol.* 2012;189(7):3430-3438.

210. Walter M, Simanovich E, Brod V, Lahat N, Bitterman H, Rahat MA. An epitope-specific novel anti-EMMPRIN polyclonal antibody inhibits tumor progression. *Oncoimmunology.* 2016;5(2):e1078056.

211. Yun C, Gang L, Rongmin G, Xu W, Xuezhi M, Huanqiu C. Essential role of Her3 in two signaling transduction patterns: Her2/Her3 and MET/Her3 in proliferation of human gastric cancer. *Mol Carcinog.* 2015;54(12):1700-1709.

212. Kjaer I, Lindsted T, Frohlich C, et al. Cetuximab Resistance in Squamous Carcinomas of the Upper Aerodigestive Tract Is Driven by Receptor Tyrosine Kinase Plasticity: Potential for mAb Mixtures. *Mol Cancer Ther.* 2016;15(7):1614-1626.

213. Nonagase Y, Yonesaka K, Kawakami H, et al. Heregulin-expressing HER2-positive breast and gastric cancer exhibited heterogeneous susceptibility to the anti-HER2 agents lapatinib, trastuzumab and T-DM1. *Oncotarget.* 2016.

214. Iida M, Brand TM, Starr MM, et al. Overcoming acquired resistance to cetuximab by dual targeting HER family receptors with antibody-based therapy. *Mol Cancer.* 2014;13:242.

215. Wang D, Qian G, Zhang H, et al. HER3 targeting sensitizes HNSCC to cetuximab by reducing HER3 activity and HER2/HER3 dimerization - evidence from cell line and patient derived xenograft models. *Clin Cancer Res.* 2016.

216. Gizzi M, Pautier P, Lhomme C, Leary A. Novel membrane-based targets - Therapeutic potential in gynecological cancers. *Crit Rev Oncol Hematol.* 2015;93(3):293-303.

217. Bon G, Loria R, Amoreo CA, et al. Dual targeting of HER3 and MEK may overcome HER3-dependent drug-resistance of colon cancers. *Oncotarget.* 2016.

218. Mancini M, Gaborit N, Lindzen M, et al. Combining three antibodies nullifies feedback-mediated resistance to erlotinib in lung cancer. *Sci Signal.* 2015;8(379):ra53.

219. Takikita M, Xie R, Chung JY, et al. Membranous expression of Her3 is associated with a decreased survival in head and neck squamous cell carcinoma. *J Transl Med.* 2011;9:126.

220. Kugel CH, 3rd, Hartsough EJ, Davies MA, Setiady YY, Aplin AE. Function-blocking ERBB3 antibody inhibits the adaptive response to RAF inhibitor. *Cancer Res.* 2014;74(15):4122-4132.

221. Sadekar S, Figueroa I, Tabrizi M. Antibody Drug Conjugates: Application of Quantitative Pharmacology in Modality Design and Target Selection. *Aaps j.* 2015;17(4):828-836.

222. Wahl K, Siegemund M, Lehner F, et al. Increased apoptosis induction in hepatocellular carcinoma by a novel tumor-targeted TRAIL fusion protein combined with bortezomib. *Hepatology.* 2013;57(2):625-636.

223. Hutt M, Fellermeier-Kopf S, Seifert O, Schmitt LC, Pfizenmaier K, Kontermann RE. Targeting scFv-Fc-scTRAIL fusion proteins to tumor cells. *Oncotarget.* 2018;9(13):11322-11335.

Acknowledgements

First of all, I want to thank Prof. Roland Kontermann for the supervision of this thesis, for the provision of a fascinating research topic and for sharing his excellent knowledge in the field of antibody engineering.

Sincere thanks go to Dr. Tilman Brummer, for being second reviewer of this thesis and for introducing me to the field of cancer research in the first place.

I thank Jonas Zantow, Michael Hust and Stefan Dübel from TU Braunschweig for providing the herein used scFv clones. Furthermore I would like to thank Prof. Klaus Pfizenmaier for giving me the opportunity to be part of the Predict project. I also want to thank Prof. Monilola Olayioye for many helpful discussions, tips and cooperation.

Big thanks go to my Master students Jonas Honer and Alexander Rau, who did a great job working on the HER3 project. I really enjoyed the opportunity working together facing the same objective. I am grateful for the great time, for the interesting discussions with Jonas and that Alexander hold the fort after I left.

I would like to thank all present and former Members of the Kontermann group, for all the support I received, a good working atmosphere and some nice evenings we spent together. Special thanks go to Oliver Seifert for his support concerning the *in vivo* study, to Meike Hutt for many helpful tips and to Fabian Richter for helpful advice concerning the affinity measurements and the written form of this thesis.

I thank Sabine Münkel for technical assistance regarding the cloning of the IgG molecules. Thanks go also to Alex and Beatrice from the animal facility, to Elke Gerlach for her assistance with the suspension cells and to Stephan Eisler for his help with the microscope. I want to thank the whole institute, especially Angelika Hauser, Simone Schmid and the girls from the Mo-Lab for helpful advice, good cooperation and a supporting atmosphere.

Last but not least I want to thank Michael who supported me in many respects. I am very grateful for his love and patience and for believing in me all the time.

Declaration

I hereby declare that I performed the present study independently without any illegitimate help or other materials than stated. All sources used have been quoted adequately.

Lisa Schmitt
Stuttgart, 30th of April 2018

Curriculum Vitae

Personal details

Name	Lisa Christine Schmitt
Address	Burgstraße 56, 70569 Stuttgart
Date of birth	February 18th, 1988
Place of birth	Karlsruhe

Education and professional experience

Since 04/2018	Remote Site Monitor at PPD Germany GmbH & Co. KG
05/2017 – 04/2018	Project Assistant II at PPD Germany GmbH & Co. KG
10/2016 – 02/2017	Professional education as CRA (Clinical Research Associate) at Pharmaakademie GmbH & Co. KG
04/2013 – 03/2016	PhD student at the University of Stuttgart, Institute of Cell Biology and Immunology, Biomedical Engineering laboratory of Prof Roland E. Kontermann “Novel EGFR family member binding antibodies as cancer therapeutics”
06/2014	“Training for the handling of laboratory animals” (FELASA-B)
10/2007 – 03/2013	Diploma in Biology at the University of Freiburg Major: Neurobiology und Biophysics Minors: Molecular Immunology, Cell biology, Biologic Anthropology Final grade: 1.2
04/2012 – 03/2013	Diploma thesis at the University of Freiburg, Institute of Molecular Medicine and Cell Research, group of Dr. Tilman Brummer. “Establishment of a conditionally immortalized MEF culture system to study the role of the B-Raf activation loop”

07/2012 – 11/2012	Student assistant at the University of Freiburg, International Graduate Academy Handling of western blot analyses
03/2011 – 02/2012	Scientific assistant at the University of Freiburg, Institute of Biology III, group of Dr. Tilman Brummer Processing of PCR analyses for mouse genotyping
09/2010 – 12/2010	Scientific assistant at the University of Freiburg, Institute of Biology I, group of Dr. Tonio Ball Continuation of the research project dealing with high resolution surface-based fMRI analyses
07/2010 – 08/2010	Research project at the University of Freiburg, Institute of Biology I, group of Dr. Tonio Ball: “High resolution surface-based fMRI of prefrontal cortex”
03/2010 – 04/2010	Research project at the University of Freiburg, Institute of Biology III, group of Prof. Karl-Friedrich Fischbach dealing with neurogenetic studies of Drosophila melanogaster
09/1994 – 06/2007	General qualification for university entrance Freie Waldorfschule Karlsruhe, Germany Final grade: 1.0

Patent application

15.09.2016	Schmitt LC, Seifert O, Hutt M, Zantow J, Hust M, Dübel S, Olayioye MA, Kontermann RE. Antigen binding protein against HER3. Patent application. Nr. 16188871.4

Publications

Hutt M, Fellermeier-Kopf S, Seifert O, **Schmitt LC**, Pfizenmaier K, Kontermann RE. Targeting scFv-Fc-scTRAIL fusion proteins to tumor cells. Oncotarget 2018 Jan 31. DOI: 10.18632/oncotarget.24379.

Schmitt LC, Rau A, Seifert O, Honer J, Hutt M, Schmid S, Zantow J, Hust M, Dübel S, Olayioye MA, Kontermann RE. Inhibition of HER3 activation and tumor growth with a human antibody binding to a conserved epitope formed by domain III and IV. mAbs 2017 Jul 9. DOI: 10.1080/19420862.2017.1319023

Möller Y, Morkel M, Schmid J, Beyes S, Hendrick J, Strotbek M, Riemer P, Schmid S, **Schmitt LC**, Kontermann R, Mürdter T, Schwab M, Sers C, Olayioye MA. Oncogenic Ras triggers hyperproliferation and impairs polarized colonic morphogenesis by autocrine ErbB3 signaling. Oncotarget 2016 Jul 18. DOI: 10.18632/oncotarget.10658

Köhler M, Röring M, Schorch B, Heilmann K, Stickel N, Fiala GJ, **Schmitt LC**, Braun S, Ehrenfeld S, Uhl FM, Kaltenbacher T, Weinberg F, Herzog S, Zeiser R, Schamel WW, Jumaa H, Brummer T. Activation loop phosphorylation regulates B-Raf in vivo and transformation by B-Raf mutants. EMBO J. 2016 Jan 18. DOI: 10.15252/embj.201592097

Deswal S, Meyer A, Fiala GJ, Eisenhardt AE, **Schmitt LC**, Salek M, Brummer T, Acuto O, Schamel WW. Kidins220/ARMS associates with B-Raf and the TCR promoting sustained Erk signaling in T cells. J Immunol. 2013 Mar 1. DOI: 10.4049/jimmunol.1200653